



**AUBURN UNIVERSITY**

Samuel Ginn College of Engineering

**Final Research Report**

**LOAD RATING FOR CORRUGATED METAL CULVERTS  
UNDER SHALLOW COVER DEPTHS**

Submitted to the

Alabama Department of Transportation

Prepared by

J. Brian Anderson  
James S. Davidson  
Bujing Liu  
Chukwuma C. Okafor  
Olga L. Rojas  
Kelly N. Turner

June 2023

---

---

**Highway Research Center**

**Harbert Engineering Center**

**Auburn University, Alabama 36849**

<b>1. Report No.</b>	<b>2. Government Accession No.</b>	<b>3. Recipient Catalog No.</b>	
<b>4 Title and Subtitle</b> <b>LOAD RATING FOR CORRUGATED METAL CULVERTS UNDER SHALLOW COVER DEPTHS</b>		<b>5 Report Date</b>	
		<b>6 Performing Organization Code</b>	
<b>7. Author(s)</b> J. Brian Anderson, James S. Davidson, Bujing Liu, Chukwuma C. Okafor, Olga L. Rojas, and Kelly N. Turner		<b>8 Performing Organization Report No.</b>	
<b>9 Performing Organization Name and Address</b> Highway Research Center Department of Civil Engineering 238 Harbert Engineering Center Auburn, AL 36849		<b>10 Work Unit No. (TRAIS)</b>	
		<b>11 Contract or Grant No.</b>	
<b>12 Sponsoring Agency Name and Address</b> Highway Research Center Department of Civil Engineering 238 Harbert Engineering Center Auburn, AL 36849		<b>13 Type of Report and Period Covered</b>	
		<b>14 Sponsoring Agency Code</b>	
<b>15 Supplementary Notes</b>			
<b>16 Abstract</b> The accuracy and applicability of existing methodologies and tools for load rating of corrugated metal culverts under shallow cover were thoroughly investigated through numerical modeling and field testing. The basis of three existing spreadsheet rating tools were investigated. Two existing culverts that are more than 80 years old and whose cover over the crown is significantly less than current design and construction requirements were instrumented and load tested. The test data was then used to improve the accuracy of the analytical rating factors using the approach defined in the <i>AASHTO Manual for Bridget Evaluation</i> . The plane strain finite element program CANDE that was developed specifically for culvert analysis and design and is widely used, plus two general-purpose finite element software, Abaqus and Plaxis, were extensively employed to understand the soil-structure interaction phenomena and assess culvert rating methodology. Recommendations for addressing the deficiencies of the existing “simplified” spreadsheet tools for low cover situations were developed and incorporated into a new spreadsheet-based tool.			
<b>17 Key Words:</b> culvert, pipe, arch, soil structure interaction, rating, finite element		<b>18 Distribution Statement</b> No restrictions. This document is available to the public through the National Technical Information Service, Springfield, Virginia 22161	
<b>19 Security Classification (of this report)</b> Unclassified	<b>20 Security Classification (of this page)</b> Unclassified	<b>21 No. of pages</b>	<b>22 Price</b>

---

**Research Report No.**

**LOAD RATING FOR CORRUGATED METAL CULVERTS  
UNDER SHALLOW COVER DEPTHS**

Submitted to the

Alabama Department of Transportation

Prepared by

J. Brian Anderson  
James S. Davidson  
Bujing Liu  
Chukwuma C. Okafor  
Olga L. Rojas  
Kelly N. Turner

October 2022

## **DISCLAIMERS**

The contents of this report reflect the views of the authors, who are responsible for the facts and the accuracy of the data presented herein. The contents do not necessarily reflect the official views or policies of Auburn University or the Federal Highway Administration. This report does not constitute a standard, specification, or regulation.

### **NOT INTENDED FOR CONSTRUCTION, BIDDING, OR PERMIT PURPOSES**

J. Brian Anderson, James S. Davidson, Bujing Liu, Chukwuma C. Okafor, Olga L. Rojas, and Kelly N. Turner

## **ACKNOWLEDGEMENTS**

The authors would like to acknowledge the following people who contributed to the success of this project:

- Dr. Michael Stallings for the guidance about load rating and for sharing his experience and passing it along to us.
- Daniel Jones, Michael Wall, and Eric Christie of the ALDOT Maintenance Bureau conceived the project and provided information to the project team.
- Lance Armbrester with the City of Anniston, AL provided access to the examined culverts and offered insight to the McClellan land use.
- Patricia Carcamo Barrientos, Jeff Stallings, and Dan Jackson provided support for geotechnical tests at the culverts.
- John “Jip” Pitts and his crew mobilized the ALDOT load truck and provided traffic control during the field load tests.
- Ashton Babb, Frank Russell, and Sam Dunlop from Auburn assisted with the culvert load testing.
- Russ Davis with the Alabama National Guard provided access to the Pelham Range to inspect BIN 18609.



## ABSTRACT

The accuracy and applicability of existing methodologies and tools for load rating of corrugated metal culverts under shallow cover were thoroughly investigated through numerical modeling and field testing. The basis of three existing spreadsheet rating tools were investigated. Two existing culverts that are more than 80 years old and whose cover over the crown is significantly less than current design and construction requirements were instrumented and load tested. The test data was then used to improve the accuracy of the analytical rating factors using the approach defined in the *AASHTO Manual for Bridge Evaluation*. The plane strain finite element program CANDE that was developed specifically for culvert analysis and design and is widely used, plus two general-purpose finite element software, Abaqus and Plaxis, were extensively employed to understand the soil-structure interaction phenomena and assess culvert rating methodology. Recommendations for addressing the deficiencies of the existing “simplified” spreadsheet tools for low cover situations were developed and incorporated into a new spreadsheet-based tool.

## TABLE OF CONTENTS

ABSTRACT.....	v
LIST OF TABLES.....	ix
LIST OF FIGURES.....	x
CHAPTER 1: INTRODUCTION.....	1
1.1 Background.....	1
1.2 Objectives.....	3
1.3 Scope and Methodology.....	3
CHAPTER 2: LITERATURE REVIEW.....	7
2.1 Metal Culverts.....	7
2.2 Specifications and Guides.....	12
2.3 NCHRP Projects.....	12
2.3.1 McGrath et al. (2002).....	13
2.3.2 Mlynarski et al. (2008).....	14
2.3.3 Petersen et al. (2010).....	14
2.3.4 Mlynarski et al. (2019).....	15
2.4 Field Test Projects.....	15
2.4.1 Webb et al. (1999).....	16
2.4.2 Sezen et al. (2009).....	23
2.4.3 Sargand et al. (2018).....	27
2.4.4 Mlynarski et al. (2019).....	29
2.5 Literature Survey Conclusions.....	31
CHAPTER 3: LOAD RATING OF CORRUGATED METAL CULVERTS.....	32
3.1 Definition and General Philosophy.....	32
3.2 Evaluation Load Definitions.....	36
3.3 Load Factors.....	38
3.4 Corrugated Culvert Methodology.....	38
3.5 Advanced Analytical Approaches.....	40
CHAPTER 4: SITE CHARACTERIZATION AND CONDITION ASSESSMENT.....	41
4.1 Background.....	41
4.2 Project Culverts.....	42
4.2.1 BIN 18609.....	44
4.2.2 BIN 18615.....	45
4.2.3 BIN 19875.....	46

4.2.4 BIN 20431 .....	47
4.2.5 BIN 20432.....	49
4.2.6 BIN 20433.....	50
4.2.7 BIN 20441.....	52
4.2.8 BIN 20442.....	54
4.2.9 BIN 20444.....	56
4.3 Preliminary Site Visits .....	57
4.3.1 November 25, 2019.....	57
4.3.2 October 16, 2020.....	60
4.4 Condition Assessment.....	61
CHAPTER 5: LOAD TESTS .....	63
5.1 Test Sites.....	63
5.1.1 Bain’s Gap Road (BIN 20433) .....	63
5.1.2 Berman Road (BIN 20441).....	65
5.2 Load Tests.....	68
5.2.1 General Methodology .....	68
5.2.2 Instrumentation .....	70
5.2.3 Testing Procedure .....	73
5.2.4 Load Line and Truck Stopping Locations .....	77
5.2.5 Strain Gage and Potentiometer Installation .....	79
5.2.6 Data Storage Settings.....	81
5.2.7 Load Test .....	82
5.3 Data Analysis.....	85
5.3.1 Test Data .....	85
5.3.2 Calculations.....	92
5.3.3 Results.....	97
5.4 Field Test Summary.....	97
CHAPTER 6: FINITE ELEMENT ANALYSES .....	101
6.1 Background.....	101
6.2 CANDE.....	101
6.3 ABAQUS .....	108
6.4 PLAXIS 3D.....	116
6.5 Analytical method comparisons.....	122
CHAPTER 7: SIMPLIFIED RATING FACTOR METHODOLOGY FOR SHALLOW FILL SCENARIOS .....	129
7.1 Background.....	129
7.2 Definition and Origin of Minimum Cover Requirements.....	130
7.3 Rating Factor Analysis Methodology .....	135
7.3.1 Modified ODOT Minimum Cover Definition .....	135
7.3.2 Definition of “Span” for Long-Span Structures.....	137
7.3.3 Tire Contact Area.....	139
7.3.4 Thrust due to Live Load.....	140

7.3.5 Maximum Moment by the Duncan Method.....	141
7.3.6 Maximum Moment by Castigliano’s method .....	142
7.4 Pavement Effect .....	143
7.4.1 Culvert under Rigid Pavement.....	144
7.4.2 Culvert under Flexible Pavement.....	148
7.4.3 Pavement Effect in Duncan Method .....	151
7.4.4 Pavement Effect in Castigliano’s Method .....	152
7.5 Worst-Case Position for Load Rating .....	152
7.6 Rating Factor Equations for Culverts with Shallow Cover .....	157
7.7 Rating Factors based on Moment by Castigliano Method.....	161
7.8 Proposed ALDOT Simplified Method.....	161
7.9 Example and Comparison .....	161
7.9.1. Refined ODOT Approach .....	162
7.9.2 Refined MDOT Simplified Approach (Duncan and Drawsky 1983) .....	168
7.9.3 Rating Factor Based on AASHTO.....	174
7.9.4 Rating Factor Based on Duncan (1983).....	174
7.9.5 Comparison between Simplified Approaches and CANDE .....	175
7.9.6 Rating Factors Based on Castigliano’s Equation.....	176
7.9.7 Comparison between Simplified Approaches and CANDE .....	179
7.10 Simplified Methodology Summary.....	180
 CHAPTER 8: RATING OF THE ANNISTON CULVERTS .....	 182
8.1 Rating Factor Methodology Summary.....	182
8.1.1 Original ODOT Spreadsheet.....	182
8.1.2 Modified ODOT Spreadsheet .....	182
8.1.3 MDOT Spreadsheet .....	183
8.1.4 AU Modified MDOT (ALDOT Spreadsheet).....	183
8.1.4 2D / Plane Strain (CANDE).....	184
8.1.5 3D Nonlinear FEM .....	185
8.1.6 Load Testing .....	185
8.2 Rating Factor Calculation using Field Test Data.....	186
8.3 Rating Factor Comparison .....	193
8.4 Anniston Culverts Rating Factors .....	195
8.4.1 Input and Methodology .....	195
8.4.2 Modeling Approach and Assumptions.....	196
8.4.3 Load Case Definitions.....	197
8.4.4 Rating Factor Results.....	197
 CHAPTER 9: CONCLUSIONS AND RECOMMENDATIONS.....	 202
 REFERENCES .....	 206

## LIST OF TABLES

Table 4.1. Culvert locations.....	42
Table 5.1. Bain’s Gap strain gage and potentiometer readings for load line 1.....	88
Table 5.2. Bain’s Gap strain gage and potentiometer readings for load line 2.....	89
Table 5.3. Berman Road strain gage and potentiometer readings for load line 1.....	90
Table 5.4. Berman Road strain gage and potentiometer readings for load line 2.....	91
Table 5.5. Calculated stresses from measured strain for Bain’s Gap load line 1. ....	93
Table 5.6. Calculated stresses from measured strain for Bain’s Gap load line 2. ....	94
Table 5.7. Calculated stresses from measured strain for Berman Road load line 1. ....	95
Table 5.8. Calculated stresses from measured strain for Berman Road load line 2. ....	96
Table 6.1. Dimensions and cross-section properties of corrugated steel plates used in the Anniston culverts.....	102
Table 6.2. Resistance Factors.....	104
Table 6.3. Load factors and load modifiers for buried corrugated metal pipe or arch. ....	104
Table 6.4. Multiple Presence Factors $m$ .....	107
Table 6.5. Elastic soil properties for backfill (Selig 1990).....	110
Table 6.6. Triaxial Test Parameters (Selig 1988). ....	110
Table 6.7. Mohr-Coulomb properties for Backfill ML95.....	111
Table 6.8. Summary of orthotropic structural properties for corrugated metal pipe and arch. ..	112
Table 6.9. Boundary conditions.....	114
Table 6.10. Modified equivalent plate properties used in PLAXIS 3D.....	118
Table 7.1. Minimum cover definition Table 12.6.6.3-1 of the AASHTO <i>LRFD Bridge Design Specifications</i> (2020). ....	133
Table 7.2. Critical-load parameter for uniform elastic arches in pure compression (Galambos 1998). ....	137
Table 7.3. Elastic soil properties for backfill (Selig 1990).....	145
Table 7.4. Distribution Angle between Pavement Layers .....	146
Table 7.5. Distribution Angle between Pavement Layers .....	149
Table 8.1. Quantities used in calculating rating factors for culverts 1 and 2 for the 33T concrete truck. ....	190
Table 8.2. Rating factor (RF) comparisons for BIN 20441 using 33T concrete truck .....	194
Table 8.3. Anniston culvert properties.....	196
Table 8.4. Rating factors for Anniston Culverts based on CANDE Level 1 Analyses .....	199
Table 8.5. Operating Rating Factors Comparisons between Level 1 and Level 2 CANDE Analyses .....	201

## LIST OF FIGURES

Figure 2.1. Mechanisms of soil arching (a) rigid pipe and positive arching; (b) flexible pipe and negative arching (Kang et al. 2009).....	9
Figure 2.2. Comparison of positive projection conduits for (a) rigid and (b) flexible pipe (Tehrani et al. 2020). .....	9
Figure 2.3. Common cross section shapes of metal culverts (Duncan and Drawsky 1983).....	10
Figure 2.4. Spangler’s Assumptions for Derivation of the Iowa Formula (Watkins and Spangler 1958; Whidden 2009). .....	11
Figure 2.5. (a) Cross-sectional view of culvert installation; (b) End-to-end installation of concrete and metal culverts (Webb et al. 1999). .....	17
Figure 2.6. Monitoring deformation in a corrugated metal culvert (Webb et al. 1999). .....	18
Figure 2.7. Longitudinal deflection profile of crown locations from live-load test (Webb et al. 1999). .....	19
Figure 2.8. Bending moments from live-load axles over culvert crown (Webb et al. 1999). .....	21
Figure 2.9. Bending moments from live-load axles over south shoulder (Webb et al. 1999). .....	22
Figure 2.10. Displacement sensors and strain gage locations (Sezen et al. 2009).....	25
Figure 2.11. Maximum deflections and strains versus backfill height (Sezen et al. 2009). .....	26
Figure 2.12. Close-up view of instrumentation point (Sargand et al. 2018).....	28
Figure 2.13. Model 5 instrumentation locations (Mlynarski et al. 2019). .....	30
Figure 3.1. Alabama posting loads (ALDOT 2021). .....	37
Figure 4.1. Culvert locations on broad map.....	42
Figure 4.2. Fort McClellan culvert locations. ....	43
Figure 4.3. BIN 18609 (Google Earth). .....	44
Figure 4.4. BIN 18609 from site visit.....	45
Figure 4.5. BIN 18615 (Google Earth). .....	46
Figure 4.6. BIN 19875 end view.....	47
Figure 4.7. BIN 20431 end view.....	48
Figure 4.8. BIN 20431 road surface.....	48
Figure 4.9. BIN 20432 road surface.....	49
Figure 4.10. BIN 20432 underside.....	50
Figure 4.11. BIN 20433 exterior.....	51
Figure 4.12. BIN 20433 road surface.....	51
Figure 4.13. BIN 20433 foundation.....	52
Figure 4.14. BIN 20441 cross-section. ....	53
Figure 4.15. BIN 20441 road surface.....	53
Figure 4.16. BIN 20441 close-up.....	54
Figure 4.17. BIN 20442 and fence.....	55
Figure 4.18. BIN 20442. ....	55
Figure 4.19. BIN 20444 (Google Earth). .....	56
Figure 4.20. Seismic tests at Lennox Avenue.....	58
Figure 4.21. Seismic tests at Brigadier Stern Avenue. ....	58
Figure 4.22. Seismic wave testing at Lennox Avenue.....	59

Figure 4.23. Accelerometers to measure wave transmission Lennox Avenue. ....	59
Figure 4.24. Fill characterization at Berman Road and Lenox Avenue.....	60
Figure 4.25. October 16, 2020 site visit.....	61
Figure 5.1. BIN 20433 dimensions. ....	63
Figure 5.2. BIN 20433 end view.....	63
Figure 5.3. BIN 20433 longitudinal view. ....	64
Figure 5.4. BIN 20433 Bain’s Gap Road culvert aerial photo (Google Earth). ....	64
Figure 5.5. BIN 20441 dimensions. ....	65
Figure 5.6. BIN 20441 end view.....	65
Figure 5.7. BIN 20441 longitudinal view. ....	66
Figure 5.8. BIN 20441 Berman Road culvert aerial photo (Google Earth).....	67
Figure 5.9. Tested culverts aerial photo (Google Earth).....	67
Figure 5.10. ALDOT load test vehicle.....	68
Figure 5.11. LC-5 configuration of the load truck.....	69
Figure 5.12. Instrumentation locations. ....	70
Figure 5.13. BDI ST350; strain transducer for strain measurements. ....	71
Figure 5.14. Micro-Epsilon P60; String pot potentiometers for deflection measurement.....	71
Figure 5.15. Tripod with potentiometer mounted. ....	72
Figure 5.16. CR6 datalogger. ....	72
Figure 5.17. Load lines; truck shown in the first load line position. ....	73
Figure 5.18. Truck stopping positions: start, 1/4, crown, 3/4 and end.....	74
Figure 5.19. Truck shown in the second load line position. ....	75
Figure 5.20. Location of instrumentation points at the Bain’s Gap Road culvert. ....	76
Figure 5.21. Location of instrumentation points at the Berman Road culvert.....	76
Figure 5.22. Location of truck stopping points on the road.....	77
Figure 5.23. Signal flags located at the Bain’s Gap Road culvert. ....	78
Figure 5.24. Truck stopping points located at the Berman Road culvert. ....	78
Figure 5.25. Strain gage installation. ....	79
Figure 5.26. Strain gage installed at 1/4, crown and 3/4 of the Berman Road culvert. ....	80
Figure 5.27. Potentiometer installation.....	80
Figure 5.28. Potentiometers installed at 1/4, crown and 3/4 locations at Bain’s Gap Road culvert. ....	81
Figure 5.29. CR6 Datalogger. ....	81
Figure 5.30. Connection of strain gages and potentiometers to the datalogger.....	82
Figure 5.31. Verification of truck location in stopping point (load line 1) at the Bain’s Gap Road culvert. ....	83
Figure 5.32. Load truck in 1/4 stopping point (load line 2) at the Bain’s Gap Road culvert. ....	84
Figure 5.33. Load truck in crown stopping point (load line 2) at Berman Road culvert.....	84
Figure 5.34. Load truck in reverse pass at Berman Road culvert. ....	85
Figure 5.35. Bain’s Gap (BIN 20433) culvert cross-section with sensors locations (dimensions in inches).....	86
Figure 5.36. Berman Road (BIN 20433) culvert cross-section with sensors locations (dimensions in inches).....	86
Figure 5.37. Deformed shapes of the Bain’s Gap culvert for each load truck position (scale x100). ....	98

Figure 5.38. Deformed shapes of the Berman Road culvert for each load truck position (scale x100). .....	99
Figure 6.1. Mesh plot of arch culvert.....	103
Figure 6.2. First construction increment for installation of metal structure. ....	105
Figure 6.3. Construction increments for soil along sides of culvert. ....	105
Figure 6.4. Construction increments for soil over the culvert. ....	106
Figure 6.5. Final construction increment for live load.....	106
Figure 6.6. ABAQUS model dimensions. ....	113
Figure 6.7. Boundary fixities. ....	114
Figure 6.8. Typical soil mesh.....	115
Figure 6.9. Typical mesh for arch (left) and pavement (right). ....	116
Figure 6.10. Typical deformed structure under loading (different shadings represent the vertical displacement). ....	116
Figure 6.11. Model Geometry.....	120
Figure 6.12. Typical mesh for soil clusters.....	120
Figure 6.13. Typical mesh for metal arch. ....	121
Figure 6.14. Mesh sensitivity analysis.....	121
Figure 6.15. 2-barrel culvert model in Plaxis 3D.....	122
Figure 6.16. Comparison of the output for single and double barrel models. ....	122
Figure 6.17. BIN 20443 measured and predicted responses: (left) deflection, (right) strain with load truck at “start” load position (load line 2).....	123
Figure 6.18. BIN 20443 measured and predicted responses: (left) deflection, (right) strain with load truck at “1/4” load position (load line 2).....	124
Figure 6.19. BIN 20443 measured and predicted responses: (left) deflection, (right) strain with load truck at “peak” load position (load line 2). ....	124
Figure 6.20. BIN 20443 measured and predicted responses: (left) deflection, (right) strain with load truck at “3/4” load position (load line 2).....	125
Figure 6.21. BIN 20443 measured and predicted responses: (left) deflection, (right) strain with load truck at “end” load position (load line 2).....	125
Figure 6.22. BIN 20441 measured and predicted responses: (left) deflection, (right) strain with load truck at “start” load position (load line 2).....	126
Figure 6.23. BIN 20441 measured and predicted responses: (left) deflection, (right) strain with load truck at “1/4” load position (load line 2).....	126
Figure 6.24. BIN 20441 measured and predicted responses: (left) deflection, (right) strain with load truck at “peak” load position (load line 2). ....	127
Figure 6.25. BIN 20441 measured and predicted responses: (left) deflection, (right) strain with load truck at “3/4” load position (load line 2).....	127
Figure 6.26. BIN 20441 measured and predicted responses: (left) deflection, (right) strain with load truck at “end” load position (load line 2).....	128
Figure 7.1. “Figure 12.6.6.3-1—Minimum Cover Orientation” of AASHTO LRFD Section C12.6.6.3.....	132
Figure 7.2. Circumferential thrust in non-circular culvert (Sezen et al. 2009). ....	138
Figure 7.3. Tangential thrust in arch culvert (White and Layer 1960). ....	138
Figure 7.4. Width of culvert on which the live load is applied parallel to span. ....	140
Figure 7.5. Moment due to earth fill and live load at the quarter point. ....	142



Figure 7.6. Mechanics of flexible pipe under a surface load (Watkins and Anderson 1999).....	143
Figure 7.7. Vertical pressure distribution under rigid pavement (Han et al. 2013). .....	147
Figure 7.8. Distributed Pressure over the Culvert under a Rigid Pavement .....	148
Figure 7.9. Vertical Pressure Distribution through Flexible Pavement Layers .....	150
Figure 7.10. Distributed Pressure over the Culvert under a Flexible Pavement.....	151
Figure 7.11. Moment distribution due to backfill at final cover without live load (outside values denote outer fiber in tension, inside values denote inner fiber in tension). .....	153
Figure 7.12. Live load is over the crown (outside values denote outer fiber in tension, inside values denote inner fiber in tension). .....	154
Figure 7.13. Live load is over the quarter point (outside values denote outer fiber in tension, inside values denote inner fiber in tension). .....	156
Figure 14. Live load is over the middle point between the crown and the quarter point (outside values denote outer fiber in tension, inside values denote inner fiber in tension). .....	157
Figure 15. Concrete Truck Configuration.....	162
Figure 7.16. Top radius definition (NCSPA 1995).....	162
Figure 8.1. Concrete truck used for RF comparisons .....	188
Figure 8.2. Annotated CANDE 2019 Model for a low profile arch culvert typical of this project. ....	197
Figure 8.3. Load case definitions.....	198
Figure 8.5. Test truck LC-5 configuration. ....	199

## CHAPTER 1: INTRODUCTION

### 1.1 Background

A “culvert” can be broadly defined as a conduit that conveys water through a roadway embankment or past other flow obstructions. The term “culvert” also sometimes refers to under-roadway transmission applications other than water passage where soil is between the roadway and the structure, such as railway underpasses, animal passages, etc. Culverts used for cross-drainage applications (moving water from one side of a roadway to the other) must support construction traffic, vehicle traffic, and earth loads. Therefore, culvert design involves both hydraulic and structural analyses. The ideal cross drain culvert placement is on a straight alignment with constant slope. Curved alignments or jointed culverts should only be used to accommodate unusual conditions as abrupt changes in direction or slope may negatively affect the hydraulic efficiency and lead to unforeseen maintenance issues. Today, culvert structures are most commonly made from cast-in-place concrete, precast concrete, metal, or plastic, but also have occasionally been made from masonry and wood. Culverts can be constructed with a wide range of geometries and dimensions/diameters that depend on the site conditions, cost factors, and water flow demand.

Culverts spanning more than 20 ft are classified by the National Bridge Inspection Standards (NBIS) as bridges and must receive routine inspections. This includes the total span of multi-barrel culverts such as those involved in this study. Structures are usually designed and constructed to accommodate loads from heavy vehicles. However, there are cases when, for various reasons, structures are unable to safely carry the heaviest possible loads and therefore must be posted with a maximum permissible load, which can result in traffic detouring that is a

significant added travel distance burden and cost. Furthermore, posted structures may be impassable by critical vehicles such as fire trucks, garbage trucks, and school buses.

Bridge load rating is used to provide bridge maintenance personnel with a rational method for determining the safe load capacity of a bridge. A “rating factor” (RF) is determined, which is essentially a live load factor of safety. The process can include theoretical calculation, numerical modeling, load testing, or a combination of methods. The result of the rating is either a load posting or no posting. While the ability to rate common steel and concrete bridges is reasonably well established, guidance for load rating corrugated metal structures is recognized as lacking.

The Maintenance Bureau of the Alabama Department of Transportation identified nine corrugated metal culverts recently annexed by the City of Anniston that have never been rated. The former military base, Fort McClellan, is being converted into a mixed use development by the City of Anniston and Calhoun County. The property will feature residential, business, and industrial space. To satisfy FHWA requirements, load rating of the culverts is required. Eight are “low profile arch” double barrel culverts that have pavement and one is a pipe arch with no pavement. These structures are nearly 80 years old and were constructed to serve the original needs of the Army installation.

ALDOT initially used a spreadsheet tool developed by the Ohio DOT (Wang 2016, Sargand et al. 2018) to rate these culverts, which indicated that posting was required. However, since the soil cover was less than the minimum required by AASHTO for new designs, the low rating output was controlled by the soil cover rather than strength or stability. Given that the culverts have been performing satisfactorily for many decades and that there are no signs of significant distress or deterioration, the general opinion was that the load capacity of these culverts is higher than that indicated by the Ohio DOT spreadsheet rating analyses and that a more detailed

analysis approach would result in sufficient ratings. Moreover, the Anniston situation is not unique, and therefore need exists to develop a methodology to load rate corrugated metal structures with low cover.

## **1.2 Objectives**

The objectives of the research are to load rate the nine corrugated metal culverts that are on the former Fort McClellan military base in Anniston Alabama and to develop methodology for load rating shallow cover circular arch and pipe arch corrugated metal culverts that is applicable to Alabama posting vehicles and rating processes.

## **1.3 Scope and Methodology**

The research program included literature survey, load testing, finite element modeling, and theoretical developments. The Anniston culverts provided a unique opportunity to conduct load tests on several similar culverts that provide a unique perspective into the issue. The following tasks were undertaken to complete the research objectives:

**Task 1 – Kickoff Meeting.** Soon after notice to proceed a meeting was held to inform all stakeholders of the project objectives, work plan and schedule. Members of the project advisory committee, ALDOT rating and load testing engineers, engineering representatives from the City of Anniston, the research team and others identified by ALDOT were invited. This meeting provided an opportunity to identify points of contact and to obtain input from all stakeholders.

**Task 2 – Literature Review.** A thorough literature review was performed of all relevant published information. Specific areas of interest included load-deflection behavior of in-place corrugated metal culverts, culvert rating methodologies, past load tests of corrugated metal culverts, validated finite element models of culvert and soil systems, and culvert rating software.

**Task 3 – Nondestructive Testing and Field Measurements.** The load resistance of the culverts is dependent on their condition, geometry, material properties and properties of the soils. Culvert sites were visited to determine the overall condition of the pipe and soil systems and to identify any significant imperfections in the geometry of the culverts. Measurements of the overall system geometries were made to confirm ALDOT records. Shear wave velocity testing was performed to estimate the density of the soil at each culvert. This information provided input for the finite element modeling and provide relative comparisons of the conditions at each site.

**Task 4 – Finite Element Modeling and Analyses.** Advanced finite element models of the arch culvert, footing and soil systems were developed using geometry and material properties specific to subject group of culverts in Anniston. The modeling and analysis were performed to capture the nonlinear behavior up to and including failure. Planning of appropriate instrumentation and field load testing procedures were based on the load-displacement behavior defined through finite element analysis. Final rating of the culverts was based on the results of the field load tests and finite element analyses.

**Task 5 – Field Load Test Planning.** Results from Task 1 through 4 were used to develop a detailed plan for field load tests. The geometry, pipe and soil characteristics, stream flow and/or standing water conditions, site access and traffic conditions were considered in planning the tests. Finite element predictions of the load-deflection behavior of the systems were used to develop an instrumentation plan that consisted of displacement transducers and bonded electrical resistance strain gages. The projected ratings and rating methodologies were used to establish test loading magnitudes and critical load positions. Traffic volumes and traffic control requirements were considered in establishing the time of day the tests were performed and how many repetitions of

each test loading were performed. The field load test plan was submitted to ALDOT for approval and scheduling.

**Task 6 – Field Load Tests.** The field load test plan developed in Task 5 was implemented as a cooperative effort between ALDOT and the research team. All instrumentation, data acquisition and reduction, pavement marking, and test layout and supervision was provided by the research team. Traffic control and load test vehicles with operators was provided by ALDOT.

**Task 7 – Validation of Finite Element Models.** Load, displacement and strain data collected in the field load tests was used to refine and validate the finite element models. These refined models were then used to predict the behavior of failure loads of the culverts for use in the culvert ratings.

**Task 8 – Rating of Anniston Circular Arch Culverts.** Rating factor analyses were performed for each of the Anniston culverts. Inventory and operating ratings were determined for each of ALDOT's standard vehicles. Standard rating methodologies were used along with a procedure developed in this project to account for the load test results and finite element analyses. The ratings considered the culvert's condition, the soil conditions, the potential for flooding and typical structural limit states such as the formation of a plastic hinge at the crown of the culvert and buckling of the culvert wall.

**Task 9 – Procedure for Rating Circular Arch and Pipe Arch Culverts.** Based on the knowledge gained from the first eight tasks, a procedure for rating circular arch culverts and pipe arch culverts was developed. Development of this procedure required advanced finite element modeling and analyses of pipe arch culverts to supplement the previously described analyses for circular arch culverts. The goal of these analyses was to identify the expected behavior of the pipe arch culverts. The validated finite element models were used to investigate a range of geometric and material parameters to achieve the objectives of the project. The recommended rating

procedure was incorporated into spreadsheets. Guidelines and commentary for proper use and interpretation of the results in the context of rating was also provided.

**Task 10 – Final Report.** At the conclusion of Task 1 through 9, this comprehensive final report of the project was prepared. The final report contains the rating results for the Anniston culverts in and documentation of the recommended procedure for rating of circular arch and pipe arch culverts. Implementation was in the form of final load rating values for the Anniston structures and a spreadsheet tool for load rating of circular and pipe arch culverts that can be used for other similar structures.

## CHAPTER 2: LITERATURE REVIEW

### 2.1 Metal Culverts

Broad explanations of buried metal pipe mechanics and design are provided in (Duncan and Drawsky 1983), (Whidden 2009) and (NCSPA 2008). Also, metal pipe conduits share many resistance mechanics traits with plastic pipe conduits, and there have been many important research works and developments on those topics over the past two decades. Only aspects of particular importance to the present project are highlighted herein.

As noted in the introduction, culverts are fabricated and constructed using a wide variety of materials and cross section shapes. Some approaches can only be used for limited spans, plus aesthetics can be a factor, but in general, the culvert type decision is driven by cost, which is a function of both materials and installation.

From a resistance mechanics standpoint, culverts pipes can be generally categorized as rigid or flexible. Rigid culverts are constructed (cast-in-place) or manufactured (precast) of concrete and resist load through the structural integrity of the pipe, without significant flexural displacements and without significant soil-structure interaction. Flexible pipes are metal (aluminum or steel) and plastic (high density polyethylene (HDPE), polyvinyl chloride (PVC), polypropylene (PP), or hybrid), and due to their relatively low flexural rigidity, depend upon soil arching to satisfy their load carrying demands. Soil is not merely a load on the pipe; it is part of the composite conduit structural system. This means that proper installation, especially backfill material and compaction during construction, is far more critical for flexible pipe culverts than rigid structure conduits. Illustrations of the difference between rigid and flexible buried conduits is provided in Figures 2.1 and 2.2. It should be recognized though that deep corrugation steel plate



culverts can approach rigidities that alleviate significant soil-structure interaction, but that is not the focus of the present investigation. Metal pipes and plate components that are commonly used for culverts are available in a variety of shapes and corrugation profiles, as illustrated in Figure 2.3. Details of modern steel pipe options and design are provided in the *Corrugated Steel Pipe Design Manual* (NCSPA 2008) and construction provided in *Installation Manual for Corrugated Steel Pipe, Pipe Arches, Structural Plate* (NCSPA 2013). The present work focuses on low profile arch and pipe arch culverts with shallow cover.

The origin of soil-structure interaction theory applied to metal culvert pipes is credited to Spangler (1941). Using a “soil box,” Spangler demonstrated that the horizontal soil support on the sides of flexible pipes as it deflects under soil load is sufficient for flexible pipes to be used as culverts. He derived the “Iowa Formula” for predicting the horizontal expansion of buried, flexible pipe based on a horizontal soil modulus. However, the Iowa Formula was subsequently recognized as flawed because it assumed elastic soil, and a “Modified Iowa Formula” was published by Watkins and Spangler (1958). The resulting horizontal soil modulus concept was simplistic and reflects that ring deflection is controlled primarily by the soil rather than the pipe. The formula is not the basis for design of pipe, but rather, is a prediction of long-term deflection of the circular pipe into an oval during the time of soil placement and subsequent settlement. Pipe ring stiffness is defined as resistance to deflection. The resistance to buried flexible steel pipe deflection primarily depends on the soil stiffness, however the ring stiffness is important during installation because it helps to keep the pipe shape while backfill is placed and compacted. Spangler’s assumptions for derivation of the Iowa Formula are illustrated in Figure 2.4. (Whidden 2009)

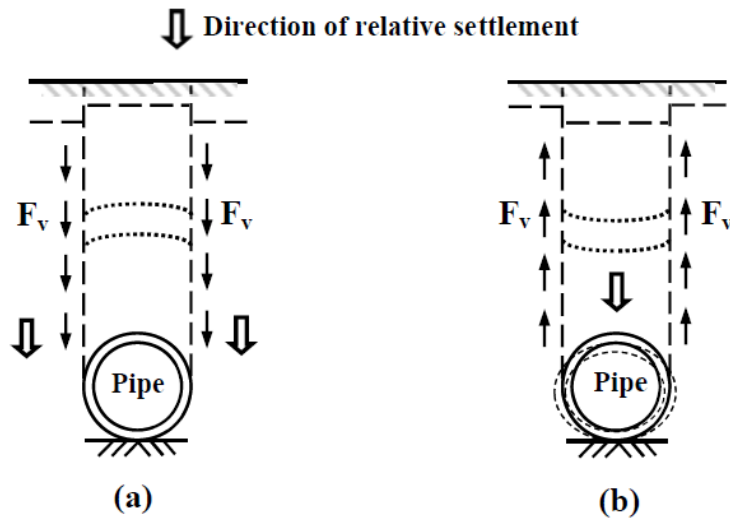


Figure 2.1. Mechanisms of soil arching (a) rigid pipe and positive arching; (b) flexible pipe and negative arching (Kang et al. 2009).

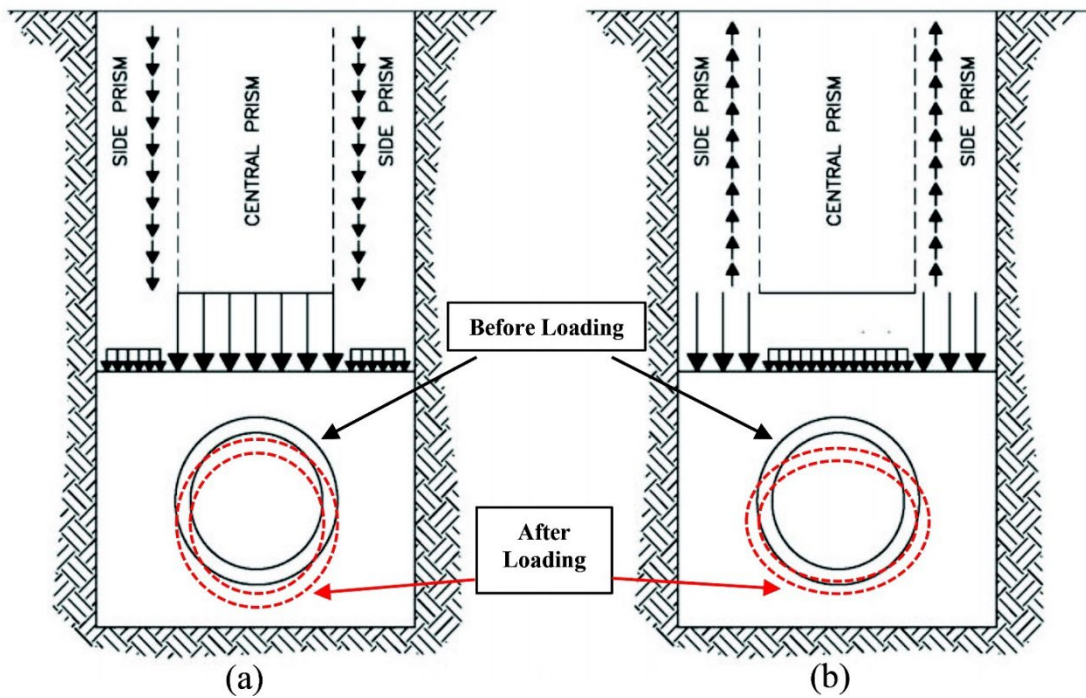
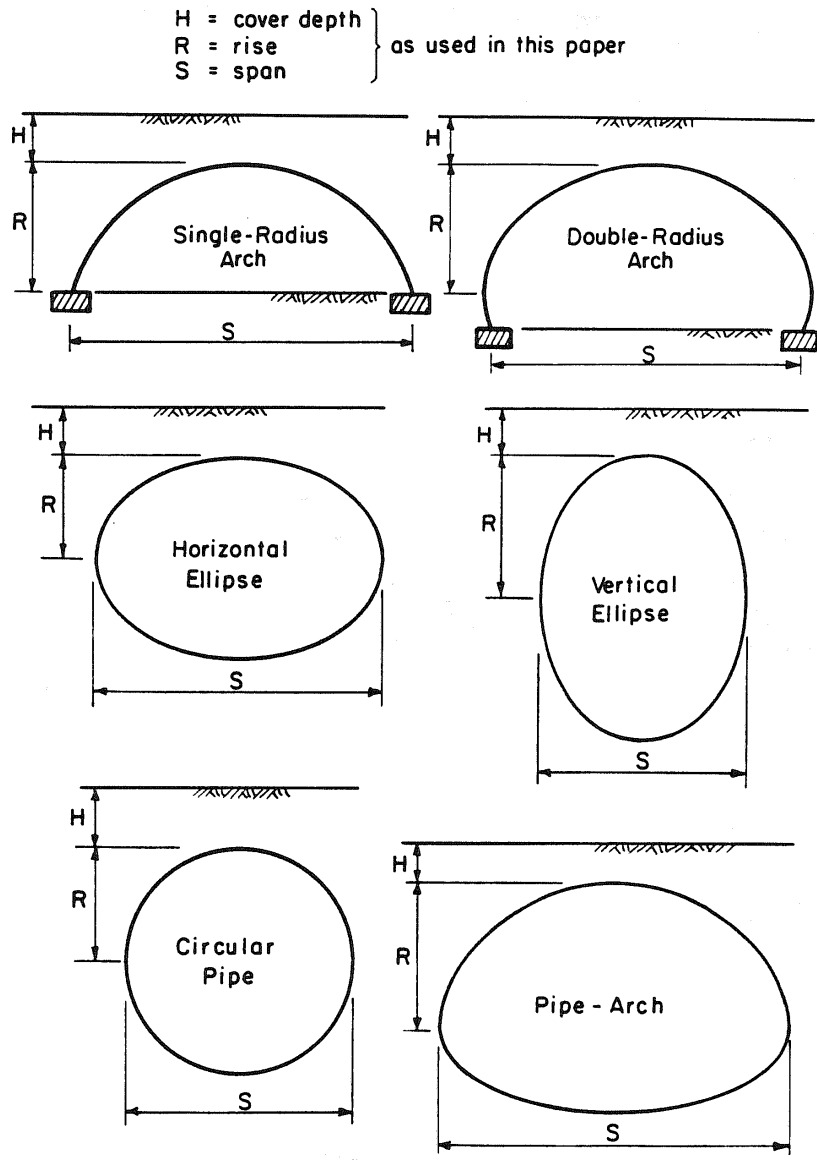
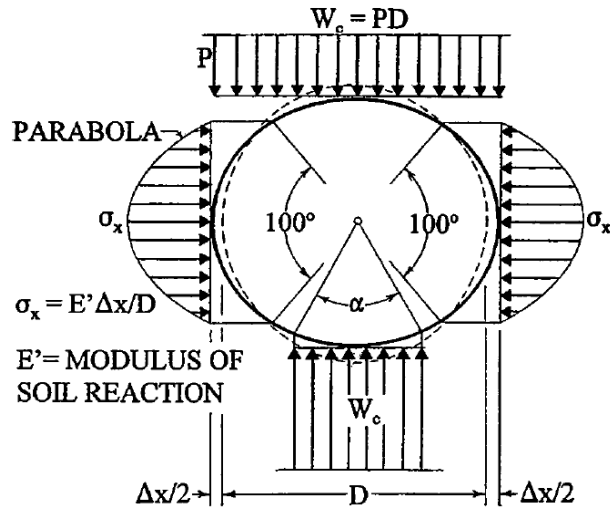


Figure 2.2. Comparison of positive projection conduits for (a) rigid and (b) flexible pipe (Tehrani et al. 2020).



**Figure 2.3. Common cross section shapes of metal culverts (Duncan and Drawsky 1983).**

Ring instability is a spontaneous deformation that progresses toward inversion (reversal of curvature) and represents a performance limit. Pipes can invert only if the ring deflects and the soil slips at the same time and must be analyzed as a soil–structure interaction problem. Structural performance of buried flexible steel pipe depends on the pipe-soil boundary interaction. Therefore,



**Figure 2.4. Spangler's Assumptions for Derivation of the Iowa Formula (Watkins and Spangler 1958; Whidden 2009).**

pipe–soil interaction is critical to maintaining the ring stability of the pipe under earth, construction and surface loads, and preventing collapse under soil pressure. (Whidden 2009)

Although other factors must be considered, the effects of gravity loads typically control design. For deep buried culverts, forces on the conduit are dominated by the soil weight, and traffic loading is relatively negligible since those forces attenuate and are resisted by soil outside of the projection of the pipe. For shallow cover pipes, the forces are dominated by traffic loading. The minimum cover required for a given culvert system depends on a range of obvious factors such as the rigidity of the pipe wall, span, soil type, compaction, pavement thickness, etc. However, current design codes recognize that the cover is important for providing protection against unforeseen events, and therefore an absolute minimum is defined. For example, Table 12.6.6.3-1—Minimum Cover, in Section 12: Buried Structures and Tunnel Liners of AASHTO LRFD Bridge Design Specifications (AASHTO 2020). The present project involves shallow buried culverts, so that will be the focus herein. Since some of the culverts involved in this study did not meet current minimum

cover standards, the origins of minimum cover requirement is a critical and therefore discussed in detail in Chapter 7.

## **2.2 Specifications and Guides**

Today the design standards for new culverts are defined by “Section 12: Buried Structures and Tunnel Liners” of the AASHTO Standard and LRFD Bridge Design Specifications. Procedures for evaluating and rating highway bridges are defined by the AASHTO *Manual for Bridge Evaluation* (MBE) (AASHTO 2018). The MBE does not specifically address rating of metal culverts, but some aspects of the MBE that are important for this project are included in the following discussion. Additional details of rating methodology are provided in Chapter 3.

Some state DOTs have developed specifications and guidance for evaluating and rating of metal culverts. State DOT documents reviewed during the present research included Connecticut, Michigan, Minnesota, Ohio, and Texas. The National Corrugated Steel Pipe Association (NCSPA) provides a recommended procedure for rating corrugated steel culvert, titled “NCSPA Design Data Sheet 19: Load Rating and Structural Evaluation of In-Service, Corrugated Steel Structures.” This data sheet was the basis for developments by Ohio (Sezen et al. 2009; Wang 2016; Sargand et al. 2015, 2018) and subsequently addressed by Michigan (MDOT 2016), which are very pertinent to this project and therefore are discussed in detail in Chapter 7.

## **2.3 NCHRP Projects**

The National Cooperative Highway Research Program (NCHRP) has sponsored important research on culvert performance and design over recent years. The following briefly highlights the projects that are critical to the present research. Specific important information from NCHRP reports are integrated and cited throughout the various relevant portions of this report.

### **2.3.1 McGrath et al. (2002)**

NCHRP Project 12-45 / NCHRP Report 473 “Recommended Specifications for Large-Span Culverts” included a thorough review and evaluation of the state-of-the-art in design and construction of large-span reinforced concrete and metal culverts, investigated culvert behavior through full-scale field tests and extensive computer modeling, and developed recommended specifications for design and construction. The key focus of the project was to develop new design models for large-span culverts: (1) a simplified procedure that would accurately model most culvert installations and be suitable for incorporation into AASHTO specifications, and (2) a comprehensive procedure that could be used for unusual installation or design conditions. The full-scale field tests evaluated the performance of a 9.5 m (31.2 ft) span metal arch culvert and a 9.1 m (30 ft) span precast, reinforced concrete arch culvert. At the minimum depth of fill (0.3 m), the metal culvert, which would be limited to a minimum depth of fill of 0.9 m (3 ft) under current practice, deflected vertically approximately 50 mm (2 inch), but no yielding was noted. Computer models were calibrated using the field-test data. Two-dimensional analysis, with nonlinear elastic-plastic soil modeling, was used to analyze the effects of earth loads, and three-dimensional linear elastic analysis was used to analyze for live-load effects. The computer models were then extended to analyze five shapes and sizes of metal culvert and two shapes of concrete culvert to develop a body of data that could be used to generate simplified design equations. For metal culverts, the approach used was to develop equations for moments and thrusts due to earth and live loads; for concrete culverts, the approach was to develop simplified pressure distributions that could be used as input into computer-based frame analysis. Detailed design examples are provided to demonstrate application of the procedures for both metal and concrete culverts.

### **2.3.2 Mlynarski et al. (2008)**

**NCHRP Project 15-28 / NCHRP Report 619 “Modernize and Upgrade CANDE for Analysis and LRFD Design of Buried Structures.”** CANDE (Culvert ANalysis and Design) is a finite element program developed especially for the structural design, analysis and evaluation of buried structures including culverts made of corrugated metal, reinforced concrete, and plastic as well as other soil-structure interaction problems such as underground storage facilities and storm water chambers. The first version of CANDE was developed in the 1970s (Katona et al. 1976) and has been revised several times since. The project resulted in an enhanced version of the CANDE software with many new analysis capabilities, a graphical user interface (GUI), explanatory tutorials demonstrating the various program applications, and a comprehensive context-sensitive help system. Additional background and implementation of CANDE is provided in Chapter 6.

### **2.3.3 Petersen et al. (2010)**

**NCHRP PROJECT 15-29 / NCHRP REPORT 647 “Recommended Design Specifications for Live Load Distribution to Buried Structures.”** NCHRP Project 15-29 investigated how surface live loads distribute through the soil and load various culvert structures. The differences between the AASHTO Standard and LRFD Specifications live load distribution approaches are emphasized in the report. Three-dimensional (3D) numerical modeling was used to investigate how live loads spread with depth as a function of soil and culvert type. Six culvert types, including corrugated metal pipe and corrugated metal arch were involved. This modeling provided a basis for developing simplified design equations for structural response. Given that the present project focused on shallow cover flexible culverts, accurate live load distribution is essential, and the work of NCHRP Project 15-29 was carefully scrutinized and incorporated to the current effort.

### **2.3.4 Mlynarski et al. (2019)**

**NCHRP Project 15-54 / NCHRP Web-Only Document 268: “Proposed Modifications to AASHTO Culvert Load Rating Specifications.”** NCHRP Project 15-54 developed recommendations for changes to the AASHTO *Manual for Bridge Evaluation* (MBE) through the load testing of seven culverts and the review and data analysis of culvert models of varying types. Part of the impetus was that it is known that MBE rating methods were developed for larger bridge structures and tend to result in overly conservative ratings when applied to buried culverts. The objectives were accomplished through: (1) surveying the DOTs for current culvert practices and issues related to culvert rating; (2) developing and executing full scale field tests on seven culverts; (3) conducting full analyses of culverts in both 3D and 2D analysis; and (4) identifying areas of the MBE and LRFD specifications for improvement and recommendations for updates to those specifications based on the field testing and analysis results.

### **2.4 Field Test Projects**

Guidance for bridge load rating is provided in the MBE, but guidance is limited for the treatment of culverts. This is a significant issue for state departments of transportation as culverts constitute about 130,000 of the structures listed in the National Bridge Inventory. Furthermore, there are millions of other culverts with spans less than 20 ft that are not accounted for in the NBI, but nonetheless need methodology for verifying that they are safe. To help fill this gap and to validate existing or new methodologies for culvert rating, field tests have been conducted. This section summarizes some of the most prominent field tests presented in the literature that are relevant to this project. Chapter 5 presents additional background and load testing of the Anniston low profile culverts. Chapter 8 presents and demonstrates the use of the Anniston load test data towards refining analytically derived rating factors.



### **2.4.1 Webb et al. (1999)**

A 1999 publication by Webb et al. titled “Field Tests of a Large-Span Metal Culvert” describes full-scale field tests that were conducted on a low profile arch culvert to provide input for development of improved large-span culvert load and resistance factor design specifications. While the tests were conducted in order to evaluate the effects of construction methods for placing side fill and to study the effects of live loads to advance culvert design and construction, the study is still relevant today because culvert behavior, soil behavior, and culvert-soil interaction of shallow-cover culverts were examined closely and were well-documented.

Two load tests were conducted with SW backfill material, each compacted to 87 and 92 percent of maximum standard Proctor density. Live-load tests were conducted with a truck with tandem axles loaded to 35,000-lb per axle at depths of fill of 1, 2, and 3-ft. Measurements were made of culvert deformation, culvert strain, culvert-soil interface pressure, soil density, soil strain, foundation movement, and temperature. Thrusts and moments were determined from the culvert strain.

In this experiment, a 42-ft long reinforced concrete arch and 40-ft long structural plate metal arch culvert were installed end-to-end in a pre-excavated trench as presented in Figure 2.5. The culverts were buried with tops about 2-ft above the existing ground surface (Figure 2.5a). Each culvert was founded on separate reinforced concrete strip footings. A level surface width of about 50-ft over both culverts was obtained (Figure 2.5b) with this arrangement.

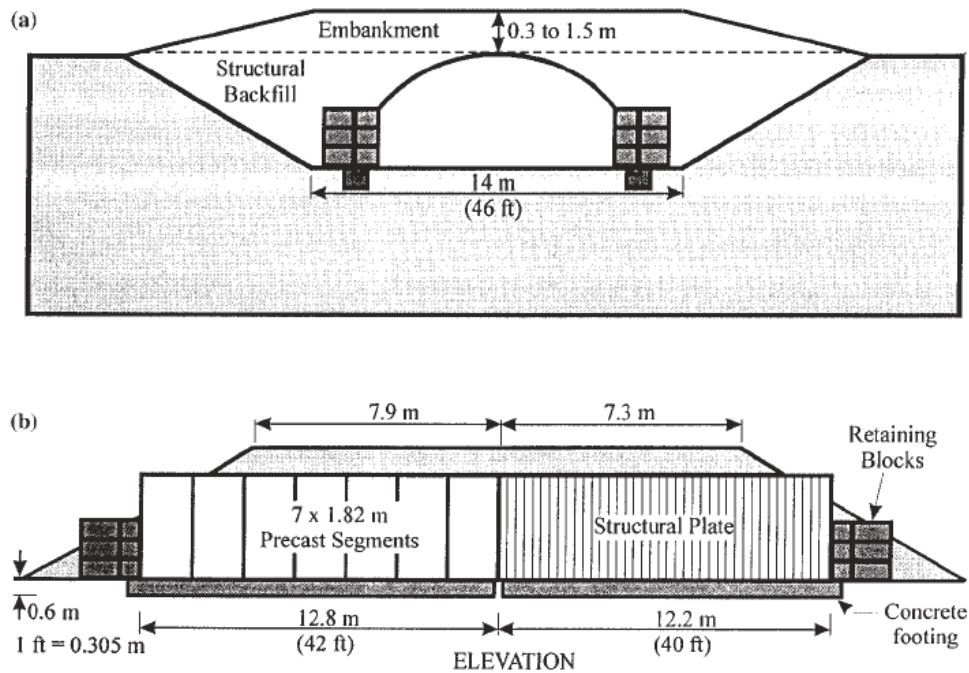


**Figure 2.5. (a) Cross-sectional view of culvert installation; (b) End-to-end installation of concrete and metal culverts (Webb et al. 1999).**

The trench was backfilled and a shallow earth embankment was constructed over both culverts. Existing site material taken from the excavated trench was used for backfilling the culverts and for building the embankment. Live-load testing with a loaded truck was carried out at various stages of shallow cover.

The metal culvert was top loaded in both tests to prevent excessive peaking (upward movement of crown) during backfilling operations. After both tests were completed, embankment material was added over the top of the culverts to bring the height of cover to about 4.5 ft. This cover height remained in place while long-term measurements of culvert performance under constant dead load were collected.

Instrumentation was used to measure deflection and strain during the study. The deformation measurement locations are presented in Figure 2.6. A total of 25 locations around the circumference of the metal culvert were selected for the detailed laser measurements at each of the three monitoring stations. Extensometers were used to measure relative horizontal movement between points of radius change at two stations along the length of each culvert as indicated in Figure 2.6. At each of the 25 locations on the inside wall of the metal culvert, four weldable electrical resistance strain gauges were installed (circumferential and longitudinal directions on inside crest and valley locations) to compute wall thrust and bending moment. From the experiment, measurements of displacement and strain were collected before backfilling, during backfilling, under live loads, and under long term dead-loads.

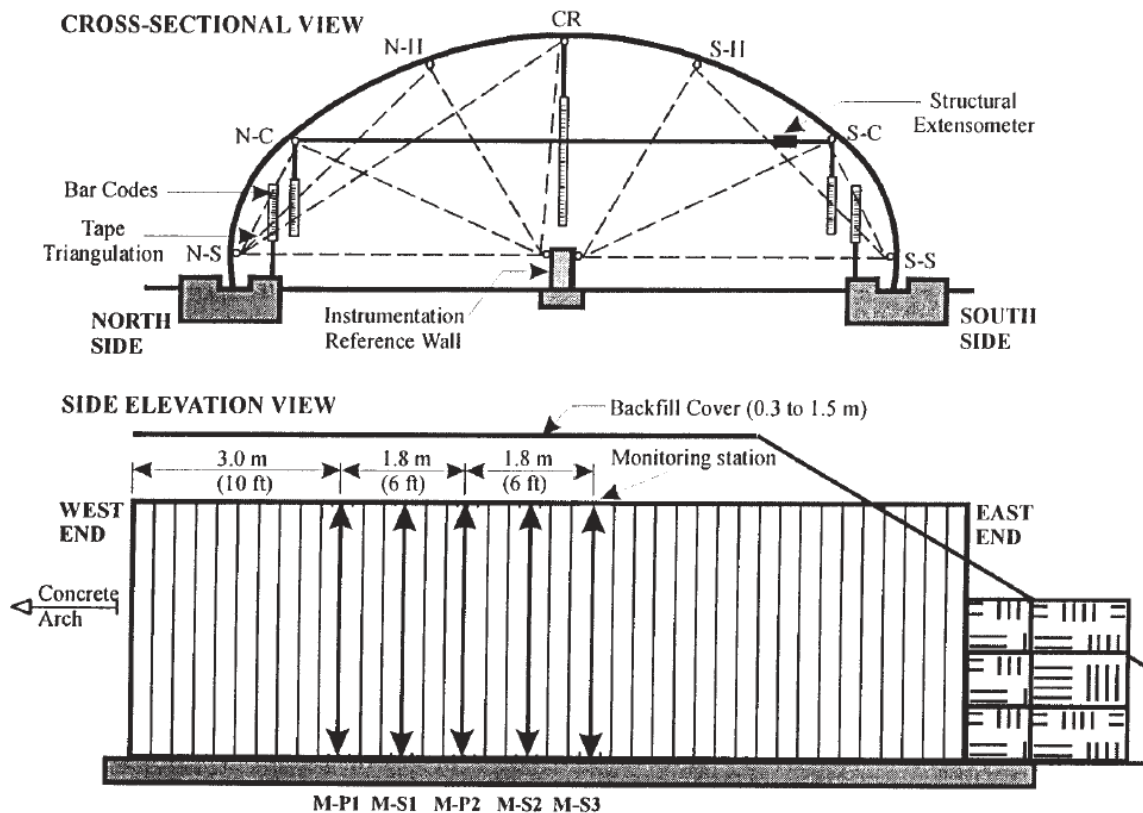
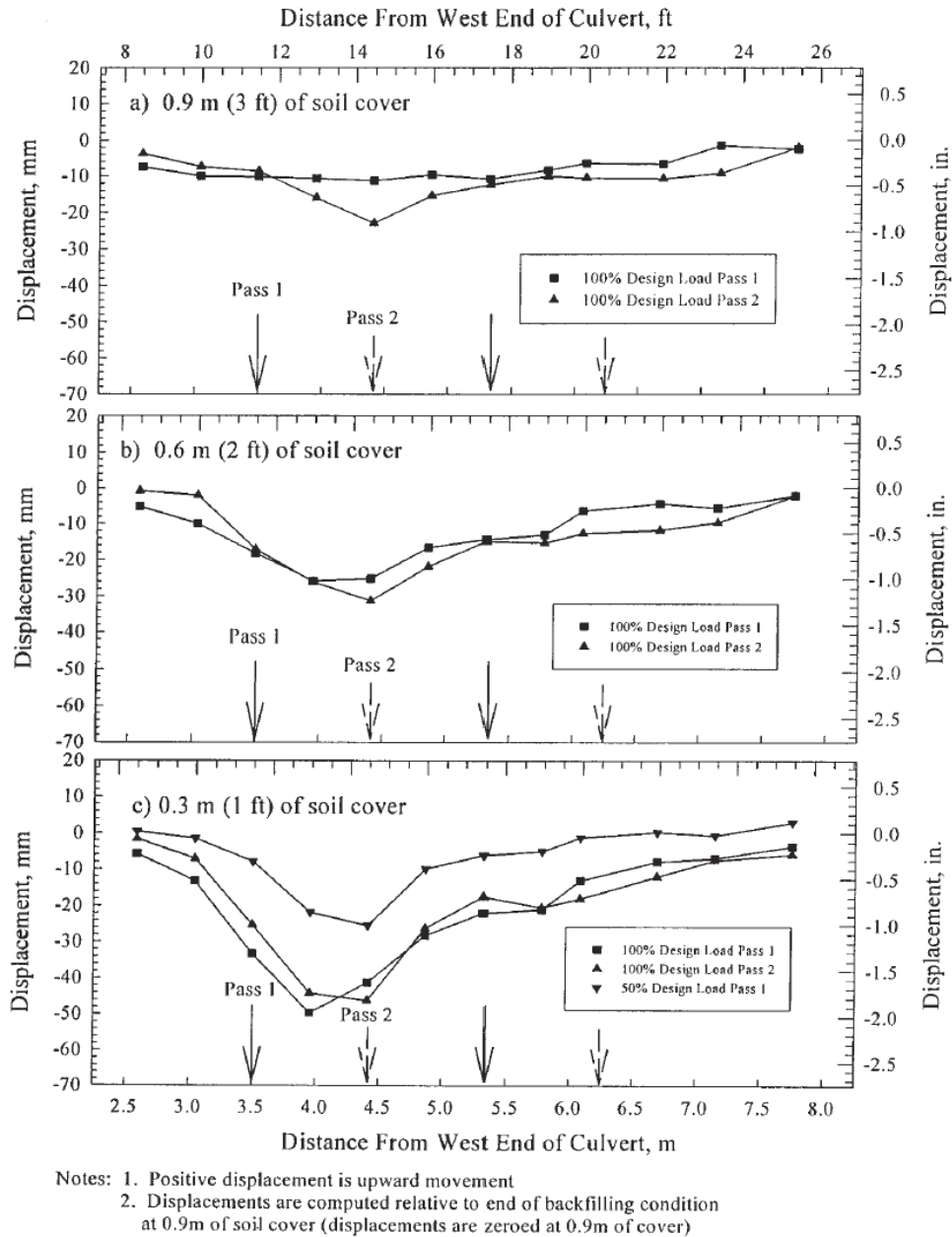


Figure 2.6. Monitoring deformation in a corrugated metal culvert (Webb et al. 1999).

Figure 2.7 shows displacement data from the live load tests. The researchers found that during the live load testing, the displacements did not increase as much as expected between the two passes.



**Figure 2.7. Longitudinal deflection profile of crown locations from live-load test (Webb et al. 1999).**

The distribution of the change in bending moment due to the tandem axles of the live-load vehicle positioned over the culvert crown during Pass 1 is plotted in Figure 2.8. The distribution of the change in bending moment due to the tandem axles of the live-load vehicle positioned over the south shoulder during Pass 1 is plotted in Figure 2.9. Three depths of soil cover and five measurement stations are included. “These figures indicate that the live-load bending moments at the shoulders measured at the stations under the wheel paths of the live-load vehicle (Stations P1 and P2) are inversely related to the depth of soil cover—that is, decreasing cover results in a substantial increase in moment.” This was as expected, as less cover causes more strain in the corrugated metal. Additionally, it was found that no significant moments developed at the spring line and curvature changes from the live-load vehicle.

Positive moment at the crown measured at the longitudinal station between the wheel paths of the live-load vehicle (Station S1) also is inversely related to the depth of soil cover. This crown moment measured between the wheel paths at Station S1 is larger than those measured underneath the wheel paths (Stations P1 and P2), which implies that the maximum bending moment and thus maximum deflection of the structure at the crown occurred between the wheel paths. It was found that the maximum live-load moments did not develop directly underneath the tandem axles but at locations outside the tandem axles (south curvature and crown locations). This was also true for the case in which the tandem axles were positioned over the crown of the culvert.

Measurement collection continued during long-term monitoring. Metal culvert bending moments under constant earth load were monitored for 9 months after construction. It was found that the spring line moments increased by about 28 to 46 percent (1.9 to 2.1 kN m/m) until about 6 months after the final soil cover was added. The moment at the crown decreased by about 10 percent in the 3-month period after the final soil cover was added and remained essentially

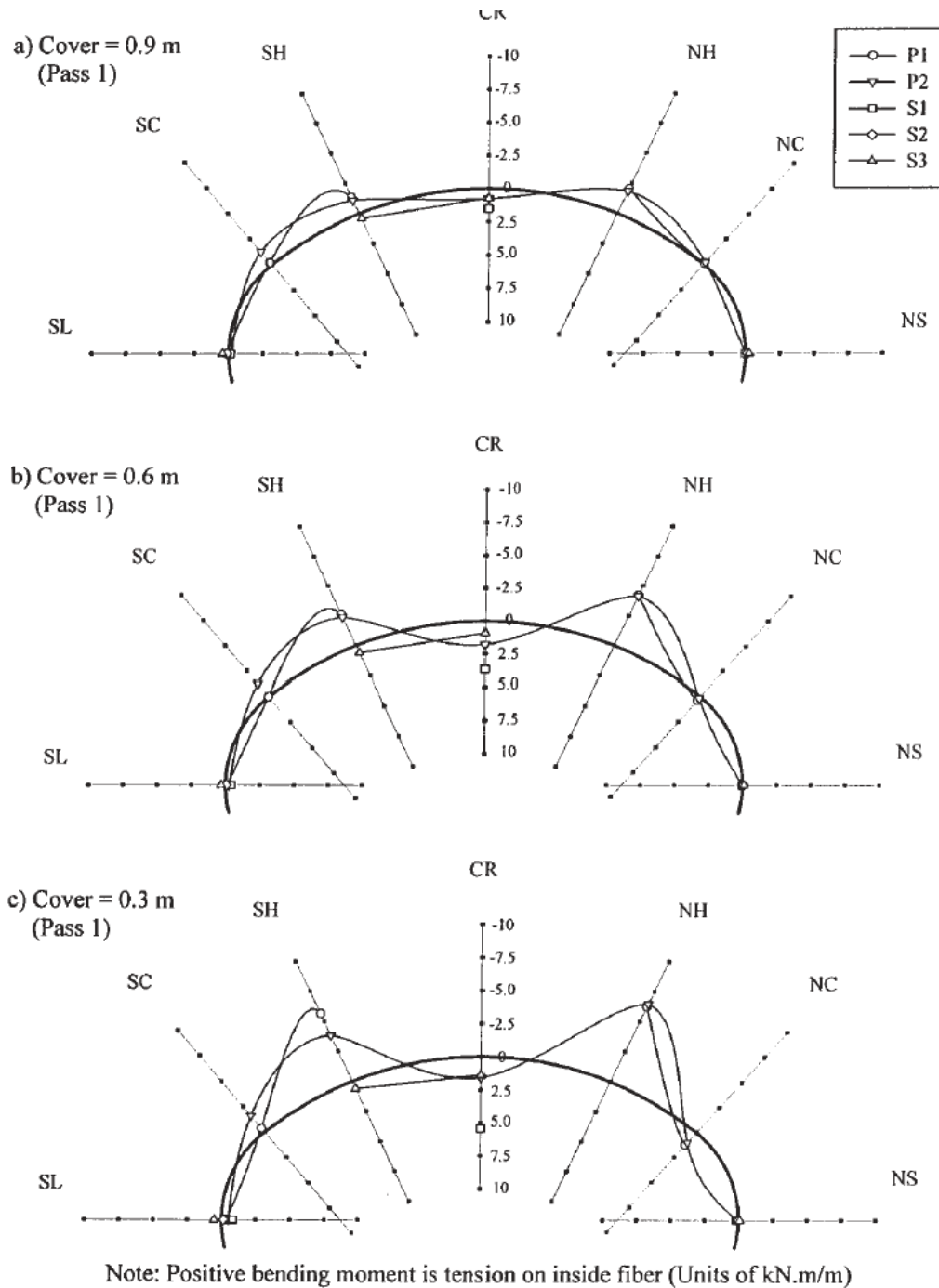


**Figure 2.8. Bending moments from live-load axles over culvert crown (Webb et al. 1999).**

unchanged during the winter months. Small increases in moments also occurred at the curvature and shoulder locations.

The goals of the full-scale tests were to evaluate the effects of construction methods for placing side fill and to study the effects of live loads in order to gather sufficient data to advance the state of the art in the design and construction of large-span culverts. The difference in performance between backfilling a flexible metal culvert with well-compacted material and

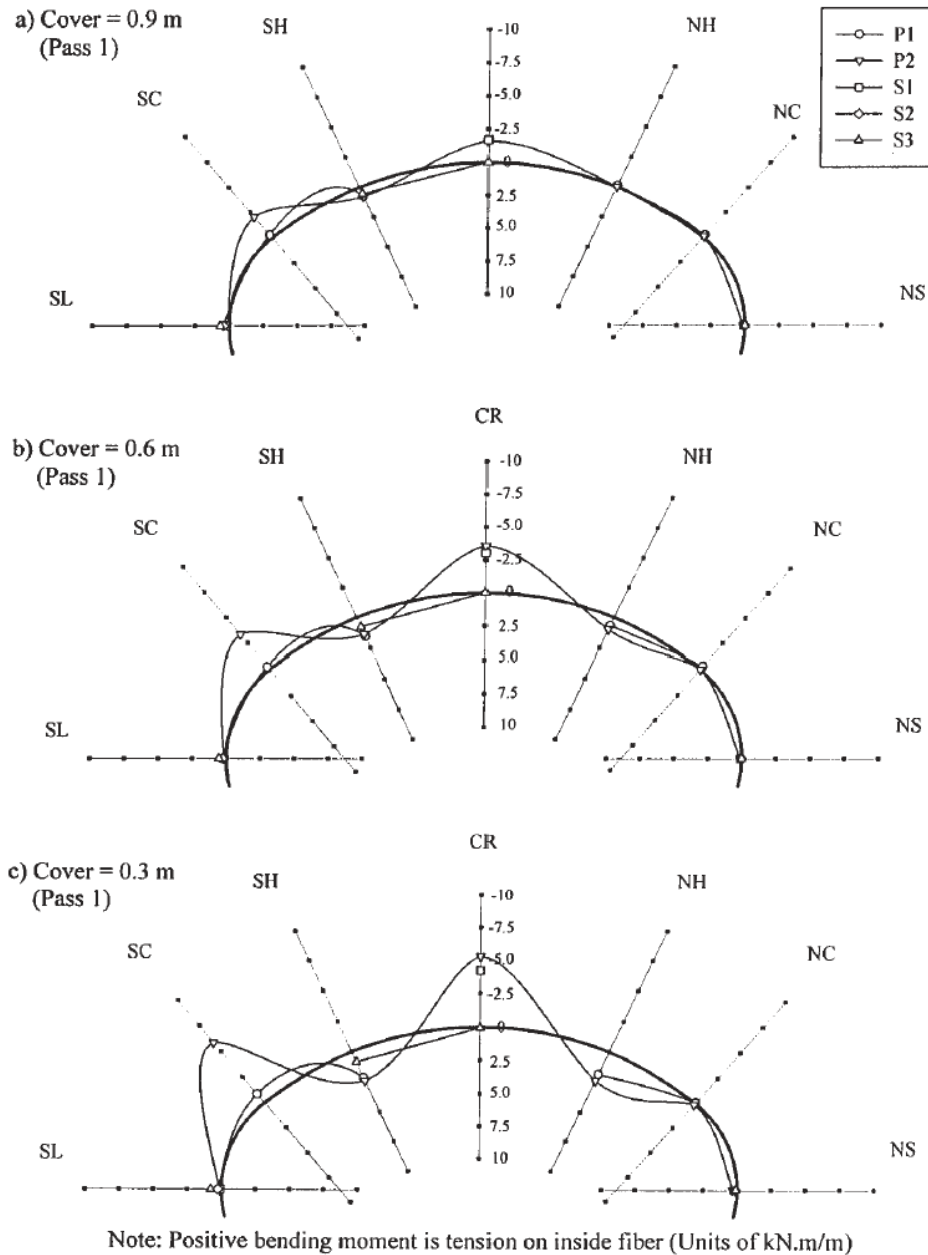


Figure 2.9. Bending moments from live-load axles over south shoulder (Webb et al. 1999).

material loosely placed without compaction effort was shown. Deformation of the metal culvert during backfilling resulted mostly from placement and spreading procedures instead of from backfill compaction. The maximum live-load moments did not develop directly underneath the tandem axles but at locations outside the tandem axles. It was concluded that the effects of live loads were distinctly different from what was assumed in their current design practice, and that the current live-load design could not be assumed to be conservative because it gives a more uniform pressure distribution than what really occurs. The actual pressure distributions create large moments that can be a controlling factor in the design for shallow cover culverts. Even so, the structure performed well and supported very heavy live loads under shallow cover conditions.

#### **2.4.2 Sezen et al. (2009)**

An initial review of the literature early in the project yielded several documents directly and indirectly related to the Ohio DOT Method. In particular, there were two studies out of Ohio that were conducted to verify the method. The first was by Sezen et al. (2009) from the Ohio State University, which was followed by Sargand et al. (2015) at Ohio University. The results of both studies were summarized in a paper by Sargand et al. published in 2018.

In the Sezen et al. (2009) report titled “Load Performance of In-Situ Corrugated Steel Highway Culverts,” 39 metal culverts including circular pipes, pipe arches, and arches were load tested. The culverts had span lengths varying from 10.6 ft to 23.1 ft and backfill soil heights over the crown varying from 0.9 ft to 24.5 ft. Static and dynamic load tests were conducted by driving heavy trucks across the culverts. Static loads were applied at ten different locations above each culvert while dynamic load tests were conducted at six truck speeds varying from 5 mph to 40 mph.



Instrumentation was required to measure the strain and deflections of the culverts. The spatial variation of deformation for each culvert cross section was monitored by measuring displacements at several predetermined locations on the culvert wall during truck loading. Six displacement sensors were installed at a single transverse cross section of the culvert directly under the center of the test truck. Each sensor was able to measure a maximum of 50 mm or 100 mm of displacement perpendicular to the wall. Figure 2.10a shows a photograph of the portable aluminum instrumentation frame installed inside a test culvert and a diagram showing the five sensor locations at the culvert wall. The instrumentation frame consisted of five adjustable arms with a displacement sensor mounted on each. The displacement sensor attached to the middle arm was used to measure vertical displacements at the crown. The body of the frame was 5 ft long and 3 ft tall. The arms were constructed using interconnecting rectangular hollow aluminum sections. The frame was designed so that the smaller sections could slide inside the larger sections and extend from 4 ft to 15 ft to adjust to the height and span of each culvert. Using clamps and bolts, each arm was attached to the body at the desired angle within a range of  $10^\circ$  from the standard position shown in Figure 2.10b. A sixth displacement sensor was installed between the ends of two plates connected at the crown of the culvert to measure possible slippage between corrugated plates at the connection bolts during a load test. However, no joint slippage was recorded at the crown for any of the culverts tested.

Fourteen channels were used to monitor changes in strain on the culvert walls in the transverse (nine gauges) and longitudinal (five gauges) directions. Electrical resistance unidirectional strain gauges were attached to the inside walls of each culvert. Twelve gauges were placed on the same culvert transverse section with the displacement sensors. The other two gauges were installed 1-ft and 2-ft away from the center section to monitor strain variations in the

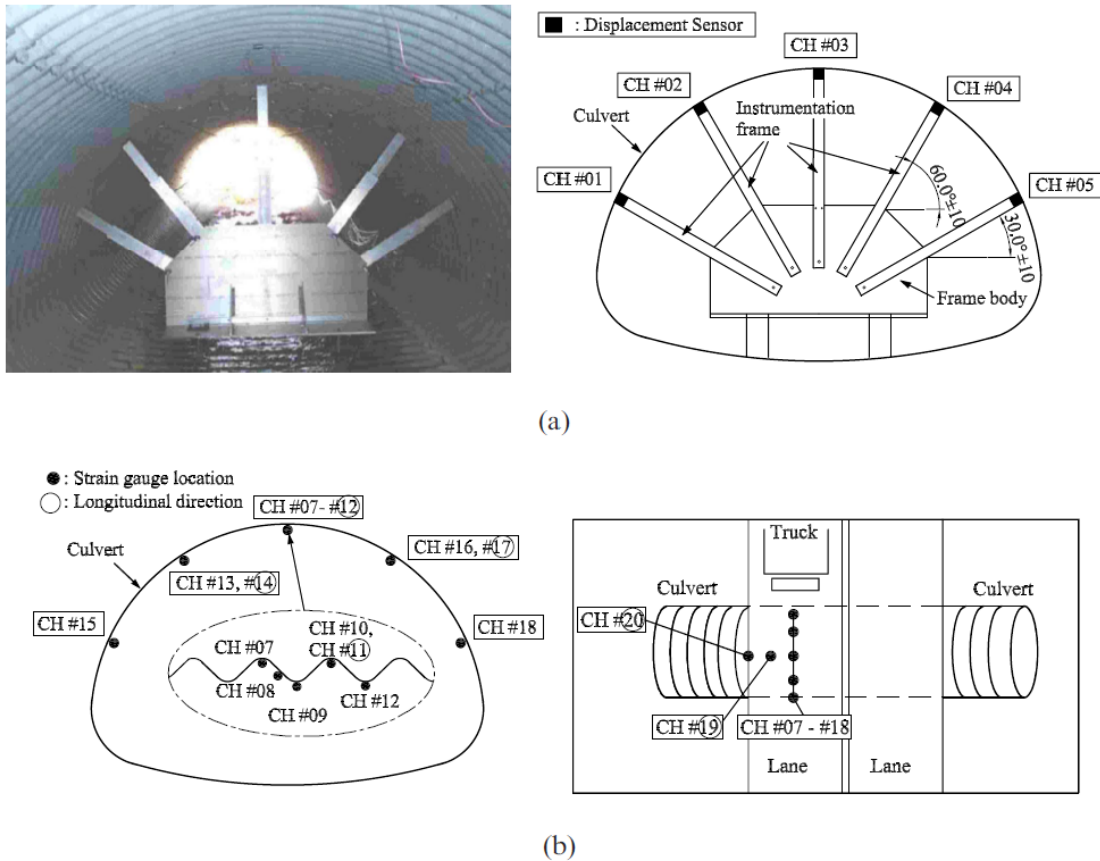
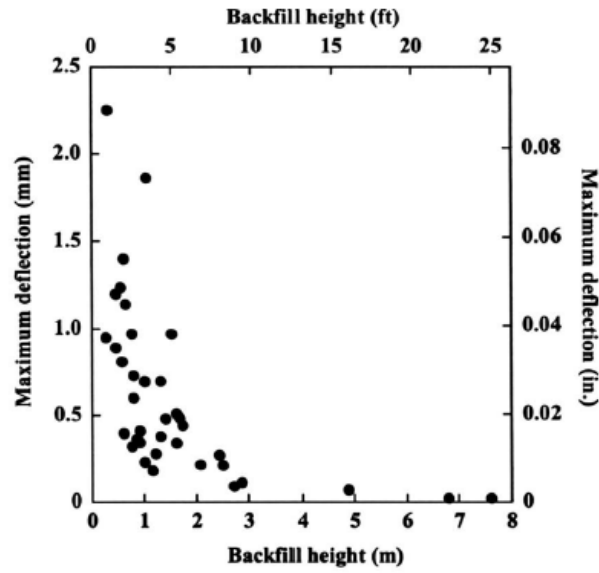


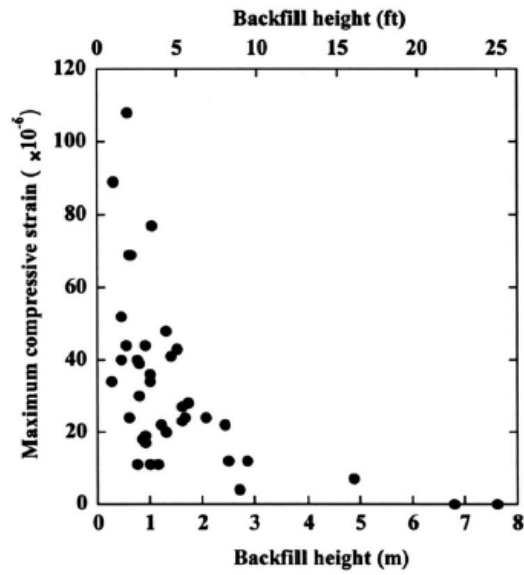
**Figure 2.10. Displacement sensors and strain gage locations (Sezen et al. 2009).**

longitudinal direction. Each strain gauge was positioned with axes oriented parallel and perpendicular to the direction of plate corrugation to measure strains in the circumferential and longitudinal directions, respectively. In order to obtain more reliable strain measurements, six strain gauges were mounted near the crown of the culvert.

A plot of maximum culvert deflection versus backfill height shows a nonlinear relationship (Figure 2.11). Additionally, maximum static load deflections were found to be consistently larger than the maximum dynamic deflections obtained using the same test truck. Deflections were nearly zero for deep culverts with backfill heights exceeding 13 ft. It was also found that maximum deflections correlated more closely to equivalent line loads than to total truck weight.



(a)



(b)

Figure 2.11. Maximum deflections and strains versus backfill height (Sezen et al. 2009).

The data indicated that culvert behavior is more difficult to predict when backfill heights are shallow because other factors, such as culvert age and condition and soil type, likely play a significant role. The objective was to develop a new load rating method and make recommendations for improving current load rating methods for corrugated metal culverts. The conclusions of that study were that the current rating method, at the time of the research, was highly subjective, unconservative, and generally ineffective in identifying possible unsafe culverts. The researchers recommended new procedures to rate the culverts but pointed out the impact of cover depth.

#### **2.4.3 Sargand et al. (2018)**

The Sargand et al. (2018) study titled “Evaluation of Load-Rating Procedure for Metal Culverts under Shallow Soil Covers” performed in Ohio aimed to evaluate the method being employed by the Ohio Department of Transportation (ODOT) for load rating corrugated metal culverts installed under extremely shallow soil covers. The authors used three-dimensional finite element modeling and load testing of corrugated metal culverts of various types to evaluate the ODOT method. The failure of large-span culverts serving major roadways under shallow soil covers can negatively impact the integrity of the overlying pavement structures and motorists more severely than smaller span culverts under shallow cover or long-span culverts under deeper depths. In the study, six metal culvert structures built between 1946 and 1996 were carefully selected, instrumented with sensors, and subjected to a series of static and dynamic live load tests.

Each culvert was instrumented with strain gauges under a wheel path located close to either its inlet or outlet end where the soil cover was the least. For strain measurements, electric resistance strain gauges were welded to the surfaces of the steel plates. The strain gauges were installed at multiple locations around the circumference at both crest and valley positions so that axial thrust

force and bending moments could be computed from each set of strain gauge readings. Gauges were placed in pairs and oriented in longitudinal and transverse orientations that were parallel or perpendicular to the corrugation. The sensors were placed under the wheel path where the greatest stresses and strains were anticipated to be under the test vehicle. For deflection measurements, linear potentiometers (Figure 2.12) were used to record the deflections experienced by the culvert structure. In each instrumentation section, sensors were installed at key positions such as the crown, shoulder, and spring line. These linear wire potentiometers were set up using a reference platform erected inside the culvert.



**Figure 2.12. Close-up view of instrumentation point (Sargand et al. 2018).**

During each load test, linear potentiometer and strain gauge readings were collected by a data acquisition unit. Linear potentiometer readings were analyzed to determine the deflections and cross-sectional shape. Strain gauge readings were processed to compute stresses, strains, thrust force, and bending moment. The ODOT load-rating procedure was applied to convert the live load

to wall thrust. The thrust forces from the field tests and the calculations were compared. The field test data was analyzed to gain insight into how shallow-installation metal structures respond to live loading. It was observed that the ODOT procedure was very conservative, as the calculated thrust values were much higher than the field values for five of the six test structures. They suggest that there is a need for further load testing to verify the ODOT method. It is worth noting that throughout this study, while it is emphasized that the soil has an impact on the performance of a corrugated metal culvert, little or no field tests were conducted to determine the in-situ stiffness and density of the soil. This appears to be a significant limitation of the research.

#### **2.4.4 Mlynarski et al. (2019)**

In 2019, the National Cooperative Highway Research Program (NCHRP), published “Proposed Modifications to AASHTO Culvert Load Rating Specifications” (Mlynarski et al. 2019). The objective of the research was to propose modifications to the culvert load rating specifications in the MBE and revise the *AASHTO LRFD Bridge Design Specifications* accordingly based on findings. Administered by the Transportation Research Board (TRB) of the National Academies of Sciences, Engineering, and Medicine, the objective was accomplished by:

- Surveying the DOTs for current culvert practices and issues related to culvert rating.
- Contacting states via telephone to inquire about current practices.
- Developing and executing full scale field tests on seven culverts.
- Developing and executing a full analysis of the subject culverts in both 3D and 2D analysis.
- Identifying areas of the MBE and LRFD Specifications for improvement and recommendations for updates to those specifications based on the field testing and analysis results.

Based on the literature survey and subsequent interaction with the project panel, a sample testing plan and target field testing matrix was developed. Upon approval by the project panel, the effort to locate target culverts was conducted by contacting the state DOTs. This process yielded a field testing plan that was developed in tandem with an analytical plan that would be used to evaluate the current processes and specifications used for culvert rating and evaluation. In all, seven culverts were field tested and analyzed in 3D using a general FEM software package and in 2D using the CANDE software updated under NCHRP Project 15-28.

As part of this report, several field testing plans were included as appendices. Models 5, 6, and 7 are the most similar to the present project and were referenced when creating the test plan. In each test plan, strain gauges and string pot gauges (potentiometers) were attached to the underside of each culvert in primary and secondary locations (Figure 2.13) to measure strain and deflection. Then, the individual wheel loads of the load truck were measured. Air and pavement temperatures were collected. Instruments were read from pre-test. Finally, the truck would pause in each load position while instruments recorded strain and deflection as detailed in the test plan.

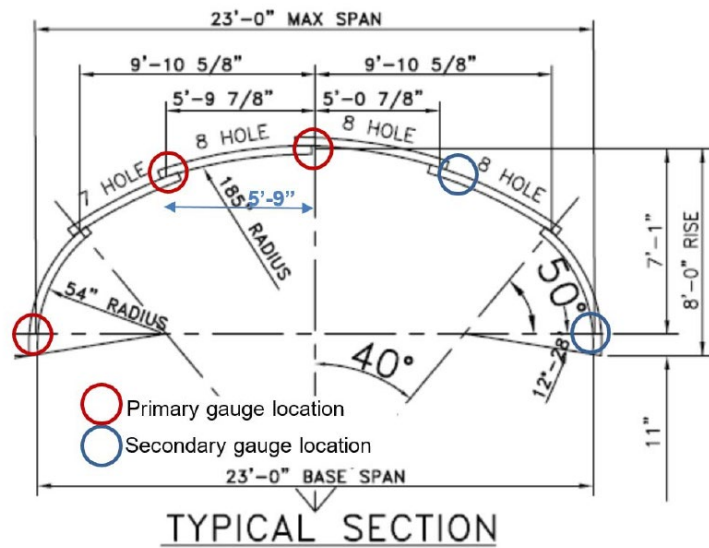


Figure 2.13. Model 5 instrumentation locations (Mlynarski et al. 2019).

## **2.5 Literature Survey Conclusions**

This chapter highlights the literature sources that are most closely related to the objectives of this project. However, more than one hundred references were collected and reviewed. Over recent years, a great amount of resources have been directed towards addressing challenges associated with design and analysis of metal culverts, including methodologies for rating low cover scenarios. The literature survey also demonstrates that other researchers have also resorted to load testing in order to accurately assess existing culvert capacities and assess currently-used analytical methods, and that many challenges still exist.



## CHAPTER 3: LOAD RATING OF CORRUGATED METAL CULVERTS

### 3.1 Definition and General Philosophy

Bridge load rating provides a basis for determining the safe load capacity of a bridge. Its primary focus is safety assessment for live loads and fatigue. The rating factor (RF) that results from the load rating process essentially represents live load factor of safety. In simplest terms, RF can be represented as:

$$RF = \frac{CAPACITY - DEAD\_LOAD\_EFFECT}{(LIVE\_LOAD + IMPACT)} \quad (3.1)$$

An RF value greater than 1 indicates a structure that is safe to carry the specified live load; an RF value less than 1 indicates a structure that must be posted. The load rating equation appears simple; however, the rating factor must be determined for each critical section, for each demand category (moment, shear, thrust, etc.), for maximum and minimum load envelopes, for both inventory and operating rating levels, and potentially for each posting vehicle. The complexity of the rating methodology for a given structure therefore depends upon the complexity of the structure and its behavior under loading (i.e., linear or nonlinear response). The lowest rating factor defines the load rating for the structure. To generate the load rating for a bridge, the rating factor is multiplied by the weight of the rating vehicle.

The *National Bridge Inspection Standards* (NBIS), as found in 23 CFR 650 Subpart C of the Code of Federal Regulations, define the regulations for the inspection and evaluation of the nation's bridges. Routine inspections required by the Code of Federal Regulations are intended to reveal any change in structural condition, thereby warranting reevaluation of the bridge if conditions significantly change. The NBIS apply to all highway bridges that are more than 20 ft in

length and located on public roads. Pertinent to the present investigation, however, it should be noted that “span” of a bridge comprised of multi-barrel culverts such as the Anniston culverts is defined as the outer-to-outer distance parallel to the roadway from the leading culvert edge to the far culvert edge. In other words, “span” is not necessarily the transverse span of a single culvert used in resistance calculations. The procedures and criteria for load rating and posting of existing bridges are defined by the *Manual for Bridge Evaluation* (MBE) (AASHTO 2018), which provides a standardized evaluation procedure and a basis to determine the safe load capacity. Definitions are provided for Allowable Stress, Load Factor, and Load and Resistance Factor ratings (ASR, LFR, LRFR, respectively). However, the MBE does not dictate which rating approach (ASR, LFR, or LRFR) must be used; rather, the rating method is typically decided based upon the original adopted design philosophy. For example, a bridge designed by the Load Factor Design (LFD) philosophy would typically be rated using the LFR method. However, the same bridge can be rated by the LRFR and ASR methods. The general forms of these definitions are the following:

$$\text{ASR and LFR: } RF = \frac{C - A_1 D}{A_2 L (1 + I)} \quad (3.2)$$

where:

$RF$  = rating factor for the live load carrying capacity;

$C$  = capacity of the member;

$D$  = dead load effect on the member;

$L$  = live load effect on the member;

$I$  = impact factor to be used with the live load effect;

$A_1$  = factor for dead loads; and

$A_2$  = factor for live load.

For ASR,  $A_1 = 1.0$  and  $A_2 = 1.0$ . The capacity,  $C$ , depends on the rating level desired, with the higher value for  $C$  used for the operating level. For the LFR,  $A_1 = 1.3$  and  $A_2$  depends on the rating level desired. For inventory level,  $A_2 = 2.17$  and for operating level,  $A_2 = 1.3$ . The nominal capacity,  $C$ , does not depend on the rating level.

$$\text{LRFR: } RF = \frac{C - (\gamma_{DC})(DC) - (\gamma_{DW})(DW) \pm (\gamma_P)(P)}{(\gamma_{LL})(LL + IM)} \quad (3.3)$$

where:

$RF$  = rating factor;

$C$  = capacity =  $f_R = \phi_c \phi_s \phi R_n$

$f_R$  = allowable stress specified in the LRFD code;

$\phi_c$  = condition factor;

$\phi_s$  = system factor;

$\phi$  = LRFD resistance factor;

$\phi_c \phi_s \geq 0.85$

$R_n$  = as inspected nominal member resistance;

$DC$  = dead load effect due to structural components and attachments;

$DW$  = dead load effect due to wearing surface and utilities;

$P$  = permanent loads other than dead loads;

$LL$  = live load effect;

$IM$  = dynamic load allowance;

$\gamma_{DC}$  = LRFD load factor for structural components and attachments;

$\gamma_{DW}$  = LRFD load factor for wearing surfaces and utilities;

$\gamma_p$  = LRFD load factor for permanent loads other than dead loads = 1.0;

$\gamma_{LL}$  = evaluation live load factor.

The limit states of interest in the present investigation are strength and stability. Furthermore, for the present project, LRFR was used and therefore will be the focus of subsequent definitions and applications. Two methods for evaluating primary load rating are defined by the MBE: empirical and analytical. The empirical load rating method requires load testing the bridge (defined and implemented in Chapter 5), whereas the analytical method is composed of three distinct procedures (AASHTO 2018):

(1) **Design Load Rating:** For LRFR, design load rating is a first-level assessment of bridges based on the HL-93 loading and LRFD design standards, using dimensions and properties of the bridge in its present as-inspected condition. It is a measure of the performance of existing bridges to current LRFD bridge design standards. Design load rating is intended to serve as a screening process to identify bridges that should be load rated for legal loads. Bridges that pass the design load check ( $RF \geq 1$ ) at the inventory level will have satisfactory load rating for all legal loads that fall within the LRFD exclusion limits.

(2) **Legal Load Rating:** Legal load rating provides a single safe load capacity for a given truck configuration applicable to AASHTO and state legal loads. Live load factors are selected based on the truck traffic conditions at the site. Strength is the primary limit state for load rating; service limit states are selectively applied. The results of the load rating for legal loads could be used as a basis for decision making related to load posting or bridge strengthening.

(3) **Permit Load Rating:** Permit load rating checks the safety and serviceability of bridges in the review of permit applications for the passage of vehicles above the legally established weight limitations. Calibrated load factors by permit type and traffic conditions at the site are specified for checking the load effects induced by the passage of the overweight truck. Guidance is also provided on the serviceability criteria that should be checked when reviewing permit applications.

Each procedure has an inventory rating and an operating rating. The inventory rating is the load that can safely utilize the bridge for an indefinite period. The operating rating is the maximum permissible live load to which a structure can be subjected. The operating rating factor is determined by multiplying the inventory rating by the ratio of the inventory live load factor to the operating level live load factor (1.75 and 1.35, respectively;  $1.75 / 1.35 = 1.30$ ). (AASHTO 2018)

### **3.2 Evaluation Load Definitions**

In general, only permanent loads and vehicular loads are considered to be of consequence in load rating. Environmental loads such as wind, ice, temperature, stream flow, and earthquake are usually not considered in rating. Permanent loads include dead loads and locked-in force effects from the construction process. Pertinent to the present investigation, significant effort must be used to define the stress condition in the culverts due to the backfill load sequence. Live load models for load rating using LRFR include (AASHTO 2018):

1. Design Load: HL-93 design load per LRFD design specifications.
2. Legal Loads: (a) AASHTO legal loads, and (b) the AASHTO notional rating load or state legal loads.

3. Permit Load: actual permit truck.

In Alabama, RFs must be defined for the posting loads defined in Figure 3.1.

ALABAMA DEPARTMENT OF TRANSPORTATION POSTING VEHICLES

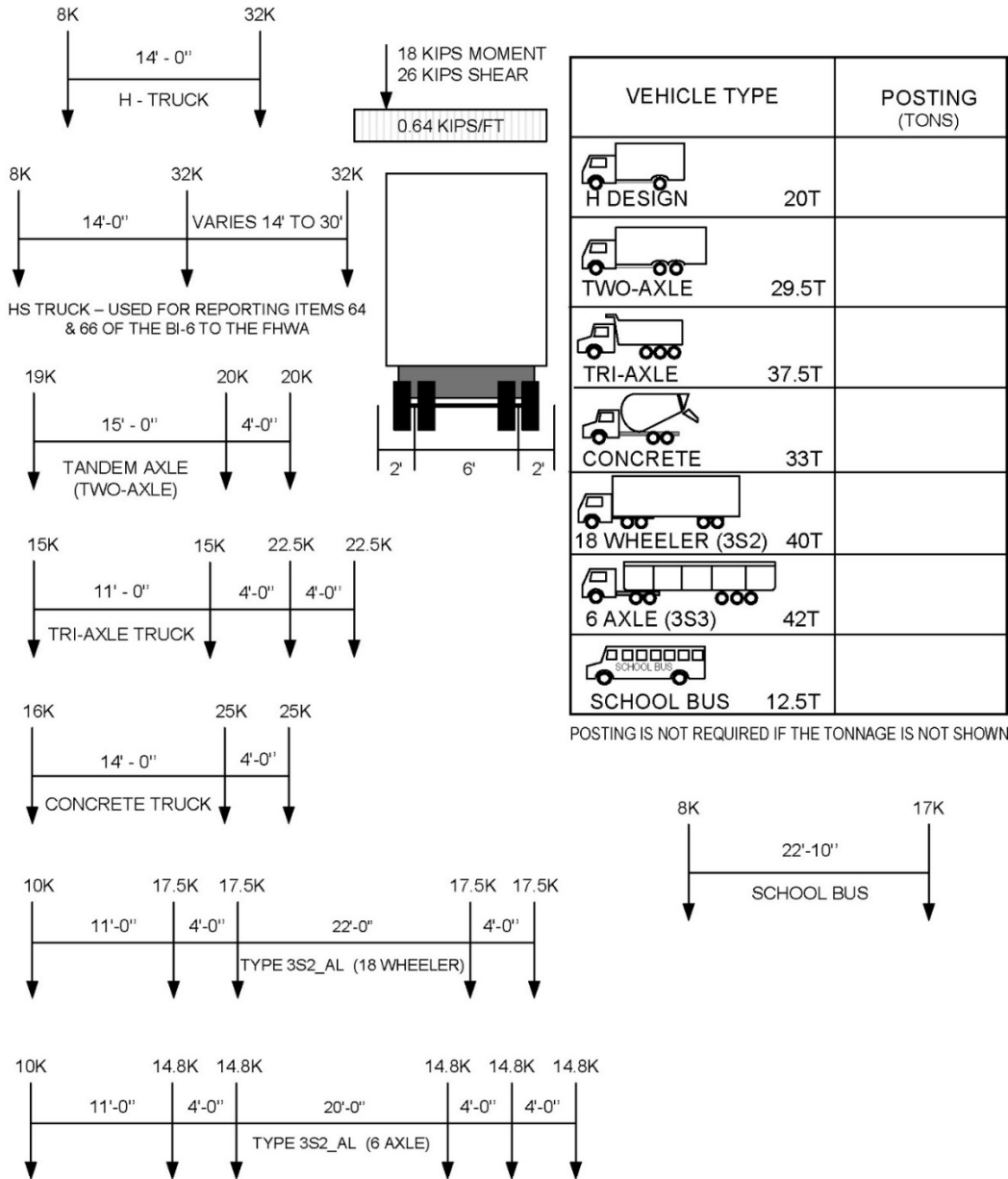


Figure 3.1. Alabama posting loads (ALDOT 2021).

The number of traffic lanes to be loaded and the transverse placement of wheel lines are defined as (1) roadway widths from 18 to 20 ft have two traffic lanes, each equal to one-half the

roadway width; and (2) roadway widths less than 18 ft carry one traffic lane only. The roadways involved in the present project were two lanes with total widths between 20 and 24 ft. Therefore, the multiple presence factor for all bridges involved in this project is 1.0. For the Anniston culverts that are the subject of this investigation, the multiple presence factors are 1.0 per AASHTO LRFD C3.6.1.1.2. The multiple presence factor does not apply for permit trucks. Dynamic load allowance (IM) must be applied to the AASHTO legal vehicles and state legal loads. The static effects of the truck loads must be increased by 33 percent for strength and service limit states to account for the dynamic effects due to moving vehicles. (AASHTO 2018)

### **3.3 Load Factors**

Load factors for vehicular live loads appropriate for use in load rating are as specified in Articles 6A.4.3.2.2, 6A.4.4.2.3, and 6A.4.5.4.2. The evaluation live load factors for the Strength I limit state are defined as 1.75 for inventory evaluation and 1.35 for operating evaluation. Live load factors for the Strength I limit state for buried structures are defined for concrete pipe, and then as 1.15 for “all other culverts and buried structures” (AASHTO 2020). If in the Engineer’s judgment, an increase in the live load factor is warranted due to conditions or situations not accounted for in the MBE when determining the safe legal load, the Engineer may increase the factors, but cannot exceed the value of the factor multiplied by 1.3 (AASHTO 2018).

### **3.4 Corrugated Culvert Methodology**

The MBE provides detailed methodologies for assessing predominate bridge structures such as steel and concrete superstructure bridges and provides procedures for cast-in-place concrete culverts. However, it does not define specific guidance for load rating metal culverts. The rating factor for corrugated metal culverts must be evaluated based on the following four criteria (per CANDE 2019): (1) thrust stress, (2) global buckling, (3) seam strength, and (4)

plastic penetration. In addition, deflection should be checked, which is generally limited to 5% for corrugated metal culverts except “long spans”, which are usually limited to 2% of the vertical rise; however deflection criteria used for load rating should not include displacements associated with construction and dead loads.

Because of the lack of guidance in the MBE for metal culverts, many states have adopted the procedures outlined in the National Corrugated Steel Pipe Association (NCSPA) Design Data Sheet 19 (NCSPA 1995) for the load rating of corrugated steel culverts. This method appears to provide reasonable results for structures with soil cover greater than 3 ft (Mlynarski et al. 2019). Based upon the NCSPA Design Data Sheet 19, the Ohio Department of Transportation (ODOT) developed a spreadsheet for rating corrugated metal culverts, which was evaluated in the report titled “Verification of ODOT’s Load Rating Analysis Programs for Metal Pipe and Arch Culverts” (Sezen et al. 2009). NCSPA Design Data Sheet 19 is LFR and assesses two categories of RF: (1) “wall strength”, and (2) “minimum cover.” The lower of the two rating factors controls. One of the primary issues with the NCSPA approach though is that the “minimum cover” criteria does not depend on any geometric or strength characteristics of the culvert – it is only a function of the cover and AASHTO minimum cover requirements – and it is therefore widely recognized as being overly conservative.

Due to the minimum cover RF issue and recommendations developed by Sezen et al. (2009), ODOT revised its spreadsheet; the primary changes are discussed in Chapter 7. Then in 2012, Michigan Tech University completed a study for the Michigan Department of Transportation titled “Assessment of ODOT Culvert Load Rating Spreadsheets for use in Michigan” (Ahlborn et al. 2013). The objective was to assess the ODOT spreadsheets for adherence to guides and specifications and to modify the spreadsheets to function with Michigan legal and overload trucks.



Spreadsheets in LFR and LRFR formats were developed. However, the project did not investigate the suitability of the technical process used in the ODOT spreadsheets to produce reasonable load rating calculations, but rather adopted the same NCSPA process.

### **3.5 Advanced Analytical Approaches**

Advanced general purpose finite element software such as ABAQUS and PLAXIS used in Chapter 6 are capable of analyzing soil-structure interaction characteristics involved in the behavior and design of flexible culverts. However, accurate modeling using such advanced tools requires expertise, time, and computing resources that are typically not available to engineers for the typical culvert design or rating tasks. Furthermore, rating factor analyses function are not built into general purpose FEM software, and therefore applying load and resistance factors, extracting the data required for rating analyses, and incorporating that data into the rating process are complex.

The Culvert ANalysis and Design (CANDE) software is a finite element program developed especially for the structural design, analysis and evaluation of buried structures including culverts made of corrugated metal, reinforced concrete, and plastic as well as other soil-structure interaction problems such as underground storage facilities and storm water chambers. The first version of CANDE was developed in the 1970's (Katona et al. 1976). The project resulted in an enhanced version of the CANDE software with many new analysis capabilities, a graphical user interface (GUI), explanatory tutorials demonstrating the various program applications, and a comprehensive context-sensitive help system. Additional background and implementation of CANDE is provided in Chapter 6.

## CHAPTER 4: SITE CHARACTERIZATION AND CONDITION ASSESSMENT

### 4.1 Background

As introduced in Chapter 1, ALDOT identified nine corrugated metal culverts annexed by the City of Anniston that have never been rated. These structures are nearly 80 years old and were constructed as part of Fort McClellan. The former military base is being converted to a mixed-use development by the City of Anniston and Calhoun County. The property will feature residential, business, and industrial space. To satisfy FHWA requirements, load rating of the culverts is required.

The ALDOT Maintenance Bureau utilized the spreadsheet tool developed by the Ohio DOT (Wang 2016, Sargand et al. 2018) to rate these culverts. Based on the spreadsheet results, the culverts require posting. However, the low rating and posting requirement is because the soil cover for all of the culverts is less than the minimum required by AASHTO for new designs, rather than strength and stability assessments of the structures; the geometric and material strength characteristics of the structure are not involved in the rating factor calculation using this method when the cover is less than the minimum design cover (discussed in detail in Chapter 7). Therefore, the general opinion is that the load capacity of these culverts is significantly higher than indicated by the spreadsheet rating analysis. This chapter describes the nine corrugated metal culverts annexed by the City of Anniston and reasoning for choosing the two culverts that were load tested.

## 4.2 Project Culverts

**Table 4.1. Culvert locations.**

<b>BIN</b>	<b>Name</b>	<b>Latitude</b>	<b>Longitude</b>
18609	Pelham Range Pipe Arch	33.688611	-86.006111
18615	Patriot Road	33.733763	-85.789746
19875	Federal Way	33.720801	-85.793575
20431	Federal Way	33.720423	-85.794266
20432	Berman Road	33.716777	-85.784409
20433	Bain's Gap Road	33.716578	-85.783472
20441	Berman Road	33.715110	-85.789994
20442	Brigadier Stern	33.708250	-85.786528
20444	Amor Road	33.729587	-85.789218

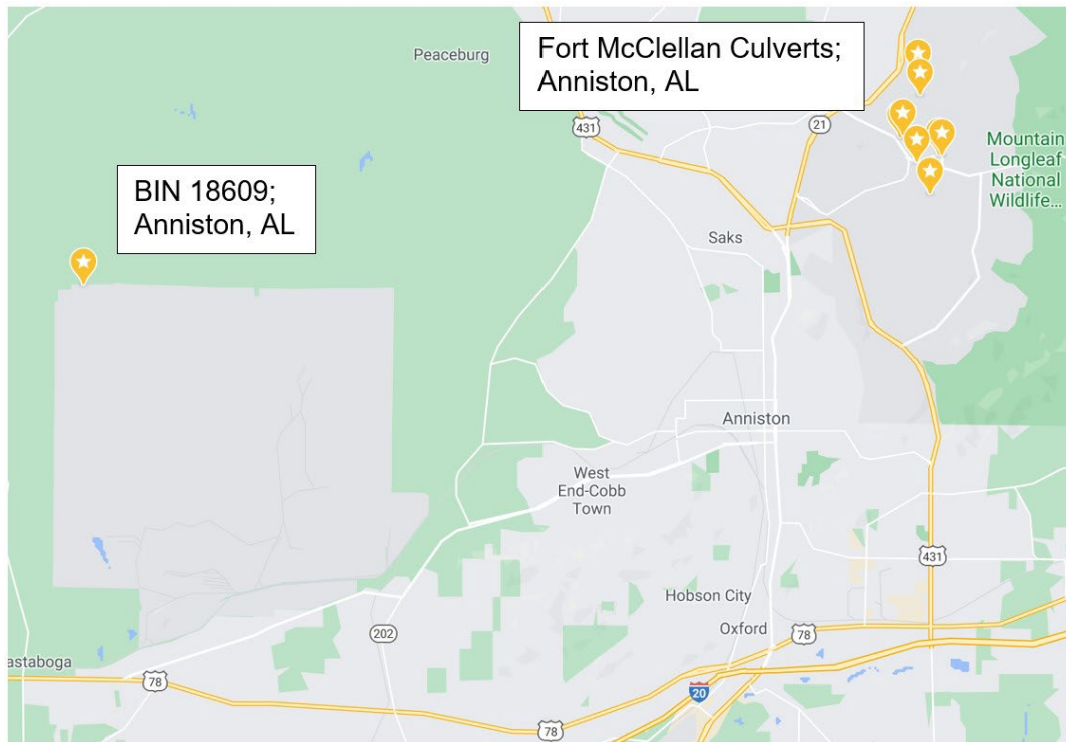


**Figure 4.1. Culvert locations on broad map.**



**Figure 4.2. Fort McClellan culvert locations.**

#### 4.2.1 BIN 18609

Owner	Material	Shape	Fill (in.)	Span (ft.)	Height (ft.)	Condition	Skew (degree)	Pavement (in.)
Nat'l Guard	Steel	Pipe Arch	12	12.67	-	7	0	0

BIN 18609 is different from the other culverts considered because it is a pipe arch instead of a low-profile arch. Because this culvert is on National Guard property, the project team was only able to visit it with an escort. Given its remoteness and access challenges, along with it being different from all of the other low-profile arch culverts, it was decided that BIN 18609 would not be a good test candidate.



**Figure 4.3. BIN 18609 (Google Earth).**





**Figure 4.4. BIN 18609 from site visit.**

#### **4.2.2 BIN 18615**

Owner	Material	Shape	Fill (in.)	Span (ft.)	Height (ft.)	Condition	Skew (degree)	Pavement (in.)
State	Steel	LPA	14	16.67	4.33	6	0	2.5

BIN 18615 was also inaccessible to the team due to it being within a restricted area, and therefore was deemed not ideal for load testing.



**Figure 4.5. BIN 18615 (Google Earth).**

**4.2.3 BIN 19875**

Owner	Material	Shape	Fill (in.)	Span (ft.)	Height (ft.)	Condition	Skew (degree)	Pavement (in.)
-	Steel	LPA	18	16.67	4.33	-	0	2.5

BIN 19875 is very close to BIN 20431. Ultimately, this culvert was not recommended for load testing because others were easier to re-route traffic during testing.





**Figure 4.6. BIN 19875 end view.**

**4.2.4 BIN 20431**

Owner	Material	Shape	Fill (in.)	Span (ft.)	Height (ft.)	Condition	Skew (degree)	Pavement (in.)
City	Steel	LPA	16	16.67	4.33	6	0	2.5

BIN 20431 is very close to BIN 19875. Ultimately, this culvert is not recommended for load testing because the others would be easier to re-route traffic around during testing.





**Figure 4.7. BIN 20431 end view.**



**Figure 4.8. BIN 20431 road surface.**

#### 4.2.5 BIN 20432

Owner	Material	Shape	Fill (in.)	Span (ft.)	Height (ft.)	Condition	Skew (degree)	Pavement (in.)
City	Steel	LPA	15	16.67	4.33	6	41	2.5

BIN 20432 is closed to traffic. While being closed to traffic would keep the team from disrupting traffic, it is desirable to test a culvert with pavement. Therefore, this culvert was not selected for testing.



**Figure 4.9. BIN 20432 road surface.**





**Figure 4.10. BIN 20432 underside.**

#### **4.2.6 BIN 20433**

Owner	Material	Shape	Fill (in.)	Span (ft.)	Height (ft.)	Condition	Skew (degree)	Pavement (in.)
City	Steel	LPA	15	16.67	4.33	7	0	2.5

BIN 20433 is the best candidate for testing because of the lack of skew, surrounding tree roots, and other variables. This culvert is also very accessible for instrumentation setup. It would be relatively easy to pause and re-route traffic around this area as there are several nearby adjacent roads.





**Figure 4.11. BIN 20433 exterior.**



**Figure 4.12. BIN 20433 road surface.**





**Figure 4.13. BIN 20433 foundation.**

#### **4.2.7 BIN 20441**

Owner	Material	Shape	Fill (in.)	Span (ft.)	Height (ft.)	Condition	Skew (degree)	Pavement (in.)
City	Steel	LPA	13	16.67	4.33	6	0	2.5

BIN 20441 was also deemed to be a good test candidate because it would be very accessible. Additionally, one quadrant of this culvert has very shallow cover, giving us a good estimate of a “worst case” scenario during loading.





**Figure 4.14. BIN 20441 cross-section.**



**Figure 4.15. BIN 20441 road surface.**





**Figure 4.16. BIN 20441 close-up.**

#### **4.2.8 BIN 20442**

Owner	Material	Shape	Fill (in.)	Span (ft.)	Height (ft.)	Condition	Skew (degree)	Pavement (in.)
City	Steel	LPA	12	16.67	4.33	7	0	2.5

BIN 20442 is closed to traffic, but adjacent to the culvert is a fence that would challenge load truck accessibility. Therefore, it was not an ideal candidate for load testing





**Figure 4.17. BIN 20442 and fence.**



**Figure 4.18. BIN 20442.**



#### 4.2.9 BIN 20444

Owner	Material	Shape	Fill (in.)	Span (ft.)	Height (ft.)	Condition	Skew (degree)	Pavement (in.)
City	Steel	LPA	19	16.33	4.33	6	0	2.5

BIN 20444 was also inaccessible to the team because it is within a restricted area.

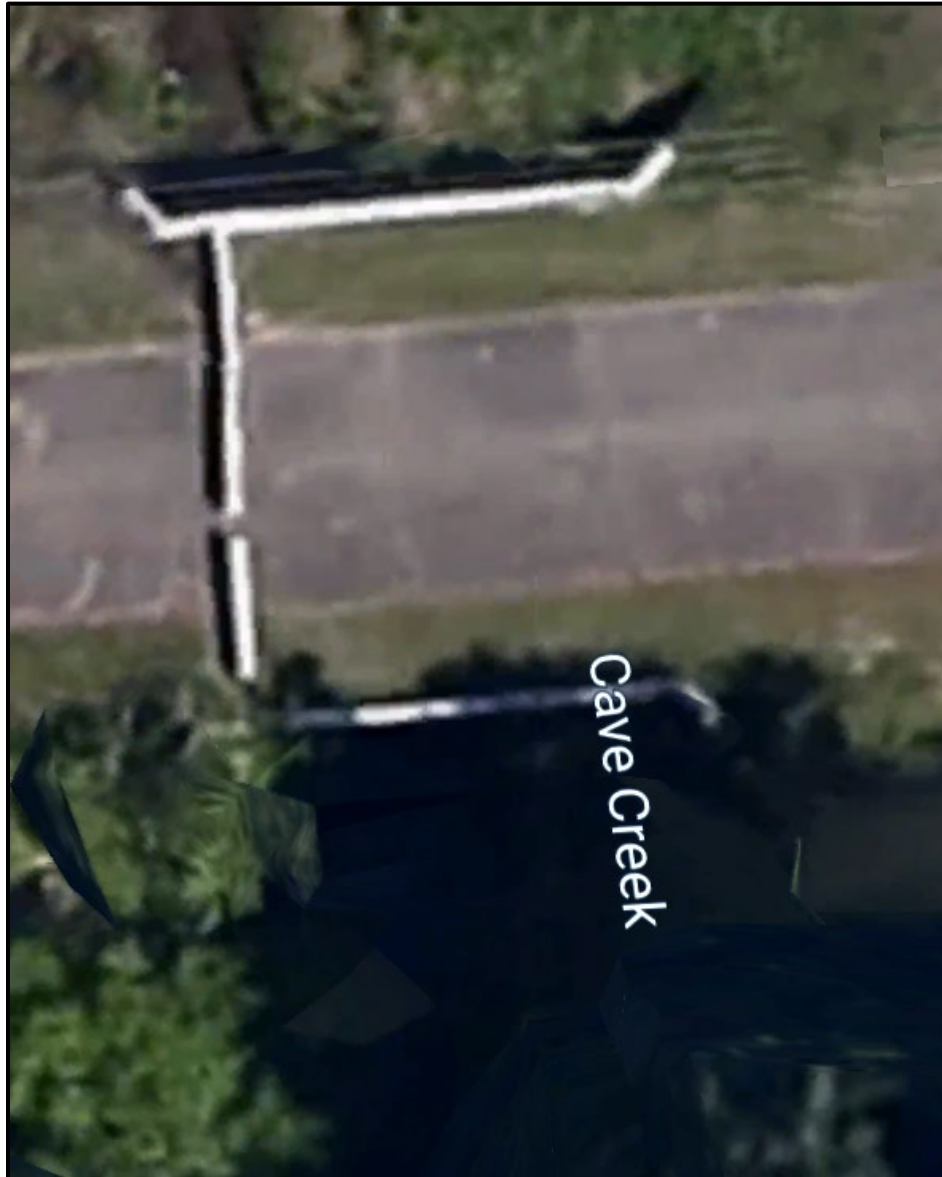


Figure 4.19. BIN 20444 (Google Earth).

## **4.3 Preliminary Site Visits**

### **4.3.1 November 25, 2019**

The research team traveled to Anniston on November 25, 2019 to conduct seismic tests at the Lennox Avenue and Brigadier Stern Avenue Culverts. Three approaches were used to characterize the culvert fill and determine the stratigraphy at over and behind the culverts. Traditional Spectral Analysis of Surface Waves (SASW) and Seismic Refraction were conducted using an array of geophones placed over the culvert backfill. A hammer was used to provide energy input into the ground and the arrival time of compression and shear waves were recorded using a seismograph. Figures 4.20 and 4.21 show testing and Lennox Avenue and Brigadier Stern Avenue, respectively.

Additional tests were conducted to measure the speed of wave transmission through the culvert cover fill to ensure the materials were in fact soil and not concrete. This was accomplished using an array of three geophones and a hammer to send compression waves through the cover. The thickness of the cover was measured using a tape. The results of both studies verified that the backfill was compacted soil transitioning to natural soil that was about twice as stiff. The thickness of the cover was 1.4 ft at Lennox Avenue and 3.4 ft at Brigadier Stern Avenue. Photographs from the wave tests at Lennox Avenue are included as Figures 4.22 and 4.23. A general profile of the culverts is shown in Figure 4.24. In general, the modulus of the compacted culvert fill was just under 2000 psf, and the modulus of the surrounding in-situ soil was about 4000 psf.



**Figure 4.20. Seismic tests at Lennox Avenue.**



**Figure 4.21. Seismic tests at Brigadier Stern Avenue.**





**Figure 4.22. Seismic wave testing at Lennox Avenue.**



**Figure 4.23. Accelerometers to measure wave transmission Lennox Avenue.**



- Easy access to underside of culvert for instrumentation application.
- Minimal factors that could disrupt data such as vastly different pavement thickness across span or culvert skew.

After visiting six of the nine culverts, the team chose the best two culverts to be instrumented and load tested, BIN 20433 and BIN 20441.



**Figure 4.25. October 16, 2020 site visit.**

#### **4.4 Condition Assessment**

Section 4 of the MBE broadly defines procedures and practices for inspecting bridges. Section 4.3.5.10 defines the procedures for “Corrugated Metal Plate Structures”. This includes the obvious concerns such as inspecting the shape for distortion and deformation, metal loss, inlet/outlet for folding and blockage, foundations for settlement and degradation, backfill for water

infiltration and apparent voids, seams for leakage, bolt conditions, etc. ALDOT provided two sets of “corrugated metal structure bridge rating data sheet[s]”, (1) inspections conducted by ALDOT personnel, and (2) inspections conducted by an external consultant. The research team also visited and inspected all of the culverts involved in the project except the two that were not accessible due to being within currently restricted areas. In general, the condition of all of the culverts is uniformly very good with nothing notable that would significantly diminish the rating factor calculations.



**CHAPTER 5: LOAD TESTS**

**5.1 Test Sites**

**5.1.1 Bain’s Gap Road (BIN 20433)**

This culvert was chosen because it is the least complicated structure. This culvert is also easily accessible for instrumentation setup. Figures 5.1 through 5.4 provide sketches and photos of BIN 20433.

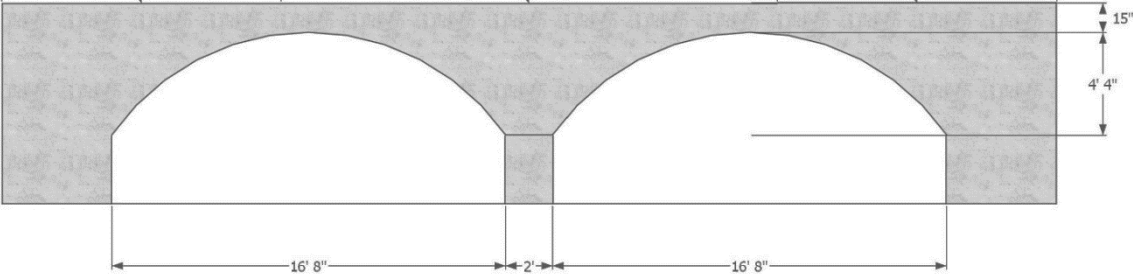


**Figure 5.1. BIN 20433 dimensions.**



**Figure 5.2. BIN 20433 end view.**





**Figure 5.3. BIN 20433 longitudinal view.**



**Figure 5.4. BIN 20433 Bain's Gap Road culvert aerial photo (Google Earth).**

### 5.1.2 Berman Road (BIN 20441)

This culvert was also chosen because of the accessibility. Additionally, one quadrant of this culvert has very shallow cover, giving a good estimate of a “worst case” scenario during loading. Figures 5.5 through 5.9 provide sketches and photos of BIN 20441.

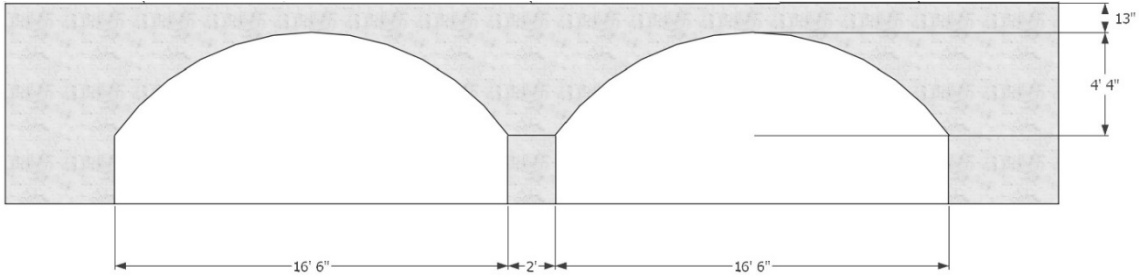


**Figure 5.5. BIN 20441 dimensions.**



**Figure 5.6. BIN 20441 end view.**





**Figure 5.7. BIN 20441 longitudinal view.**





Figure 5.8. BIN 20441 Berman Road culvert aerial photo (Google Earth).

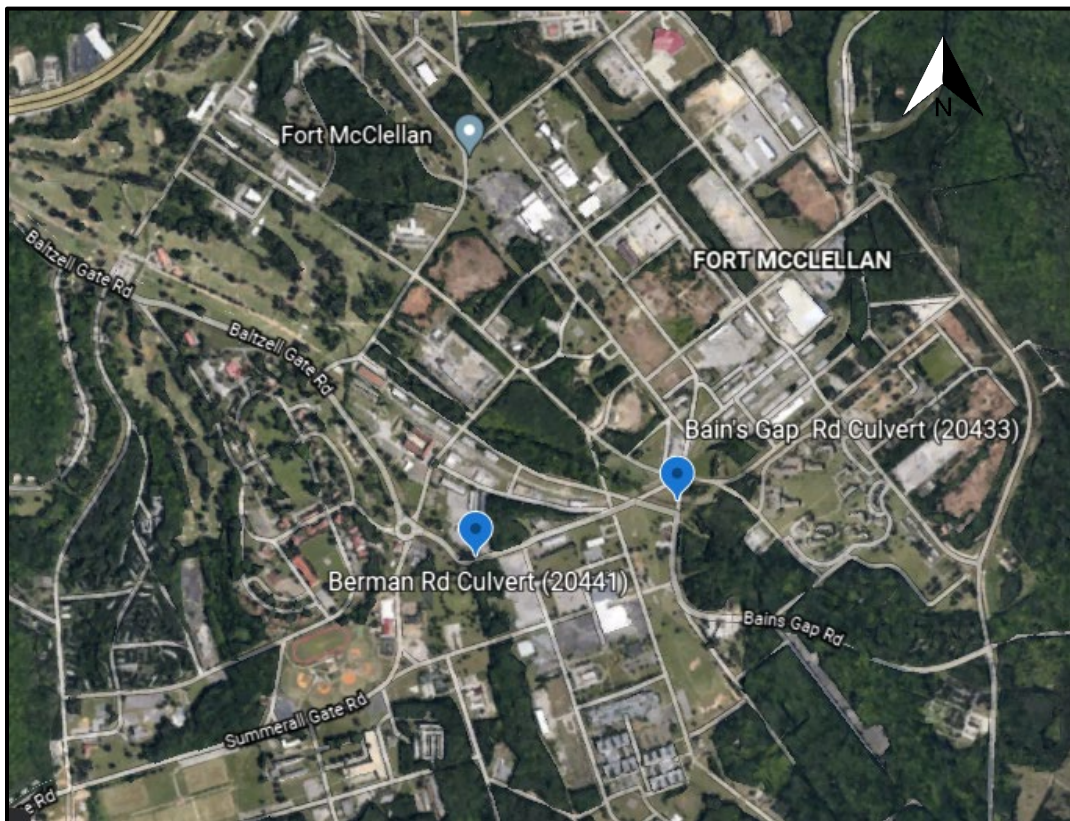


Figure 5.9. Tested culverts aerial photo (Google Earth).

## 5.2 Load Tests

### 5.2.1 General Methodology

The research team arrived at the Anniston site on June 14, the day before testing to fully instrument Gain's Gap Road culvert and to install the strain gages at Berman Road culvert. No traffic control was required during instrumentation installation.

The first day of testing, June 15, the load test truck arrived on site at morning and the test on the Bain's Gap Road culvert started around 12 pm. The truck was configured with Load Case 5 (LC5). Traffic control as well as the testing vehicle was provided by ALDOT. A photograph of the truck is shown in Figure 5.10 and LC-5 is defined in Figure 5.11.



**Figure 5.10. ALDOT load test vehicle.**

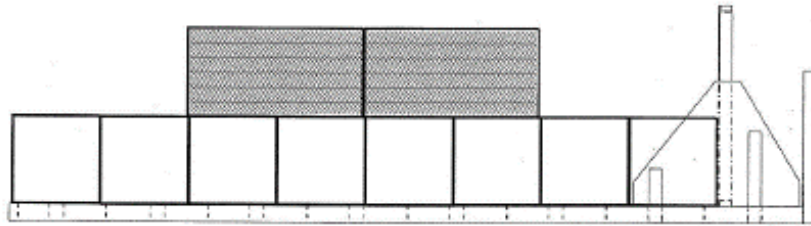
In the second day of testing, June 16, the team completed the instrumentation at Berman Road culvert. The test started around 10:30 am.



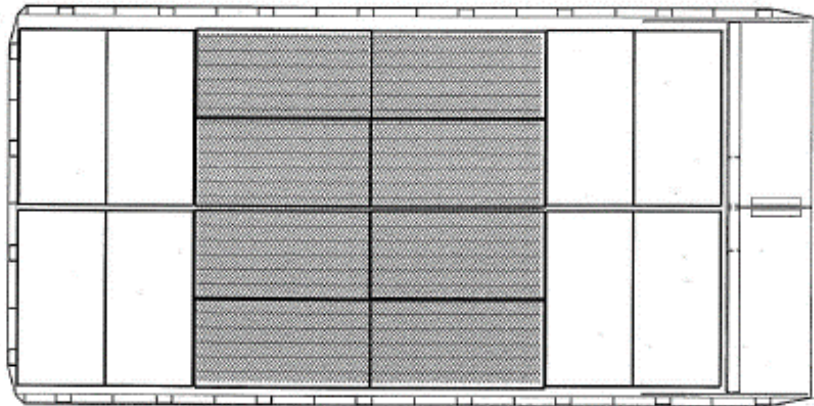
# LOAD TRUCK BLOCK CONFIGURATION



Load Case: LC-5

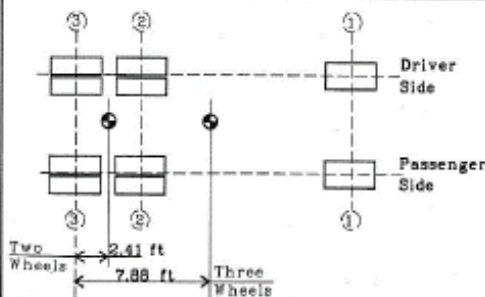
Side View



Top View



**KEY:**  Top Layer ( 8 Blocks)  Bottom Layer ( 16 Blocks)



Wheel Loads				
Total Wt (lbs)	85,700	Wheel 3 (lbs)	Wheel 2 (lbs)	Wheel 1 (lbs)
Driver		15,800	16,000	11,100
Passenger		15,600	15,800	11,400
Average		15,700	15,900	11,250

Figure 5.11. LC-5 configuration of the load truck.

## 5.2.2 Instrumentation

Based on previous studies of load-tests on culverts and finite element analyses, it was decided to place strain transducers and potentiometers at three locations for testing. These locations were the crown and each shoulder ( $\frac{1}{4}$  and  $\frac{3}{4}$  points) of the culverts. Quarter points are proportional to the culvert's width (labeled in Figure 5.12). To measure strain, BDI ST350 strain transducers were attached to mounts glued at each location. To measure displacement, string pot potentiometers were bolted to each location at the culvert and connected to stable tripods. Data was read from a CR6 datalogger and was available live during testing for visualization and verification.

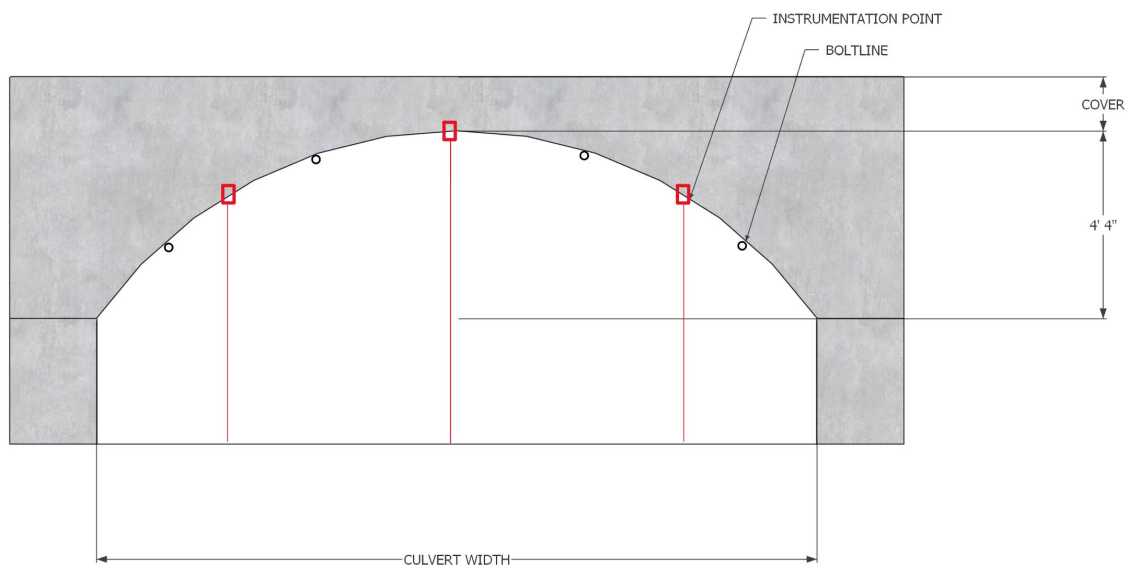


**Figure 5.12. Instrumentation locations.**

To measure strain, BDI ST350 strain transducers were bolted at each instrumentation location. The research team chose this instrument for strain measurements for many reasons. These strain transducers provide roughly 3.5 times the output of a typical foil strain gage. The reusable sensors are also ideal for measuring live-load strain on structures and can be installed within minutes in all weather conditions. In similar projects, regular strain gages are welded on to the

surface of the culvert in two directions. This is a time-consuming effort, so the strain transducer is a better choice as the transducers were attached to the culvert using Loctite glue with accelerant. The distance between the bolt holes of the transducer is 3 inches. The corrugation pitch is also 3 inches. These transducers have a typical sensitivity of  $500 \mu\epsilon/mV_{out}/V_{in}$ , with an accuracy  $< \pm 1\%$ . Figure 5.13 is a photograph of a BDI ST350.



**Figure 5.13. BDI ST350; strain transducer for strain measurements.**

String potentiometers were used to measure vertical displacements at the sensor locations. Micro-Epsilon WDS-100-P60 (Figure 5.14) potentiometers were used that had a measuring range up to 100 mm. The potentiometers were affixed to heavy stable tripods. The wire extended from the potentiometer was attached to the culvert using a self-tapping eye screw. Figure 5.15 shows the field installation of the potentiometers. The reported resolution of these sensors was “towards infinity.” These were chosen as the research team has prior experience with these instruments, which should minimize error with use.



**Figure 5.14. Micro-Epsilon P60; String pot potentiometers for deflection measurement.**





**Figure 5.15. Tripod with potentiometer mounted.**

The CR6 Measurement and Control Datalogger from Campbell Scientific, shown in Figure 5.16, is a powerful receptor data-acquisition system. The CR6 datalogger provides fast communication, low power requirements, built-in USB, compact size, and high analog input accuracy and resolution. It uses universal (U) terminals to allow a connection to the sensors. The research team had extensive experience with this datalogger and its programs, so it was chosen for this project.



**Figure 5.16. CR6 datalogger.**

### 5.2.3 Testing Procedure

The instrumentation points were chosen to measure representative deflection and strain measurements of the culvert. From FEA, it is predicted that these maximums will occur at either the crown or shoulders of the culverts. As such, these locations were instrumented with the strain transducers and potentiometers. These culverts were constructed using plates of galvanized steel that are bolted together at the seams. To minimize irregularities in the data due to forces acting at these seams, instrumentation points were mounted at the plate centers, between the bolt lines. These positions were exactly recorded to confirm data with the finite element analysis.

The truck was driven over two load lines (Figure 5.17). For the first load line, the truck itself was centered over the gages. An additional two passes were performed for this load line (3 passes total) besides one reverse pass in which the truck moved on the opposite direction. Each truck stopping point was defined by the location of the front rear axle (heaviest) as it aligns with  $\frac{1}{4}$  point, center, and  $\frac{3}{4}$  point of the arch. These locations are conceptualized in Figure 5.18. In this way, data will be able to be easily verified and compared to the predicted stresses of the finite element analysis.

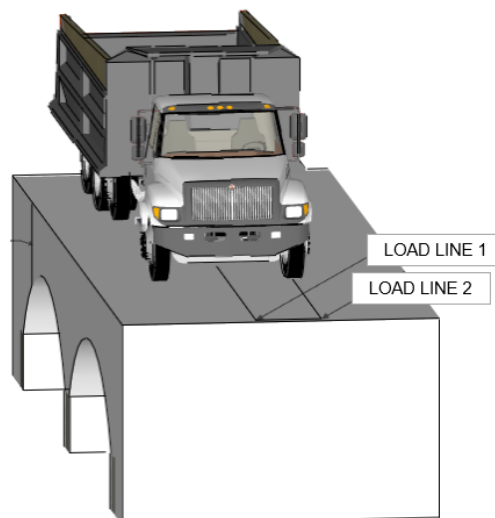


**Figure 5.17. Load lines; truck shown in the first load line position.**

For the second load line, the truck's right wheels were centered over the gages. A total of three passes were performed for this load line as well one reverse pass, and each stopping point of truck was defined by the location of the front rear axle (heaviest). Paint markings were used to assist with positioning the load truck at the correct stopping location and load line, as shown in Figure 5.19.

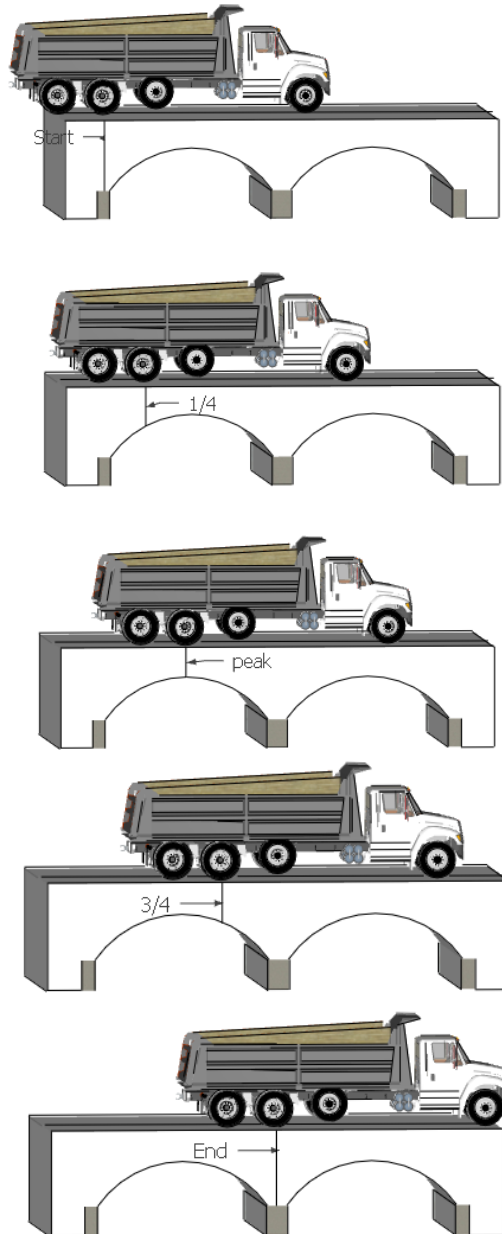


**Figure 5.18. Truck stopping positions: start,  $\frac{1}{4}$ , crown,  $\frac{3}{4}$  and end.**



**Figure 5.19. Truck shown in the second load line position.**

In order to install the instrumentation equipment, the  $\frac{1}{4}$ , crown and  $\frac{3}{4}$  points were located under the culvert. The distance from the head wall to the center of the travel lane was established. The instrument locations were set along that line, at the  $\frac{1}{4}$ , crown and  $\frac{3}{4}$  points previously established. Figures 5.20 and 5.21 show the research team establishing the sensor locations.





**Figure 5.20. Location of instrumentation points at the Bain's Gap Road culvert.**



**Figure 5.21. Location of instrumentation points at the Berman Road culvert.**

## 5.2.4 Load Line and Truck Stopping Locations

Prior to testing, the research team located the load traffic lines. The instrumentation points marked on the bottom surface of the culvert were located on the road surface, over the load lines, using spray paint to indicate load positions to the team and load truck driver. The starting and ending points of each culvert were located as well to provide additional measurements for comparison. Along with the marks painted on the road, flags were positioned on the sides of the road to signal the stopping points. Figures 5.22 through 5.24 show the marking process.



**Figure 5.22. Location of truck stopping points on the road.**





**Figure 5.23. Signal flags located at the Bain's Gap Road culvert.**



**Figure 5.24. Truck stopping points located at the Berman Road culvert.**

### 5.2.5 Strain Gage and Potentiometer Installation

Strain gages were installed by attaching the strain transducers to manufacturer supplied mounting tabs, Figure 5.25, and then adhering to the culvert surface using Loctite glue and an accelerant. As shown in Figure 5.26, the strain gages were located at  $\frac{1}{4}$ , crown and  $\frac{3}{4}$  positions in each culvert; this installation was developed by the research team the day before first test. The potentiometers were installed in each culvert the same day of the test. Figure 5.27 shows the installation of a potentiometer on a tripod, settling the tripod to the soil and checking its level to make sure the potentiometer was completely vertical to the eye-screw, previously fixed to the culvert surface. As shown in Figure 5.28, the potentiometers were located at  $\frac{1}{4}$ , crown and  $\frac{3}{4}$  positions of each culvert.



**Figure 5.25. Strain gage installation.**





**Figure 5.26. Strain gage installed at  $\frac{1}{4}$ , crown and  $\frac{3}{4}$  of the Berman Road culvert.**



**Figure 5.27. Potentiometer installation.**



**Figure 5.28. Potentiometers installed at  $\frac{1}{4}$ , crown and  $\frac{3}{4}$  locations at Bain's Gap Road culvert.**

### **5.2.6 Data Storage Settings**

The data storage settings on the CR6 Datalogger was developed after the potentiometer installation. Each instrument was connected to the datalogger according to the previous program code developed specifically for these tests. Checks were made before the start of the load test. Figures 5.29 and 5.30 depict the CR6 setup.

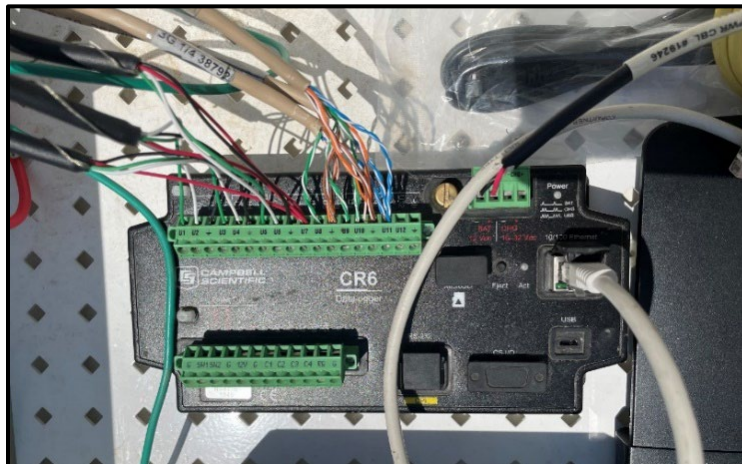


**Figure 5.29. CR6 Datalogger.**





**Figure 5.30. Connection of strain gages and potentiometers to the datalogger.**

### **5.2.7 Load Test**

Once the instrumentation was set, the load test was implemented for each culvert. As previously indicated, the load truck was driven over the culverts three times plus a reverse pass in each load line. In each pass, the truck stopped in the start, 1/4, crown, 3/4, and end points marked on the road. For each stopping point, the strain and deflection data were recorded for a minute. The load truck location at each point was verified by the research team, as shown in Figure 5.31. Figure 5.32 shows the load truck at the 1/4 point with right wheels over the sensors (line 2). Figure 5.33 and Figure 5.34 show the load truck during testing at the Berman Road Culvert.



**Figure 5.31. Verification of truck location in stopping point (load line 1) at the Bain's Gap Road culvert.**





**Figure 5.32. Load truck in 1/4 stopping point (load line 2) at the Bain's Gap Road culvert.**



**Figure 5.33. Load truck in crown stopping point (load line 2) at Berman Road culvert.**



**Figure 5.34. Load truck in reverse pass at Berman Road culvert.**

In total, there were forty measurements of strain and deflection collected for each culvert. To minimize disruptions in data during the test, at times when gage readings were being taken, no other traffic could be on the culvert structure. Taking this into account, in some cases testing was paused between each data recording to allow for traffic to pass, notes were taken to record the time at which other traffic were over the culvert. The traffic was controlled by ALDOT staff.

## **5.3 Data Analysis**

### **5.3.1 Test Data**

The strain transducers and potentiometers were installed at three points across the culvert section as shown in Figure 5.35 for the Bain’s Gap culvert (BIN20433) and Figure 5.36 for the Berman Road culvert (BIN20441). The potentiometers were installed at the top fiber of the corrugations to measure the maximum deflection at the respective sensor locations.



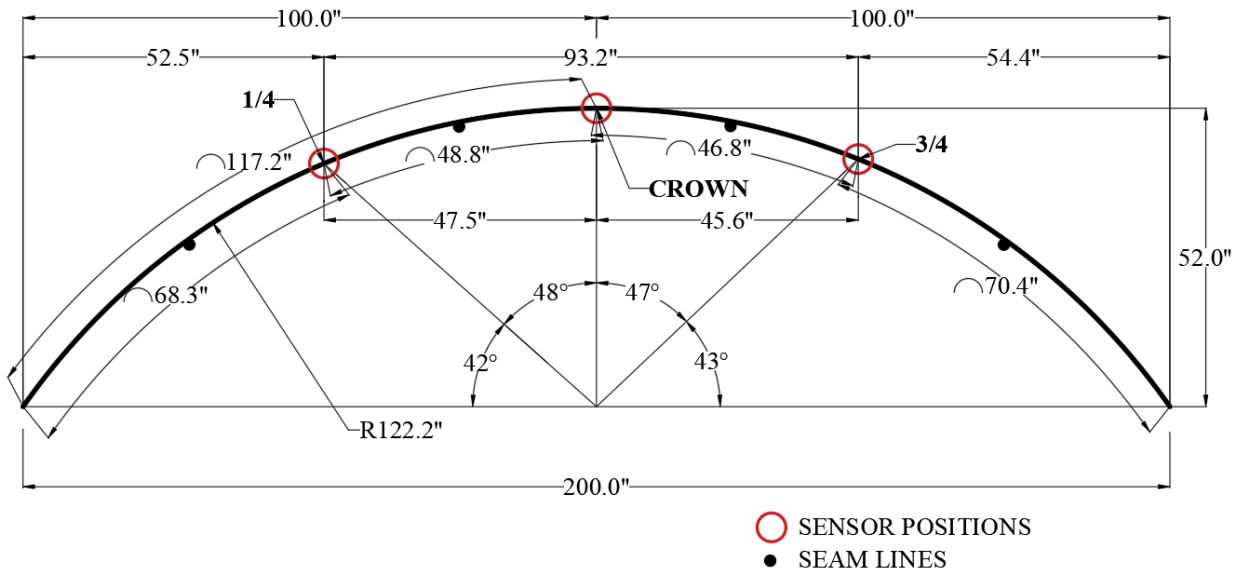


**Figure 5.35. Bain's Gap (BIN 20433) culvert cross-section with sensors locations (dimensions in inches).**

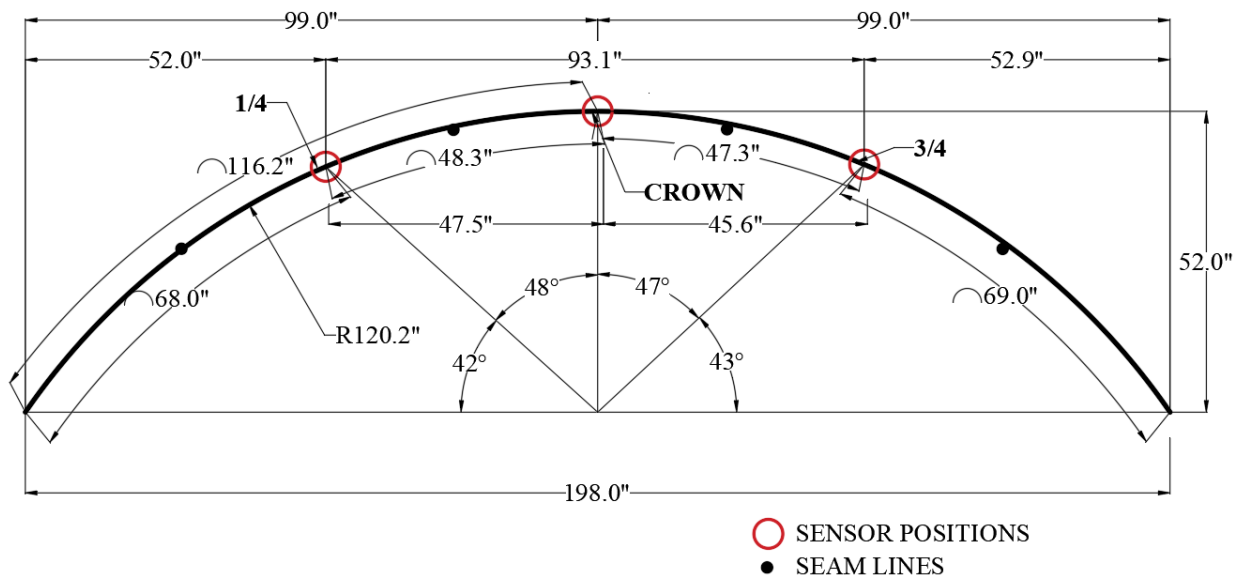


**Figure 5.36. Berman Road (BIN 20433) culvert cross-section with sensors locations (dimensions in inches).**

The load test data for each load position were extracted by matching the timesheet with the data timestamp. The sensors were scanned every 1 second and data were collected every 10

seconds. Because the load truck was left at each position for one minute, there were at least 6 sets of readings from each sensor at each load position, the maximum values from these sets were considered the worst-case responses.

Tables 5.1 and 5.2 show the maximum responses for the sensors at the Bain's Gap culvert for load line 1 and load line 2 respectively, while Tables 5.3 and 5.4 show the maximum responses for the sensors at the Berman Road culvert for load line 1 and load line 2 respectively.

For the Bain's Gap culvert, for load line 1, the maximum strain was  $-118.424 \mu\epsilon$  recorded at the crown when the load truck was at the first-quarter position (reversed), the maximum vertical deflection was 0.082 inch downwards, recorded at the crown when the load truck was at the third-quarter position (reversed).

For load line 2, the maximum strain was  $269.695 \mu\epsilon$  recorded at the crown when the load truck was positioned at the crown (pass 1), the maximum vertical deflection was 0.113 inch downwards, recorded at the crown with the load truck at the crown (pass 3).

For the Berman Road culvert, for load line 1, the maximum strain was  $-103.166 \mu\epsilon$  recorded at the first-quarter gage when the load truck was at the third-quarter position (reversed), the maximum vertical deflection was 0.076 inch downwards, recorded at the crown when the load truck was at the third-quarter position (reversed).

For load line 2, the maximum strain was  $243.213 \mu\epsilon$  and the maximum vertical deflection was 0.117 inch downwards, both were recorded from sensors at the crown, when the load truck was positioned at the crown (reversed).

**Table 5.1. Bain's Gap strain gage and potentiometer readings for load line 1.**

Load Point	Pass #	Strain ( $\mu\epsilon$ )			Deflection (in)		
		1/4	Crown	3/4	1/4	Crown	3/4
Start	1	12.149	-33.672	-0.313	-0.012	0.017	0.006
	2	2.970	-35.494	-3.406	-0.011	0.014	0.006
	3	2.136	-33.934	-3.799	-0.011	0.013	0.007
	R	-8.570	-60.175	-7.294	-0.004	0.012	-0.008
1/4	1	68.896	-63.542	-11.739	-0.051	0.016	0.025
	2	64.448	-64.040	-17.481	-0.052	0.014	0.027
	3	60.217	-67.274	-15.461	-0.052	0.015	0.026
	R	92.389	-118.424	-11.658	0.014	0.024	-0.057
Crown	1	-20.541	94.099	-86.802	-0.035	-0.051	0.038
	2	-22.201	105.585	-96.374	-0.030	-0.060	0.035
	3	-24.288	101.883	-99.713	-0.032	-0.061	0.035
	R	10.183	57.873	-86.427	0.035	-0.051	-0.045
3/4	1	-86.816	72.918	-5.491	0.016	-0.058	-0.017
	2	-85.567	70.576	-10.649	0.014	-0.060	-0.014
	3	-87.828	63.332	-12.981	0.012	-0.062	-0.013
	R	-92.825	83.575	-58.763	-0.012	-0.082	0.010
End	1	-37.437	-42.080	44.482	0.036	-0.008	-0.056
	2	-38.629	-41.242	46.702	0.036	-0.009	-0.056
	3	-38.629	-42.080	44.482	0.036	-0.009	-0.056
	R	-65.746	-6.017	-13.062	-0.052	-0.041	0.038

**Table 5.2. Bain's Gap strain gage and potentiometer readings for load line 2.**

Load Point	Pass #	Strain ( $\mu\epsilon$ )			Deflection (in)		
		1/4	Crown	3/4	1/4	Crown	3/4
Start	1	-8.851	-45.750	-10.730	-0.017	0.010	0.005
	2	-15.415	-54.441	-14.848	-0.014	0.006	0.000
	3	-17.292	-54.442	-13.805	-0.014	0.004	-0.002
	R	-13.609	-64.460	-18.119	-0.004	0.012	-0.011
1/4	1	61.474	-140.407	-11.101	-0.077	0.021	0.023
	2	74.283	-130.143	-14.125	-0.073	0.016	0.017
	3	65.668	-140.263	-15.834	-0.075	0.014	0.017
	R	146.012	-170.895	-14.828	0.015	0.030	-0.080
Crown	1	-57.236	269.695	-125.609	-0.037	-0.110	0.041
	2	-73.651	255.023	-105.553	-0.037	-0.107	0.038
	3	-54.447	265.813	-119.613	-0.038	-0.113	0.038
	R	24.723	226.196	-120.905	0.032	-0.101	-0.050
3/4	1	-191.929	32.976	39.380	0.016	-0.088	-0.035
	2	-191.683	27.254	44.535	0.018	-0.088	-0.037
	3	-195.364	3.464	41.280	0.016	-0.088	-0.037
	R	-195.345	71.989	-34.934	-0.034	-0.104	0.017
End	1	-16.272	-190.024	-39.347	0.032	-0.002	-0.079
	2	-17.010	-183.168	24.034	0.030	0.004	-0.082
	3	-18.448	-190.925	-24.843	0.030	-0.004	-0.080
	R	-30.144	-167.104	-100.083	-0.076	-0.019	0.033

**Table 5.3. Berman Road strain gage and potentiometer readings for load line 1.**

Load Position	Pass #	Strain ( $\mu\epsilon$ )			Deflection (in)		
		1/4	Crown	3/4	1/4	Crown	3/4
Start	1	0.221	-32.593	4.147	-0.005	0.018	0.001
	2	-1.439	-31.013	1.723	-0.005	0.017	0.002
	3	-3.511	-31.136	-2.529	-0.005	0.013	0.000
	R	-14.603	-44.269	-7.209	-0.011	0.009	0.001
1/4	1	60.188	-69.673	-4.393	-0.044	0.017	0.020
	2	67.617	-72.597	-7.046	-0.049	0.014	0.022
	3	64.310	-73.942	-8.405	-0.047	0.015	0.021
	R	48.713	-73.672	-15.144	-0.050	0.009	0.019
Crown	1	-15.422	83.159	-72.945	-0.032	-0.049	0.023
	2	-22.908	88.196	-71.592	-0.034	-0.052	0.027
	3	-19.586	86.939	-85.467	-0.033	-0.054	0.025
	R	-34.398	90.200	-98.196	-0.038	-0.068	0.025
3/4	1	-79.033	67.192	-33.766	0.004	-0.064	-0.014
	2	-74.675	39.049	-51.131	-0.006	-0.063	-0.009
	3	-74.901	54.647	-48.425	-0.003	-0.066	-0.011
	R	-103.166	57.223	-41.434	-0.006	-0.076	-0.014
End	1	-32.424	-14.937	4.907	0.026	-0.017	-0.045
	2	-41.629	4.763	-20.198	0.026	-0.028	-0.044
	3	-34.805	-21.222	11.773	0.026	-0.016	-0.047
	R	-51.575	-27.353	11.731	0.023	-0.032	-0.051



**Table 5.4. Berman Road strain gage and potentiometer readings for load line 2.**

Load Position	Pass #	Strain ( $\mu\epsilon$ )			Deflection (in)		
		1/4	Crown	3/4	1/4	Crown	3/4
<b>Start</b>	<b>1</b>	-14.105	-43.462	-9.511	-0.009	0.013	-0.001
	<b>2</b>	-16.061	-43.136	-15.488	-0.008	0.009	-0.004
	<b>3</b>	-17.624	-40.459	-18.529	-0.008	0.004	-0.006
	<b>R</b>	-24.959	-50.074	-14.144	-0.014	0.004	-0.001
<b>1/4</b>	<b>1</b>	47.078	-139.686	-7.618	-0.064	0.020	0.014
	<b>2</b>	58.173	-138.204	-11.037	-0.066	0.017	0.014
	<b>3</b>	58.748	-137.857	-14.907	-0.067	0.013	0.012
	<b>R</b>	43.521	-127.807	-13.830	-0.062	0.012	0.014
<b>Crown</b>	<b>1</b>	-33.735	190.826	-97.027	-0.037	-0.093	0.022
	<b>2</b>	-38.834	205.018	-104.140	-0.037	-0.101	0.023
	<b>3</b>	-32.688	204.496	-113.997	-0.038	-0.104	0.021
	<b>R</b>	-47.742	243.213	-121.242	-0.039	-0.117	0.027
<b>3/4</b>	<b>1</b>	-177.637	40.194	-45.052	0.008	-0.092	-0.024
	<b>2</b>	-174.752	60.173	-39.291	0.010	-0.099	-0.025
	<b>3</b>	-183.767	67.302	-41.868	0.010	-0.104	-0.026
	<b>R</b>	-208.898	-14.852	-28.582	-0.002	-0.093	-0.031
<b>End</b>	<b>1</b>	-26.516	-115.133	-71.842	0.022	-0.017	-0.058
	<b>2</b>	-27.925	-107.916	-81.530	0.024	-0.024	-0.058
	<b>3</b>	-30.439	-107.369	-96.312	0.023	-0.029	-0.058
	<b>R</b>	-33.565	-130.035	-21.120	0.020	-0.020	-0.068

### 5.3.2 Calculations

The measured strain values were used to estimate the stresses on the culverts in response to the load truck. The stresses were calculated using equation 5.1:

$$\sigma = \varepsilon \cdot E \quad (5.1)$$

where  $\varepsilon$  is the measured strain and  $E$  is the elastic modulus of steel taken as 29e6 psi. The calculated stresses from measured strain values are shown in Tables 5.5 and 5.6 for Bain's Gap culvert load line 1 and load line 2 respectively, and Tables 5.7 and 5.8 for Berman Road culvert load line 1 and load line 2, respectively. It should be recognized that this calculation assumes that the magnitude of the measured strain in the transverse direction is much higher than strains in the longitudinal direction.

The maximum stresses for the Bain's Gap culvert were 3.43 ksi for load line 1, calculated from strain measured at the crown when the load truck was at the first-quarter position (reversed), and 7.82 ksi for load line 2 calculated from strain measured at the crown of the culvert when the load truck was positioned at the crown.

For the Berman Road culvert, the maximum stresses were 2.99 ksi for load line 1, calculated from strain measured at the first-quarter position when the load truck was at the third-quarter position (reversed), and 7.05 ksi for load line 2 calculated from strain values measured at the crown with the load truck at the crown as well (reversed).

**Table 5.5. Calculated stresses from measured strain for Bain's Gap load line 1.**

Load Position	Pass #	Estimated stress (ksi)		
		1/4	Crown	3/4
Start	1	0.352	-0.976	-0.009
	2	0.086	-1.029	-0.099
	3	0.062	-0.984	-0.110
	R	-0.249	-1.745	-0.212
1/4	1	1.998	-1.843	-0.340
	2	1.869	-1.857	-0.507
	3	1.746	-1.951	-0.448
	R	2.679	-3.434	-0.338
Crown	1	-0.596	2.729	-2.517
	2	-0.644	3.062	-2.795
	3	-0.704	2.955	-2.892
	R	0.295	1.678	-2.506
3/4	1	-2.518	2.115	-0.159
	2	-2.481	2.047	-0.309
	3	-2.547	1.837	-0.376
	R	-2.692	2.424	-1.704
End	1	-1.086	-1.220	1.290
	2	-1.120	-1.196	1.354
	3	-1.120	-1.220	1.290
	R	-1.907	-0.174	-0.379

**Table 5.6. Calculated stresses from measured strain for Bain's Gap load line 2.**

Load Position	Pass #	Estimated stress (ksi)		
		1/4	Crown	3/4
Start	1	-0.257	-1.327	-0.311
	2	-0.447	-1.579	-0.431
	3	-0.501	-1.579	-0.400
	R	-0.395	-1.869	-0.525
1/4	1	1.783	-4.072	-0.322
	2	2.154	-3.774	-0.410
	3	1.904	-4.068	-0.459
	R	4.234	-4.956	-0.430
Crown	1	-1.660	7.821	-3.643
	2	-2.136	7.396	-3.061
	3	-1.579	7.709	-3.469
	R	0.717	6.560	-3.506
3/4	1	-5.566	0.956	1.142
	2	-5.559	0.790	1.292
	3	-5.666	0.100	1.197
	R	-5.665	2.088	-1.013
End	1	-0.472	-5.511	-1.141
	2	-0.493	-5.312	0.697
	3	-0.535	-5.537	-0.720
	R	-0.874	-4.846	-2.902

**Table 5.7. Calculated stresses from measured strain for Berman Road load line 1.**

Load Position	Pass #	Estimated stress (ksi)		
		1/4	Crown	3/4
Start	1	0.006	-0.945	0.120
	2	-0.042	-0.899	0.050
	3	-0.102	-0.903	-0.073
	R	-0.423	-1.284	-0.209
1/4	1	1.745	-2.021	-0.127
	2	1.961	-2.105	-0.204
	3	1.865	-2.144	-0.244
	R	1.413	-2.136	-0.439
Crown	1	-0.447	2.412	-2.115
	2	-0.664	2.558	-2.076
	3	-0.568	2.521	-2.479
	R	-0.998	2.616	-2.848
3/4	1	-2.292	1.949	-0.979
	2	-2.166	1.132	-1.483
	3	-2.172	1.585	-1.404
	R	-2.992	1.659	-1.202
End	1	-0.940	-0.433	0.142
	2	-1.207	0.138	-0.586
	3	-1.009	-0.615	0.341
	R	-1.496	-0.793	0.340



**Table 5.8. Calculated stresses from measured strain for Berman Road load line 2.**

Load Position	Pass #	Estimated stress (ksi)		
		1/4	Crown	3/4
Start	1	-0.409	-1.260	-0.276
	2	-0.466	-1.251	-0.449
	3	-0.511	-1.173	-0.537
	R	-0.724	-1.452	-0.410
1/4	1	1.365	-4.051	-0.221
	2	1.687	-4.008	-0.320
	3	1.704	-3.998	-0.432
	R	1.262	-3.706	-0.401
Crown	1	-0.978	5.534	-2.814
	2	-1.126	5.946	-3.020
	3	-0.948	5.930	-3.306
	R	-1.385	7.053	-3.516
3/4	1	-5.151	1.166	-1.307
	2	-5.068	1.745	-1.139
	3	-5.329	1.952	-1.214
	R	-6.058	-0.431	-0.829
End	1	-0.769	-3.339	-2.083
	2	-0.810	-3.130	-2.364
	3	-0.883	-3.114	-2.793
	R	-0.973	-3.771	-0.612

### 5.3.3 Results

According to *AASHTO Manual for Bridge Evaluation* (AASHTO 2018), the minimum yield stress of steel constructed prior to 1954 was estimated as 33 ksi (Table 6A.5.2.2-1). The maximum stresses from the load tests were 7.82 ksi for the Bain's Gap culvert and 7.05 ksi for the Berman Road culvert. Both of these values are well below the minimum yield stress of the culverts (about 24% of the yield stress).

The maximum vertical displacement from the load tests were 0.113 inch for the Bain's Gap culvert and 0.117 inch for the Berman Road culvert.

For each truck position, the deformed shapes for load line 1 and 2 for the Bain's Gap culvert are shown in Figure 5.37, the left side shows tests for which the load truck was in the forward direction while the right side shows the reversed direction. Figure 5.38 shows similar plots for the Berman Road culvert. For clarity, the plots were scaled up 100 times with the maximum deflection at each load position indicated on the plots.

### 5.4 Field Test Summary

This chapter focused on load testing and numerical analysis. Literature on similar studies were reviewed to choose best practices. Load-deflection results from numerical analyses were used to develop a comprehensive load test plan. Three instrument positions were chosen based on the finite element analysis results for maximum response points. The ALDOT load truck had 24 1-ton concrete-filled steel boxes evenly distributed on the truck bed. Five positions (start, first-quarter, crown, third-quarter and end) were established as load truck positions. Two load lines were proposed, load line one had the truck over the culvert with the sensor lines matching the centerline of the truck while load line 2 had the sensor line matching the edge of the truck footprint. The test plan included 3 passes of the load truck in the forward direction and one reverse pass for each

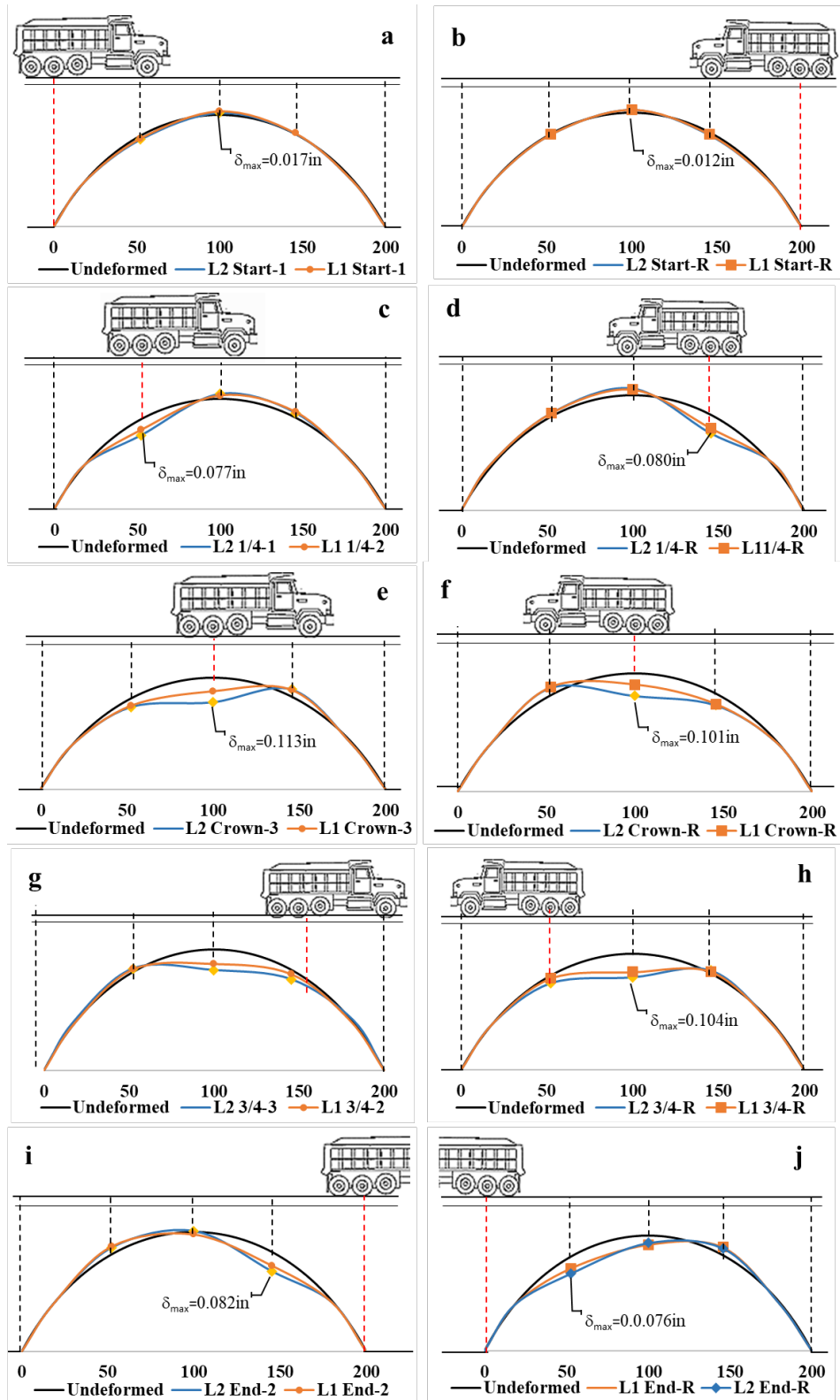


Figure 5.37. Deformed shapes of the Bain's Gap culvert for each load truck position (scale x100).

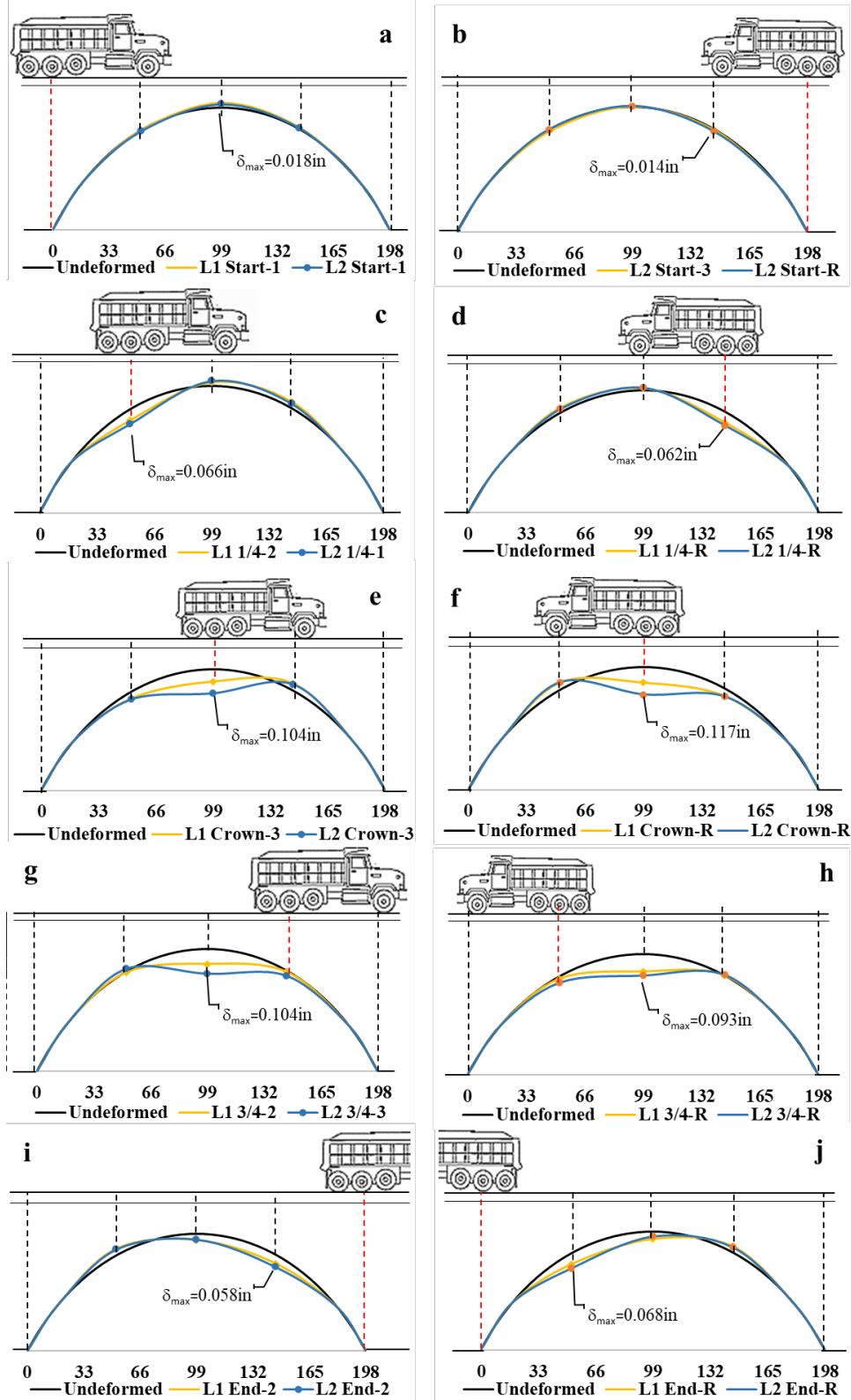


Figure 5.38. Deformed shapes of the Berman Road culvert for each load truck position (scale x100).

load position and each load line. The test plan was successfully implemented and data were collected for the selected culverts. Data analysis so far has shown satisfactory performance with a maximum deflection of 0.117 inch and a maximum stress of 7.82 ksi, which is only about 24% of the estimated yield stress of the culverts.

The load test was successfully implemented and the tested culverts performed satisfactorily. The choice of instruments and dataloggers made it very easy to perform the tests and visualize live data during the tests, however, future load tests could include more of these sensors across the culvert for better comparison with results from numerical analyses. A dynamic test would be helpful to better study the behavior of the culverts and how the responses change under a moving load. This will help validate the changes in stresses as the truck moves over the culvert.

Better investigation and consideration of other factors that could impact test results, such as the extent of damage in the pavement layer and how it affects the load transferred from the truck load down to the culverts. Better exploration programs for closer estimation of the material properties like yield stress of the culvert, strength and thickness of the pavement layer, and in-situ soil properties.



## **CHAPTER 6: FINITE ELEMENT ANALYSES**

### **6.1 Background**

Finite element modeling is perhaps the only analytical method that can accurately simulate the complexities and nonlinearities associated with soil modeling and soil-structure interaction that occurs with culverts, and therefore was used extensively for this project. Three different FEM software were used, (1) CANDE, (2) ABAQUS, and (3) Plaxis, which are introduced and discussed below. Each of these software offer particular advantages to solving the culvert problem. Furthermore, FEM was used for three overarching purposes: (1) predicting the response and assessing the safety of the Anniston culverts prior to testing; (2) validating simplified methods; and (3) conducting parametric analyses. This chapter describes the modeling approaches and highlights comparisons; FEM results from the various approaches are incorporated throughout the report.

### **6.2 CANDE**

CANDE (Culvert ANalysis and DEsign) is a special-purpose, plane-strain finite element computer program developed specifically for the structural design and analysis of soil bridges, buried culverts and underground structures. CANDE is applicable to practically all cross-sectional shapes and materials including corrugated metal, reinforced concrete and thermoplastics. It was first introduced in 1976 under sponsorship of the Federal Highway Administration (FHWA), and has been routinely upgraded since. It has the ability to simulate important construction stage effects and live load position variation (Katona 2019).

Although its development and validation over the years is robust, and its features offer great convenience for culvert design, CANDE has significant inherent weaknesses that must be

understood by any analyst that is using it. The first of these are the assumptions associated with plane-strain finite element analyses, which have significant implications with the tire pressure loading idealization. The other profound limitation specifically associated with CANDE’s use for load rating of flexible culverts is that the load response of systems such as those studied herein are extremely nonlinear. This means that the rating factor output by CANDE when the actual load intensity for a given vehicle is applied will likely be inaccurate and higher than a true reflection of capacity. The most appropriate approach is to identify the critical vehicle position and then increase the load intensity until CANDE reflects a rating of unity (approximately 1.0), and then that load magnification provides a reasonable approximation of the rating factor. This approach is subsequently denoted as “level 2” CANDE analyses. There are many other important limitations, such as lack of mesh refinement abilities and approaches for simulating pavement effect.

### **Material and section properties**

The sectional properties of corrugation 1 ½ x 6 inch for the Anniston culverts are provided in Table 6.1. Young’s modulus = 29e6 psi, Poisson’s ratio = 0.3, and density = 0.282 lb/in<sup>3</sup>. The corrugated steel behavior was modelled as elastic-plastic. All CANDE analyses included geometric nonlinear stiffness updates that capture large deformation and buckling modes.

**Table 6.1. Dimensions and cross-section properties of corrugated steel plates used in the Anniston culverts.**

<b>Corrugation (in x in)</b>	<b>Specified thickness (in)</b>	<b>Area of pipe wall (in<sup>2</sup>/in)</b>	<b>Moment of inertia (in<sup>4</sup>/in)</b>	<b>Section of modulus (in<sup>3</sup>/in)</b>	<b>Yield stress of pipe seam (psi)</b>	<b>Yield stress (ksi)</b>
1.5x6	0.249	0.27675	0.0681	0.0784	39747	33

**Pavement:** Modeled with elastic beam elements. Density = 140 lb/ft<sup>3</sup>; Young's modulus = 200,000 psi; Poisson's ratio = 0.2; thickness = 2.5 inch.

**In-situ soil:** Model type is based on SW100 in Duncan and Selig formulation. Density is considered as zero **because in-situ soil is already at rest under its own weight before the arch is installed**. Non-zero body weight would cause in-situ soil to deform and fictitiously distort the steel arch (CANDE 2019). LRFD stiffness control = 0. Moduli averaging ratio = 1.

**Backfill:** Model type is based on ML95 Duncan and Selig formulation; density = 112 lb/ft<sup>3</sup>; LRFD stiffness control = 0; moduli averaging ratio = 0.5.

**Footing:** Model type is isotropic linear elastic. **Density is set as zero to avoid arch distortion**. Young's modulus = 3.6e6 psi; Poisson's ratio = 0.17.

**Rock:** The in-situ soil beneath the footings was simulated as rock to minimize the settlement as is shown as the green layer in Figure 6.1. Model type for rock is isotropic linear elastic. Density is zero. Young's modulus = 6e6 psi; Poisson's ratio = 0.1.

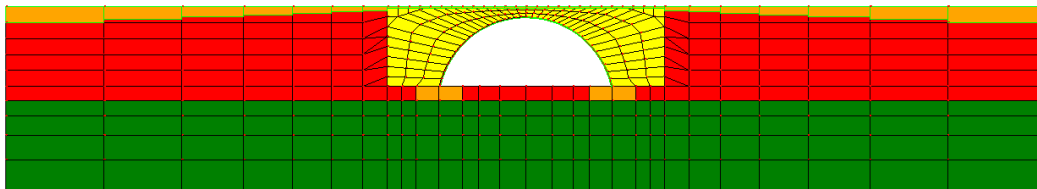


**Figure 6.1. Mesh plot of arch culvert.**

**Interface material properties between steel corrugation and soil:**

Coefficient of friction = 0.3; tensile breaking force of contact nodes = 10 lb/inch;

gap distance in normal direction = 0 inch.

## Resistance Factors for LRFR

According to AASHTO LRFD Table 12.5.5-1, the resistance factors for metal arch culvert structures are as shown in Table 6.2.

**Table 6.2. Resistance Factors**

Thrust stress yielding	1
Global buckling	1
Seam strength	0.67
Plastic penetration	0.9

## Load factors

The load factors and modifiers for buried structures are specified in AASHTO LRFD 3.4.1 as shown in Table 6.3. If the load cases produce worst-case scenario, the maximum load factor  $\gamma_{\max}$  and net load modifier  $\eta$  were used. On the other hand, the minimum load factor  $\gamma_{\min}$  and the reverse value of net load modifier  $1/\eta$  were used if the load cases do not produce worst-case scenarios but may generate over compensating results.

**Table 6.3. Load factors and load modifiers for buried corrugated metal pipe or arch.**

Culvert Type	Dead Load Culvert (DC)			Earth Fill Loading (EB)			Live Load (LL)	
	$\gamma_{\max}$	$\gamma_{\min}$	$\eta_{DC}$	$\gamma_{\max}$	$\gamma_{\min}$	$\eta_{EB}$	$\gamma_{\max}$	$\eta_{LL}$
Corrugated metal arch	1.25	0.9	1.05	1.95	0.9	1.05	1.30	1.00

$\gamma_{\max}$  = maximum load factor

$\gamma_{\min}$  = minimum load factor

$\eta_{DC}$  = net load modifier for DC load case = {(ductility)(redundancy)(importance)}

$\eta_{EB}$  = net load modifier for EB load case = {(ductility)(redundancy)(importance)}

$\eta_{LL}$  = net load modifier for LL load case = {(ductility)(redundancy)(importance)}

For the first load step (Figure 6.2) when the metal structure is present and is only loaded with its own weight, the load factor for dead load culvert (DC) =  $\gamma_{max} \times \eta_{DC} = 1.25 \times 1.05 = 1.3125$ .

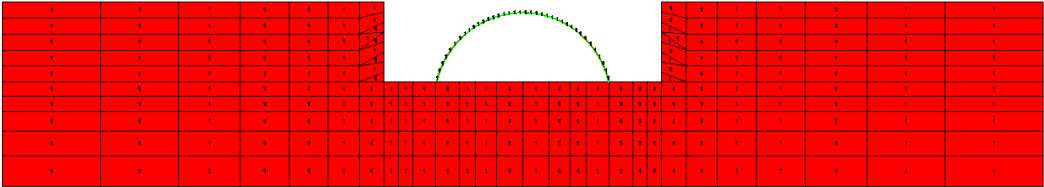


**Figure 6.2. First construction increment for installation of metal structure.**

For the load steps when earth fill layers of soil are compacted along the sides of the culvert as shown in Figure 6.3, in order to avoid overestimating the benefit from inward movement caused by lateral pressure, the load factors for earth fill loading (EB) =  $\gamma_{min} \times 1/\eta_{EB} = 0.9 \times 1/1.05 = 0.8571$ .

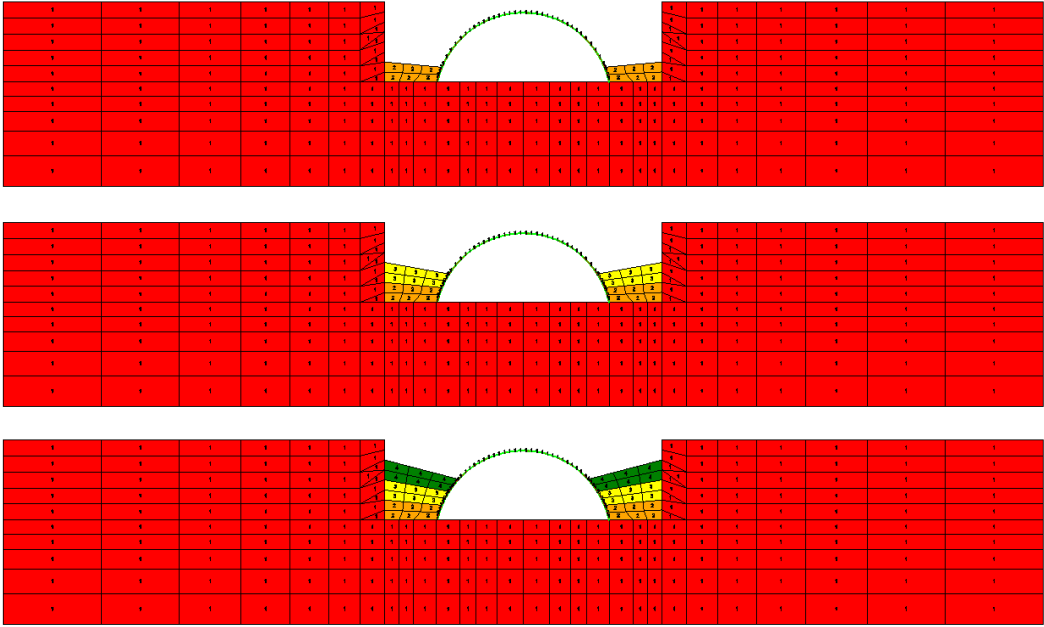


**Figure 6.3. Construction increments for soil along sides of culvert.**

For the load steps when earth fill layers of soil are placed on top of culvert as shown in Figure 6.4, the load factors for earth fill loading (EB) =  $\gamma_{max} \times \eta_{EB} = 1.95 \times 1.05 = 2.0475$ .



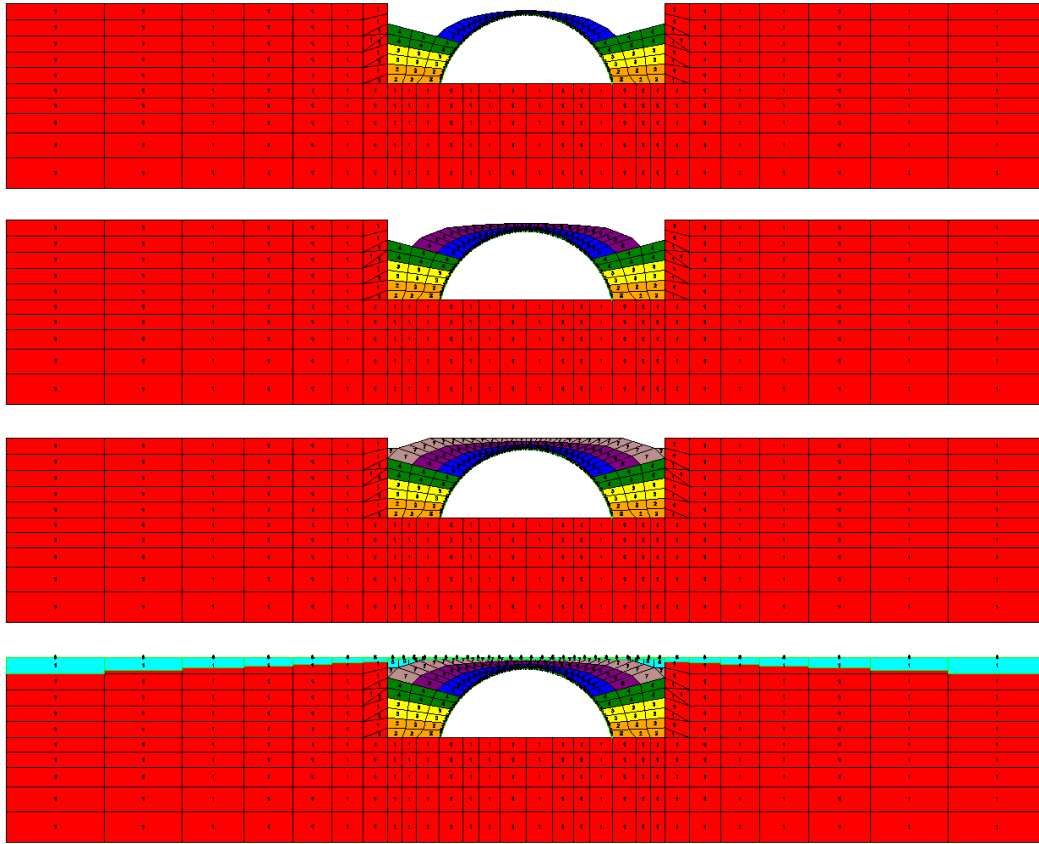


**Figure 6.4. Construction increments for soil over the culvert.**

The final load step represents the application of live load as shown in Figure 6.5. The operating load rating factor for LC-5 truck (LL) =  $\gamma_{\max} \times \eta_{LL} = 1.30 \times 1.0 = 1.30$ .

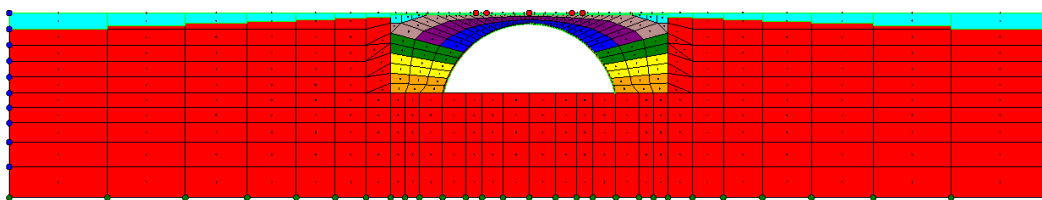


**Figure 6.5. Final construction increment for live load.**

### **Live load on culvert surface through CANDE Tool Box**

#### **Dynamic Impact Factor**

Based on AASHTO LRFD 3.6.2.2, the dynamic load allowance for culverts

$$IM = 33(1.0 - 0.125D_E)\% \geq 0\%$$

$D_E$  = the minimum depth of earth cover above the structure (ft)

### Multiple Presence Factors

Based on AASHTO LRFD 3.6.1.1.2, the multiple presence factors for ADTT of 5000 trucks in one direction are presented in Table 6.4. If  $100 \leq \text{ADTT} \leq 1000$ , factors  $m$  should be adjusted by 95%. If  $\text{ADTT} < 100$ ,  $m$  are adjusted by 90%.

**Table 6.4. Multiple Presence Factors  $m$**

Number of Loaded Lanes	Multiple Presence Factors $m$
1	1.20
2	1.00
3	0.85
>3	0.65

In this study, the effect of one loaded lane controls and ADTT was determined to be less than 100, thus, the multiple presence factor  $m = 1.20 \times 90\% = 1.08$ .

### Longitudinal load-spreading

The Continuous Load Spreading (CLS) procedure is used to account for longitudinal load-spreading. This method is more accurate because, instead of reducing the surface pressure, the CLS increases the global stiffness matrix as a continuous function of soil depth using the Elasticity-Based-Method for load-spreading. Using this procedure, all stress states throughout the entire range of soil depths are very close to the 3D solution. The 3D stiffness effect is ignored in this study because the stiffness of corrugated metal arch or pipe in longitudinal direction is too weak to provide additional bending and twisting resistance against 3D footprint load (CANDE 2019).

### Select node-loading method for axles other than the key axle

Non-key axle load is reasonably applied to both nodes in proportion to the node's proximity to the axle.

### Incremental loading for load rating

The culvert is loaded with the heaviest axle positioned directly over the crown. The wheel footprint width and length are calculated per AASHTO LRFD C3.6.1.2.5:

$$\text{Tire width (in)} = P / 0.8$$

$$\text{Tire Length (in)} = 6.4 \gamma (1 + IM / 100)$$

Where:

$\gamma$  = load factor

$IM$  = dynamic load allowance percent

$P$  = design wheel load (kip)

The centerline distance between wheels along an axle is 6 ft. The final capacity multiplier is computed by trial. Load approximate to 0.5 times the truck weight is increasingly added on the culvert until the rating factor is less than 1 or the solution does not converge, whichever occurs first. For example, 1, 1.5, 2, 2.5, 3, etc. times the truck weight, in turn, is loaded at the same position over the culvert until it fails, then the multiplier before failure is the final carrying capacity.

## 6.3 ABAQUS

### General Background

Abaqus FEA is a comprehensive and versatile software suite for computer-aided engineering, including for finite element analysis. The advantage of using ABAQUS is in its versatility, including three dimensional meshes and a wide range of element types and material

models. The disadvantage compared to CANDE is that features specific to the design and analysis of culvert structures are not embedded. The analyst must have a very high degree of advanced FEM competence, and general purpose 3D analysis requires significantly more model development time and computing power.

### Soil Properties

The Mohr-Coulomb constitutive model was used to simulate soil, not only because it captures the primary features of soil behavior under live load, but also due to its modelling simplicity. It has also been proven to be an appropriate model to produce structural response of culvert under live loads with sufficient accuracy (NCHRP 2009). Input parameters for the Mohr-Coulomb model are modulus of elasticity,  $E$ , Poisson's ratio,  $\nu$ , cohesion,  $c$ , angle of friction,  $\phi$ , and dilatancy angle,  $\psi$ .  $E$  and  $\nu$  were defined by Selig (1990) (Table 6.5) based on depth,  $c$  is given the same value as in the triaxial test parameters of Duncan-Selig model (Selig 1988) in Table 6.6.

The friction angle depends on two definitions:

$$\phi = \phi_0 - \Delta\phi \log_{10}(\sigma_3 / P_a) \text{ from Selig (1988)} \quad (6.1)$$

and

$$\sigma_3 = (1 - \sin \phi) \sigma_1 \text{ from Jaky (1944)} \quad (6.2)$$

Where

$\phi_0$ : value of  $\phi$  when  $\sigma_3 = P_a$  in Table 6.6

$\Delta\phi$ : reduction in  $\phi$  for a ten-fold increase in  $\sigma_3$  in Table 6.6

$P_a$ : atmospheric pressure (14.7 psi)

$\sigma_1$ : the first principal stress = the vertical stress

The solver function in Microsoft Excel was used to calculate  $\phi$  and the dilatation angles  $\psi$  were estimated by friction angles minus 30 deg.

**Table 6.5. Elastic soil properties for backfill (Selig 1990).**

Gravelly Sand (SW)						
Maximum Principal Stress Level (psi)	95% Standard Compaction			85% Standard Compaction		
	E (psi)	B (psi)	$\nu$	E (psi)	B (psi)	$\nu$
0 to 1	1,600	2,800	0.40	1,300	900	0.26
1 to 5	4,100	3,300	0.29	2,100	1,200	0.21
5 to 10	6,000	3,900	0.24	2,600	1,400	0.19
10 to 20	8,600	5,300	0.23	3,300	1,800	0.19
20 to 40	13,000	8,700	0.25	4,100	2,500	0.23
40 to 60	16,000	13,000	0.29	4,700	3,500	0.28
Sandy Silt (ML)						
Maximum Principal Stress Level (psi)	95% Standard Compaction			85% Standard Compaction		
	E (psi)	B (psi)	$\nu$	E (psi)	B (psi)	$\nu$
0 to 1	1,800	1,900	0.34	600	400	0.25
1 to 5	2,500	2,000	0.29	700	450	0.24
5 to 10	2,900	2,100	0.27	800	500	0.23
10 to 20	3,200	2,500	0.29	850	700	0.30
20 to 40	3,700	3,400	0.32	900	1,200	0.38
40 to 60	4,100	4,500	0.35	1,000	1,800	0.41
Silty Clay (CL)						
Maximum Principal Stress Level (psi)	95% Standard Compaction			85% Standard Compaction		
	E (psi)	B (psi)	$\nu$	E (psi)	B (psi)	$\nu$
0 to 1	400	800	0.42	100	100	0.33
1 to 5	800	900	0.35	250	200	0.29
5 to 10	1,100	1,000	0.32	400	300	0.28
10 to 20	1,300	1,100	0.30	600	400	0.25
20 to 40	1,400	1,600	0.35	700	800	0.35
60	1,500	2,100	0.38	800	1,300	0.40

**Table 6.6. Triaxial Test Parameters (Selig 1988).**

Soil Type	Standard Compaction (%)	Density (pcf)	$K$	$n$	$R_f$	$B_i / P_a$	$\epsilon_u$	$c$ (psi)	$\phi_0$ (deg)	$\Delta\phi$ (deg)
Gravelly Sand (SW)	95	141	950	0.60	0.70	74.8	0.02	0	48	8
	90	134	640	0.43	0.75	40.8	0.05	0	42	4
	85	126	450	0.35	0.80	12.7	0.08	0	38	2
	80	119	320	0.35	0.83	6.1	0.11	0	36	1
	60	91	54	0.85	0.90	1.7	0.23	0	29	0
Sandy Silt (ML)	95	127	440	0.40	0.95	48.3	0.06	4.0	34	0
	90	120	200	0.26	0.89	18.4	0.10	3.5	32	0
	85	114	110	0.25	0.85	9.5	0.14	3.0	30	0
	80	107	75	0.25	0.80	5.1	0.19	2.5	28	0
Silty Clay (CL)	60	66	16	0.95	0.55	1.3	0.43	0	23	0
	95	119	120	0.45	1.00	21.1	0.13	9.0	15	4
	90	112	75	0.54	0.94	10.2	0.17	7.0	17	7
	85	106	50	0.60	0.90	5.2	0.21	6.0	18	8
	80	100	35	0.66	0.87	3.5	0.25	5.0	19	8.5
	60	56	16	0.95	0.75	0.7	0.55	0	23	11



Duncan-Selig properties from inorganic silts and fine sands at 95 percent standard compaction (ML95) were used to compute the corresponding Mohr-Coulomb properties of backfill presented in Table 6.7. Instead of using variable angles of friction calculated from the stress state at each different depth, one friction angle was used for all depth calculated based on vertical stress  $\sigma_1$  equal to  $0.5 \text{ ft} \times 127 \text{ pcf} = 63.5 \text{ psf}$ . Only the structural responses due to live load were needed for the purposes of this research, therefore the dead load effect was extracted.

**Table 6.7. Mohr-Coulomb properties for Backfill ML95.**

Soil Type	Density (pcf)	Depth (ft)	Modulus of Elasticity (psi)	Poisson's Ratio	Angle of Friction	Angle of Dilatancy	Cohesion (psi)
Backfill ML95 (Mohr-Coulomb)	127	0 to 1	1800	0.34	34.0	4.0	4.0
		1 to 6	2500	0.29			
		6 to 11	2900	0.27			

### Corrugated steel culvert modelling approach

The metal cross section corrugation was simulated using shell elements with orthotropic properties. Equivalent orthotropic Young's moduli in the longitudinal directions  $E_l$  and circumferential directions  $E_c$  and thickness of the plate shell  $h$  were calculated to match 3 of 4 stiffnesses of the actual corrugation (circumferential and longitudinal axial stiffnesses  $A_1, A_2$  and circumferential and longitudinal bending stiffnesses  $I_1, I_2$ ). The circumferential axial and bending stiffnesses  $A_1, I_1$  and longitudinal bending stiffness  $I_2$  of actual corrugation were satisfied.

$$E_c \frac{1}{12} h^3 = EI_1 \quad (6.3)$$

$$E_c h = EA_1 \quad (6.4)$$

$$E_l \frac{1}{12} h^3 = EI_2 \quad (6.5)$$

where  $E$ : young's modulus of steel = 29e6 psi. Equivalent parameters of the orthotropic shell elements for each corrugation simulated in this study are provided in Table 6.8.

**Table 6.8. Summary of orthotropic structural properties for corrugated metal pipe and arch.**

Corrugation	Corrugation properties						
	Specified Thickness (in.)	$EI_1$ (lb * in. <sup>2</sup> /in.)	$EA_1$ (lb/in.)	$EI_2$ (lb * in. <sup>2</sup> /in.)	$EA_2$ (lb/in.)		
6"x1-1/2"	0.249	1974900	8025750	37309	7221000		
Corrugation	Equivalent plate properties						
	Wall Thickness (in.)	$E_c$ (psi)	$E_l$ (psi)	$G_{13}$ (psi)	$G_{23}$ (psi)	$G_{12}$ (psi)	Yield Stress (psi)
6"x1-1/2"	1.7184	4670520	88234	1796354	33936	246903	5222

The density of the shells was set to zero because the dead load effect from steel structure is negligible compared to earth weight. The shear moduli out of plane: shear deformation over stiff direction  $G_{13}$  and shear deformation over weak direction  $G_{23}$  were calculated by dividing the  $E_c$  and  $E_l$  by  $2(1 + \nu_{steel})$ , and for the in-plane shear modulus  $G_{12}$  the square root of  $E_c$  and  $E_l$  is divided by  $2(1 + \nu_{steel})$ .

$$G_{13} = \frac{E_c}{2(1 + \nu_{steel})} \quad (6.6)$$

$$G_{23} = \frac{E_l}{2(1 + \nu_{steel})} \quad (6.7)$$

$$G_{12} = \sqrt{\frac{E_l * E_c}{2(1 + \nu_{steel})}} \quad (6.8)$$

where  $\nu_{steel}$ , Poisson's ratio for steel = 0.3. The equivalent yield stress was calculated based on the assumption that the elastic moment causing the first yield (33000 psi) in the extreme fiber of corrugation also caused the surface yield in the orthotropic sections (Elshimi 2011).

### Model Dimensions

The width in the direction parallel to the span is 300 inch, because the culvert has span of 200 inch and rise of 52 inch, and any live load more than 50 inch away from any side of the span will only have negligible impact on the culvert. The length in the longitudinal direction is 240 inch, which was chosen because the axle distance of any rating truck is 72 inch. For shallow cover 240 inch is long enough to contain all the live load effect on the structure in longitudinal direction. (Figure 6.6)

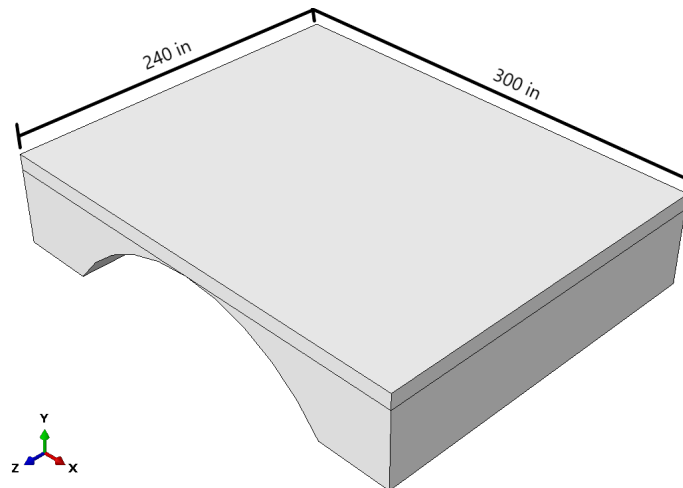


**Figure 6.6. ABAQUS model dimensions.**

### Boundary conditions

Boundary conditions for each surface and edge are defined in Table 6.9. 0 represents fixed in the designated directions, otherwise the degree of freedom is free. T1, T2, T3 are translations in the x, y, z directions, respectively; R1, R2, R3 are rotations about x, y, z directions, respectively. The x, y, z directions are parallel to the edges of model as illustrated in Figure 6.7. (The x, y, z

directions are pointing to the transverse, vertical and longitudinal direction respectively to the pipe or arch axial direction.)

**Table 6.9. Boundary conditions.**

Faces and Edges	T1	T2	T3	R1	R2	R3
Arch-Footings	0	0	0	0	0	
Pave-Edges	0		0	0	0	
Soil-Bottoms	0	0	0	0	0	0
Soil-Sides	0		0	0	0	

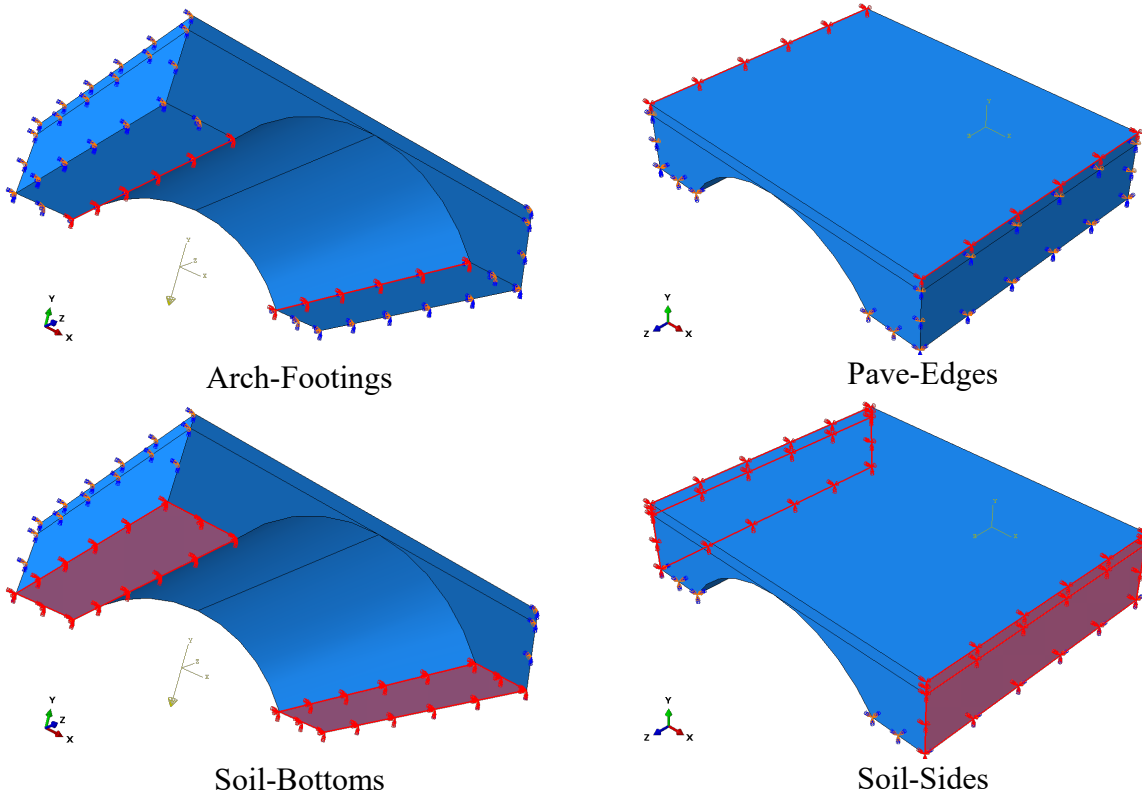


**Figure 6.7. Boundary fixities.**

## Mesh and solution approach

The soil was partitioned into several layers, each of which was assigned with different Mohr-Coulomb properties based on its depth. The soil was meshed by C3D15: 15-node triangular prism elements with 6 DOF/node (3 translations and 3 rotations) in approximate size of 10 inch (Figure 6.8). The arch was meshed by S8R5: 8-node quadrilateral shell elements with 5 DOF/node (3 translations and 2 in-plane rotations, no rotation about the shell normal) in approximate size of 8 inch while the pavement was meshed using S4: 4-node quadrilateral shell elements with 6 DOF/node (3 translations and 3 rotations) and had the approximate size of 10 inch (Figure 6.8). Only the pavement elements were assigned with linear geometric order and nonlinear material analysis; all the other elements were given nonlinear geometric order and nonlinear material analysis. Figure 6.10 shows a typical deformed mesh for structure under loading, where the deformation scale factor was magnified by 100 times.

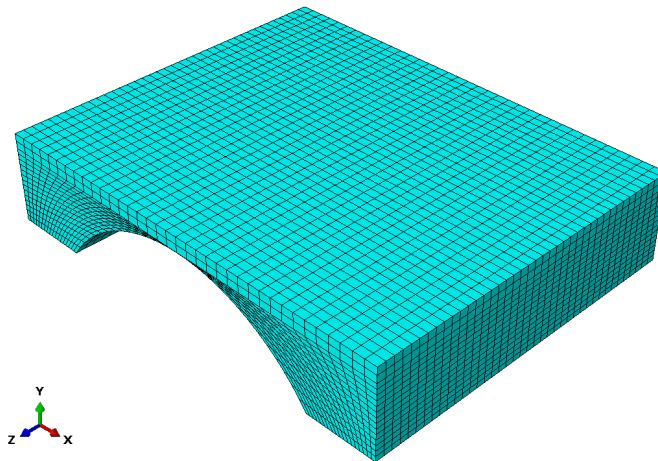


**Figure 6.8. Typical soil mesh.**

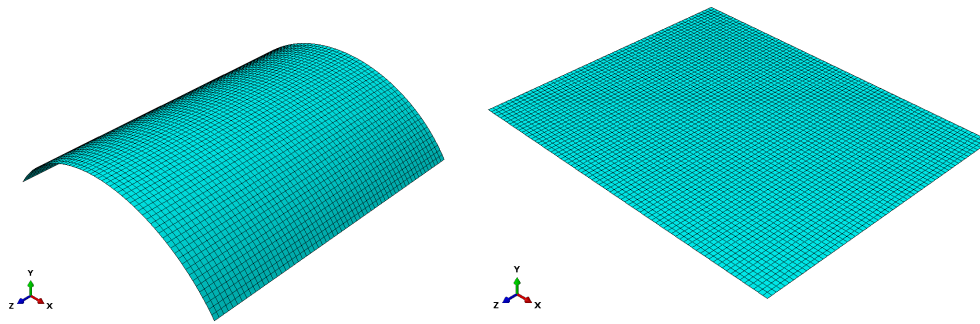


**Figure 6.9. Typical mesh for arch (left) and pavement (right).**

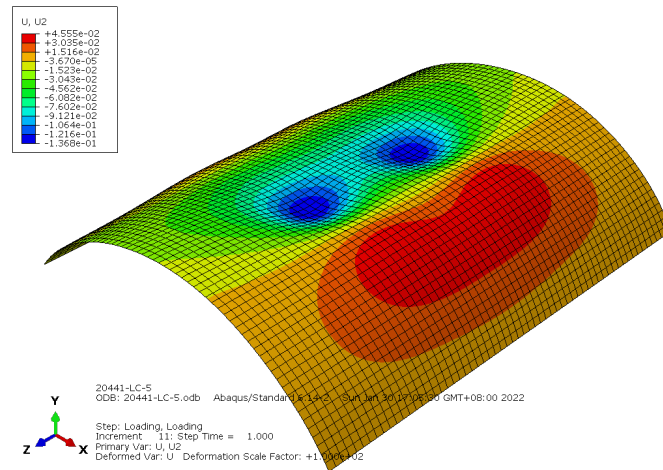


**Figure 6.10. Typical deformed structure under loading (different shadings represent the vertical displacement).**

### Interface property between soil and steel

A friction coefficient = 0.3 was assigned to the contact surface between backfill and metal culvert to simulate soil and structure interaction. This is the same soil-structure interface friction approach that is used in the design of driven piles and retaining structures (USACE, 1991).

## 6.4 PLAXIS 3D

### General

Similar to ABAQUS, PLAXIS 3D has three-dimensional modeling capabilities. However, it contains feature that are specifically developed for geotechnical analysis, and therefore was used as an additional analytical tool and results check.



## Soil Properties

The soil volumes were modelled using 10-node tetrahedral elements with three degrees of freedom per node ( $u_x$ ,  $u_y$  and  $u_z$ ) (Bentley 2021a). The ML-95 backfill was modelled using the linear elastic perfectly plastic Mohr-Coulomb soil model with input parameters for Young's modulus ( $E$ ), poisson's ratio ( $\nu$ ), cohesion ( $c$ ), friction angle ( $\phi$ ), dilatancy angle ( $\psi$ ) and tensile cut off/tensile strength ( $\sigma_t$ ). The soil properties as defined for the ABAQUS models were adapted for the PLAXIS 3D model. The bedrock layer was modeled using a linear elastic model with input parameters for Young's modulus ( $E = 263 \times 10^3$  psi) and Poisson's ratio ( $\nu = 0.25$ ).

## Corrugated steel culvert modelling approach

The corrugated steel was modelled using 6-node triangular plate elements with six degrees of freedom per node: three translational degrees of freedom ( $u_x$ ,  $u_y$ , and  $u_z$ ) and three rotational degrees of freedom ( $\phi_x$ ,  $\phi_y$ , and  $\phi_z$ ) (Bentley 2021b). The plate formulation is capable of simulating equivalent orthotropic properties and the input parameters are: equivalent plate thickness ( $d$ ), Young's modulus in the first axial direction ( $E_1$ ), Young's modulus in the second axial direction ( $E_2$ ), In-plane shear modulus ( $G_{12}$ ), out-of-plane shear modulus related to shear deformation over first direction ( $G_{13}$ ), out-of-plane shear modulus related to shear deformation over second direction ( $G_{23}$ ), and Poisson's ratio ( $\nu_{12}$ ). The input parameters are expressed in the following equations:

$$E_1 = \frac{12EI_1}{d^3} \quad (6.9)$$

$$E_2 = \frac{12EI_2}{d^3} \quad (6.10)$$

$$G_{12} = \frac{6EI_{12}}{(1+\nu)d^3} \quad (6.11)$$

$$G_{12} = \frac{EA_{13}}{2(1+\nu)d} \quad (6.12)$$

$$G_{23} = \frac{EA_{23}}{2(1+\nu)d} \quad (6.13)$$

$$\nu_{12} < \sqrt{\frac{E_1}{E_2}} \quad (6.14)$$

where:

$I_1$  = Moment of inertia against bending over the first axis.

$I_2$  = Moment of inertia against bending over the second axis.

$I_{12}$  = Moment of inertia against torsion.

$A_{13}$  = Effective material cross section area for shear forces  $Q_{13}$ .

$A_{23}$  = Effective material cross section area for shear forces  $Q_{23}$ .

The ABAQUS parameters of the orthotropic plate elements were adapted; however, because the y and z directions are flipped in PLAXIS 3D with respect to ABAQUS,  $E_1$  was switched with  $E_2$  and  $G_{13}$  was switched with  $G_{23}$ . Hence, a modified Poisson's ratio was calculated as:

$$\nu_{modified} = \nu_{12} \frac{E_1}{E_2} \quad (6.15)$$

The modified properties used in PLAXIS 3D are shown in Table 6.10.

**Table 6.10. Modified equivalent plate properties used in PLAXIS 3D.**

<b>E<sub>1</sub></b>	<b>E<sub>2</sub></b>	<b>ν<sub>12</sub></b>	<b>G<sub>12</sub></b>	<b>G<sub>13</sub></b>	<b>G<sub>23</sub></b>
<b>(psi)</b>	<b>(psi)</b>		<b>(psi)</b>	<b>(psi)</b>	<b>(psi)</b>
84152	4670520	0.005405	388803	32366	1796354

## Soil-Structure Interface

The soil-structure interaction between the backfill and the metal plate was simulated using zero-thickness, 12-node interface elements. The properties of the interface were adapted from the surrounding soil clusters and an interface strength reduction ( $R_{inter}$ ) factor of 0.7 was assigned to simulate slipping and gapping between the plate and the surrounding soil volumes. The interface reduction factor affects the interface strength according to the relationships shown in the following equations:

$$c_i = R_{inter} c_{soil} \quad (6.16)$$

$$\tan(\phi_i) = R_{inter} \tan(\phi_{soil}) \quad (6.17)$$

$$G_i = R_{inter}^2 G_{soil} \quad (6.18)$$

$c$  and  $\phi$  are cohesion and friction angle respectively. The properties with subscript “i” represent the properties at the interface and those with subscript “soil” represent the properties from the soil clusters.

## Model Geometry

The dimensions of the model in PLAXIS 3D were adapted from the ABAQUS model. Because rotational boundary conditions could not be manually defined in PLAXIS 3D, and additional 3 ft of concrete-bedrock foundation was created with a high stiffness to simulate non deformity. A prescribed line displacement with fixed translational boundaries was then created along the contact between the plate and the foundation (Figure 6.11).

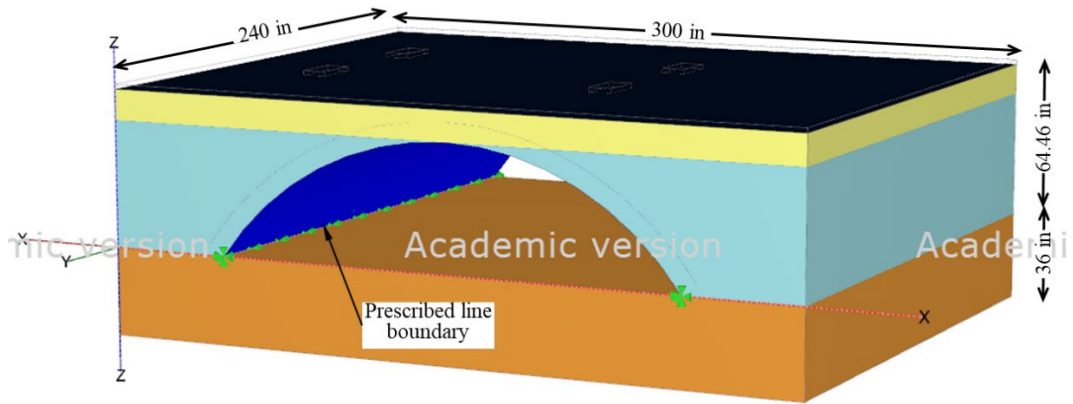


**Figure 6.11. Model Geometry**

The generated mesh used for the analyses (Figures 6.12 and 6.13) had 102852 elements and 161735 nodes, with an average element size of 8.06 inch. Mesh sensitivity was carried out to determine the proper mesh size by varying the fineness of the mesh geometry to obtain a model with negligible mesh dependency. The mesh size was reduced until a reduction in mesh size had minimal effect on the calculation output. Figure 6.14 shows a plot of the normalized maximum settlement versus the number of elements. A coarseness factor of 1.0 was used for soil volume clusters while a coarseness factor of 0.3 was used for plate elements and interface elements.

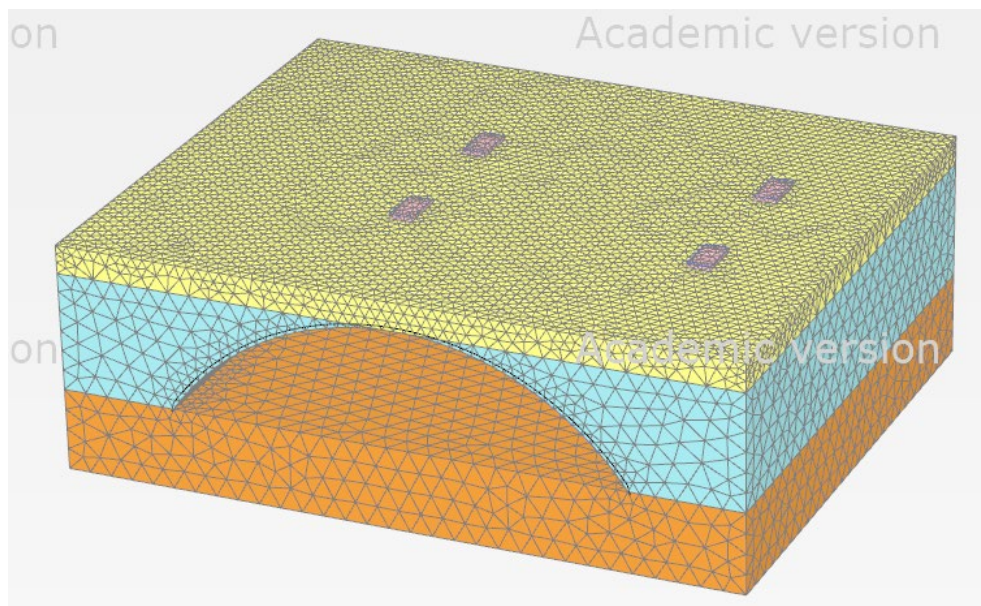


**Figure 6.12. Typical mesh for soil clusters.**

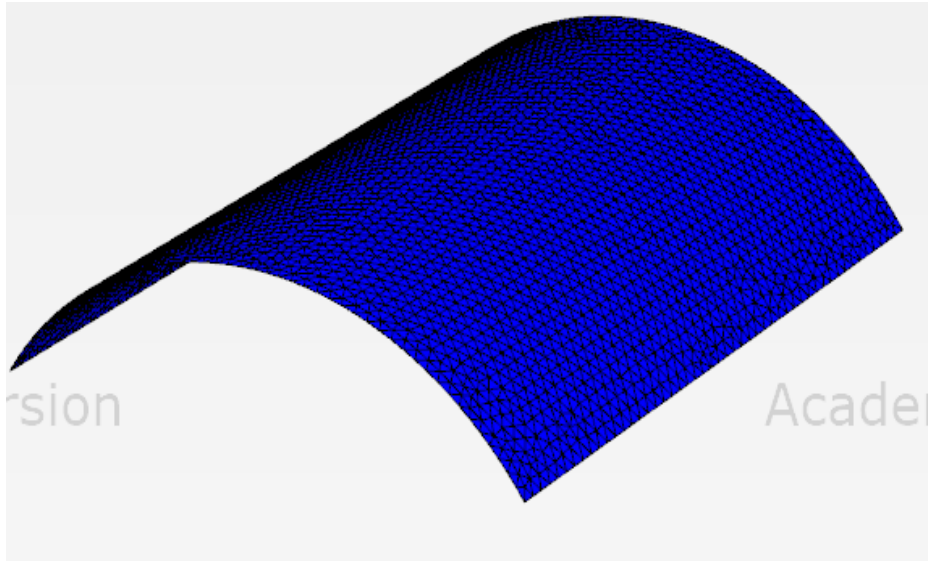


**Figure 6.13. Typical mesh for metal arch.**

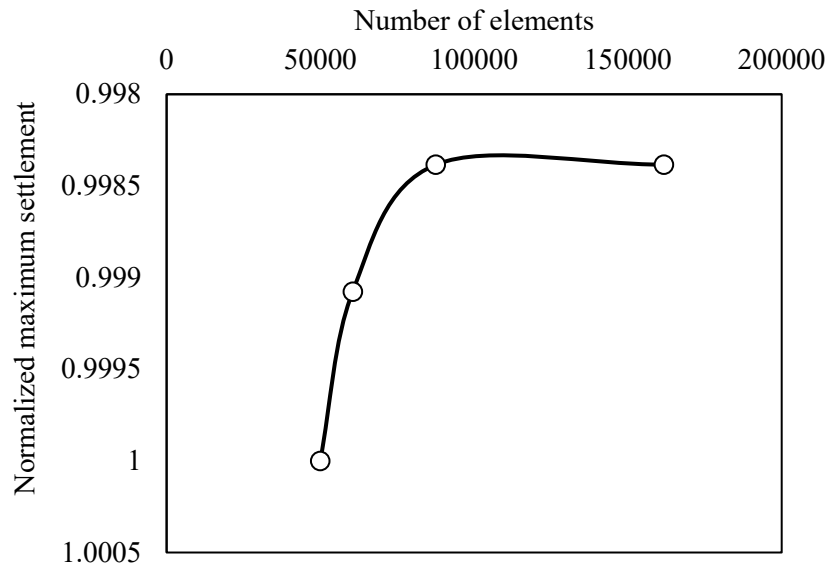


**Figure 6.14. Mesh sensitivity analysis.**

To keep the model simple, only one barrel was used in the analyses, however, a comparison was made with a model where the two barrels were used (Figure 6.15). The results showed no significant difference confirming that for the load positions considered, the presence of the second barrel does not affect the simulation results in terms of Normal forces (Figure 6.16).

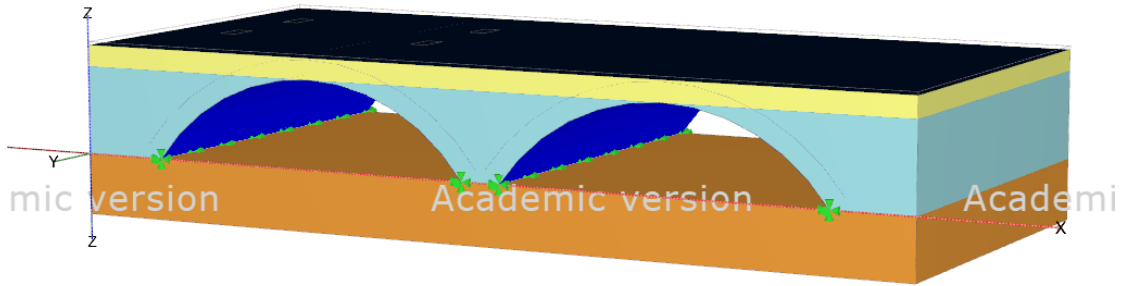


**Figure 6.15. 2-barrel culvert model in Plaxis 3D.**

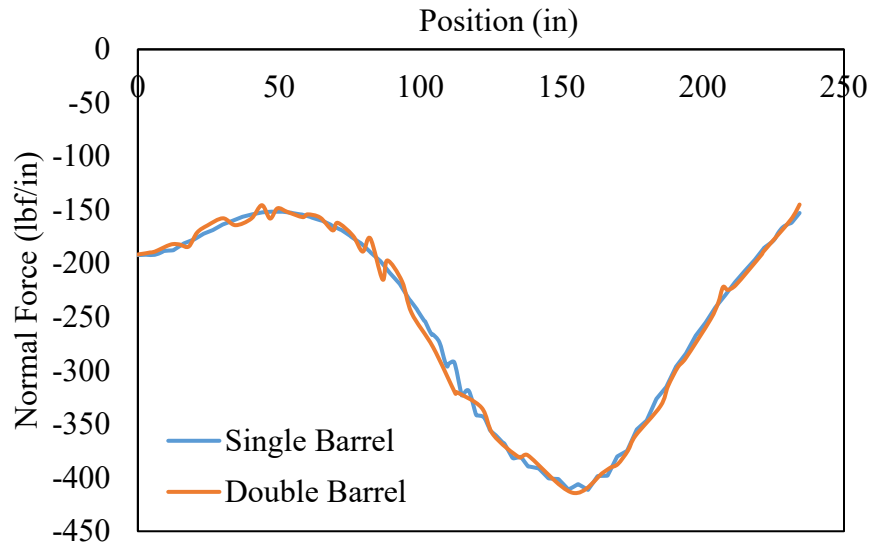


**Figure 6.16. Comparison of the output for single and double barrel models.**

### 6.5 Analytical method comparisons

The numerical approaches described above for the different programs were used to develop numerical models corresponding to each load stopping point as described in the testing program. Results were extracted at the same instrument positions relative to the truck position (a cross section at the center of the truck tire footprint and at the geometric center of the truck). Comparison of the field measured responses to the numerical simulation results for the same load and measurement positions showed reasonable agreement for both culvert structures in terms of trends and magnitude; however, the deflections predicted by the numerical analyses have been



consistently higher than the measured values.

The responses predicted by the 3D FEM programs (PLAXIS 3D and ABAQUS) showed good agreement. The responses from CANDE (plane stress) demonstrated the identical trends but were consistently higher than those predicted by PLAXIS 3D and ABAQUS. Comparing the plane stress and 3D FEM results to the field measured values, the result from 3D analyses were more accurate as the magnitudes were closer to the measured values. Load line 2 produced significantly higher responses (both measured and predicted) compared to load line 1, for both structures. Figures 6.17 to 21 show the measured and predicted deflections and strains for BIN 20433 (load line 2) while Figures 21 to 26 show the measured and predicted values for BIN 20441 (load line 2). As shown in Figures 17 through 26, the measured values were not the highest possible values as the numerical models showed higher values at locations different from the instrumented positions. Thus, because the structural responses could only be measured at a discrete number of instrument positions, the finite element models are essential for defining the magnitudes and positions of the maximum stresses and displacements.

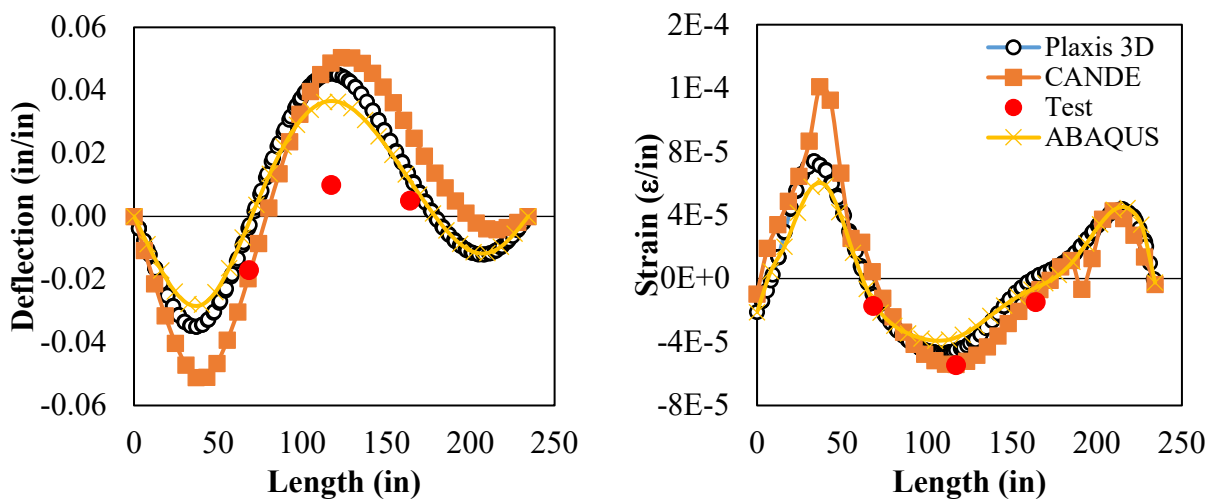


**Figure 6.17. BIN 20443 measured and predicted responses: (left) deflection, (right) strain with load truck at “start” load position (load line 2).**

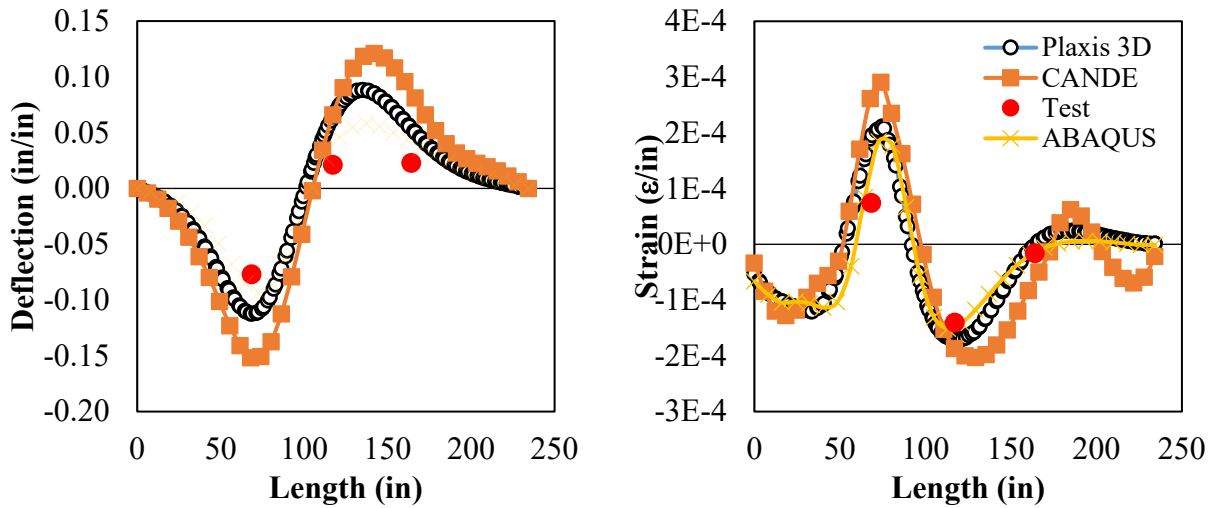


Figure 6.18. BIN 20443 measured and predicted responses: (left) deflection, (right) strain with load truck at “1/4” load position (load line 2).

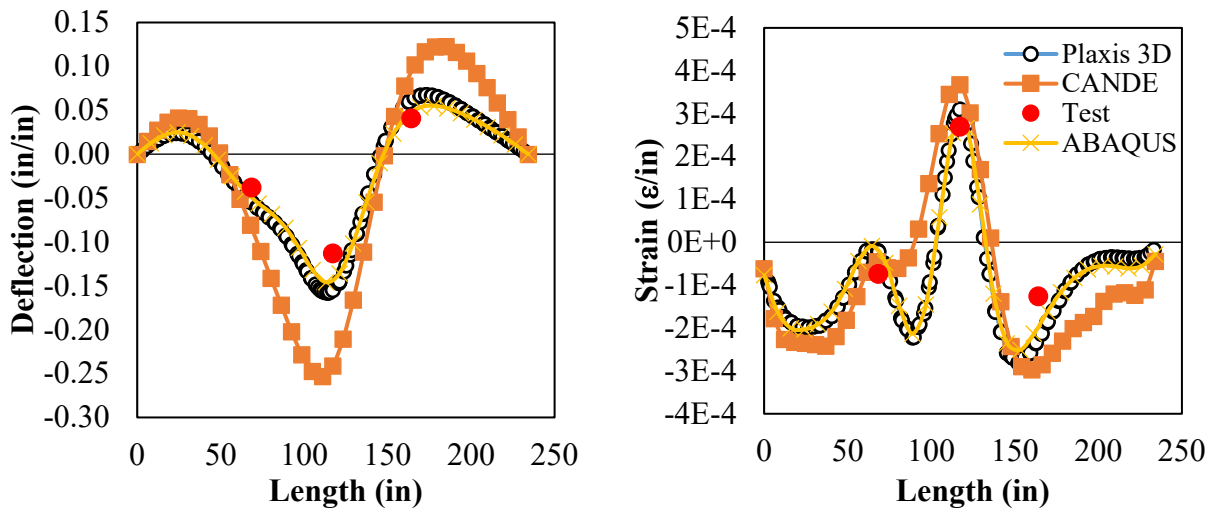
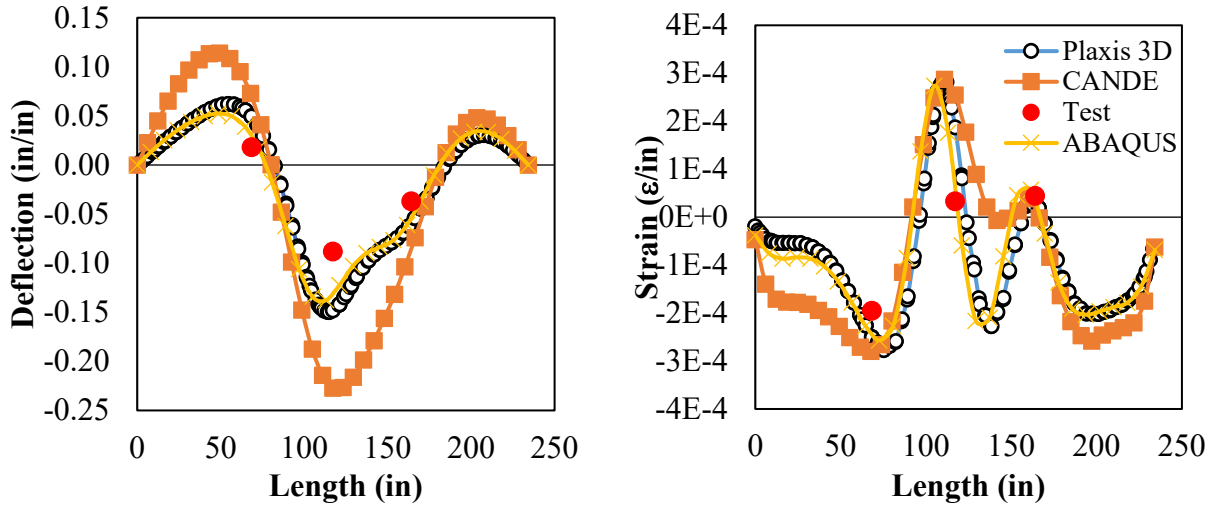
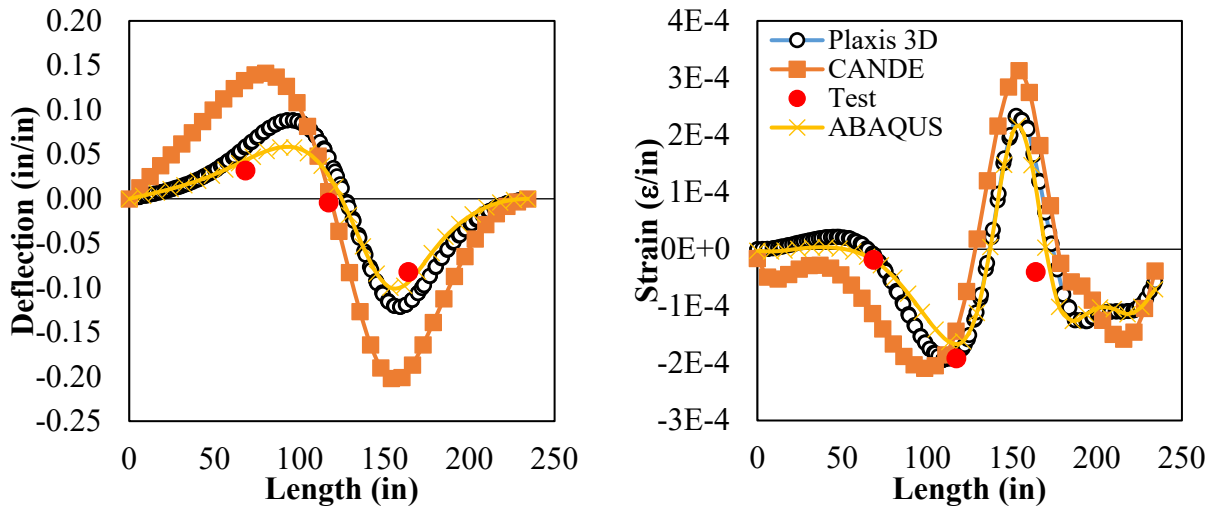


Figure 6.19. BIN 20443 measured and predicted responses: (left) deflection, (right) strain with load truck at “peak” load position (load line 2).



**Figure 6.20. BIN 20443 measured and predicted responses: (left) deflection, (right) strain with load truck at “3/4” load position (load line 2).**



**Figure 6.21. BIN 20443 measured and predicted responses: (left) deflection, (right) strain with load truck at “end” load position (load line 2).**

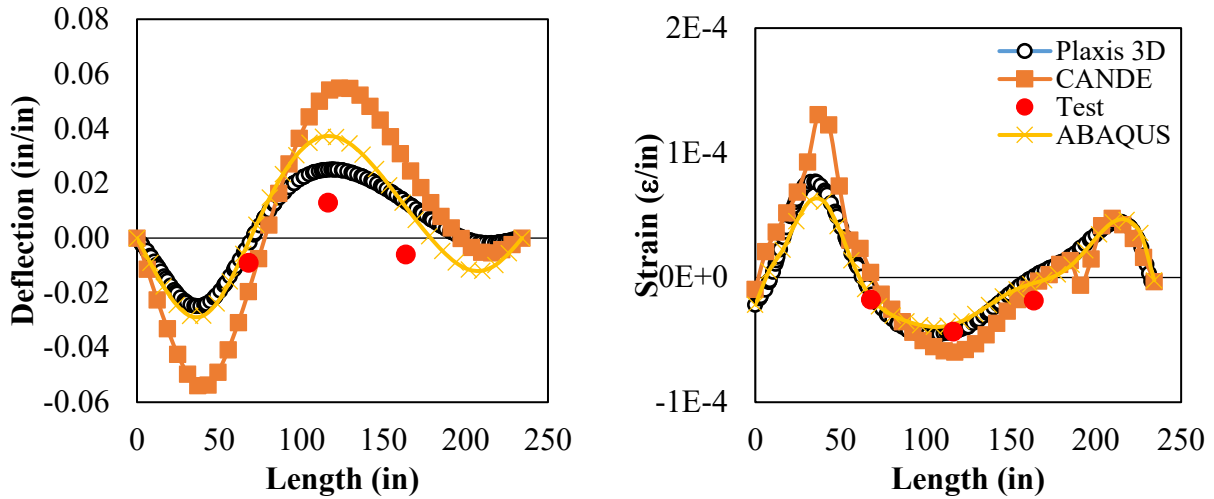


Figure 6.22. BIN 20441 measured and predicted responses: (left) deflection, (right) strain with load truck at “start” load position (load line 2).

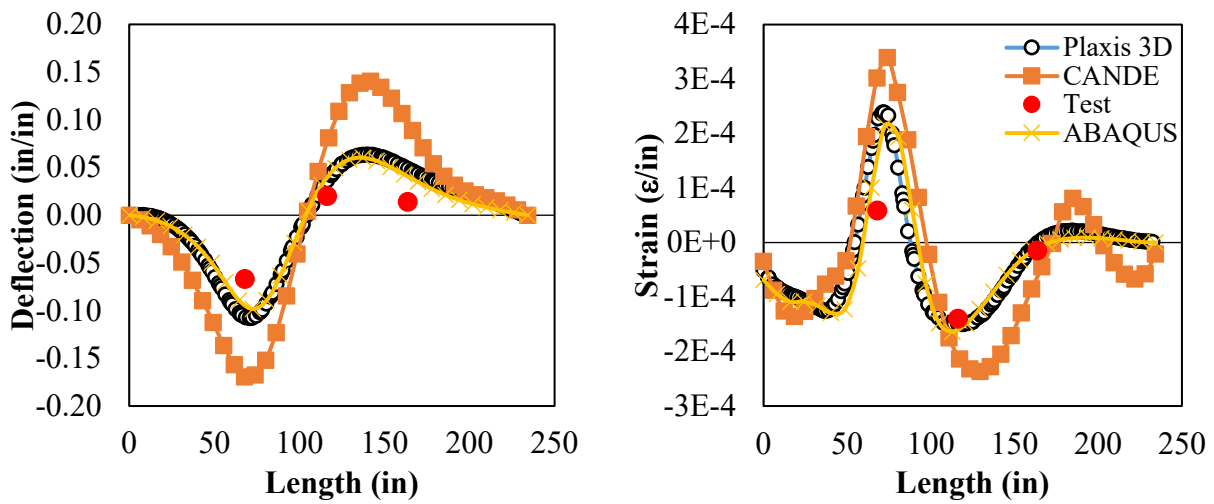


Figure 6.23. BIN 20441 measured and predicted responses: (left) deflection, (right) strain with load truck at “1/4” load position (load line 2).

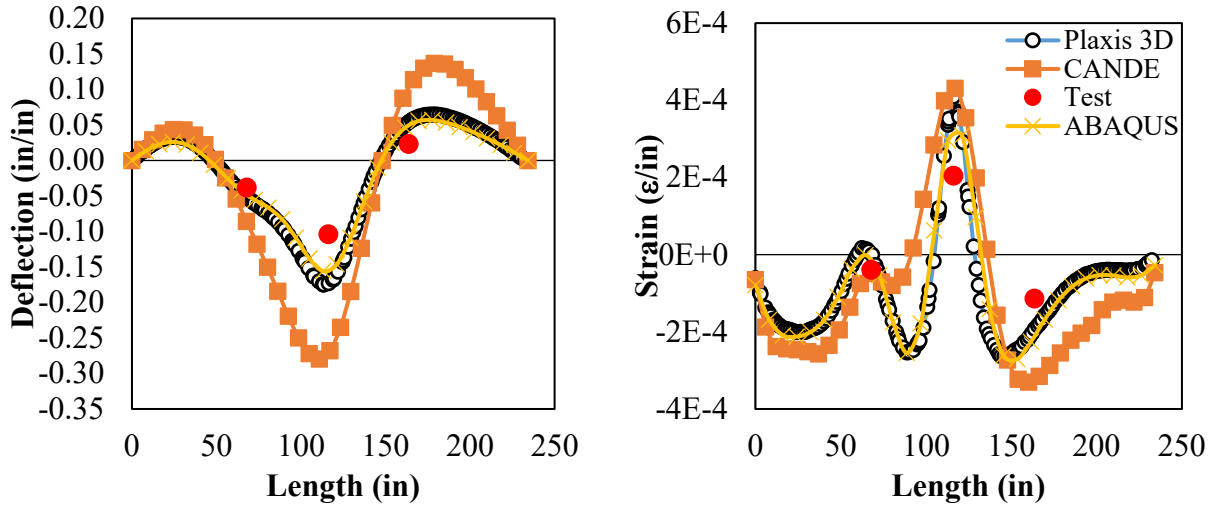


Figure 6.24. BIN 20441 measured and predicted responses: (left) deflection, (right) strain with load truck at “peak” load position (load line 2).

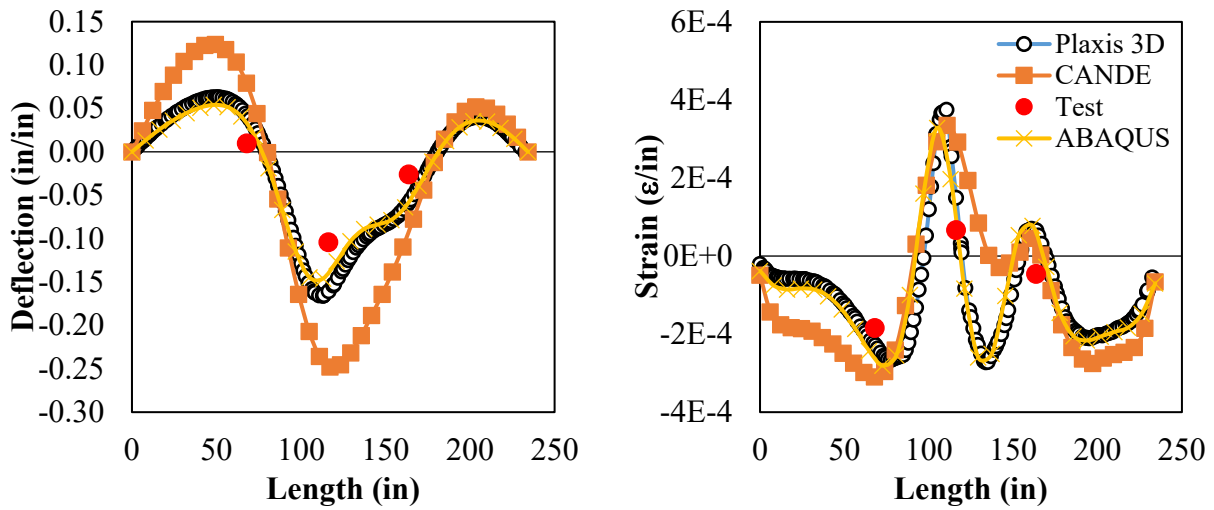
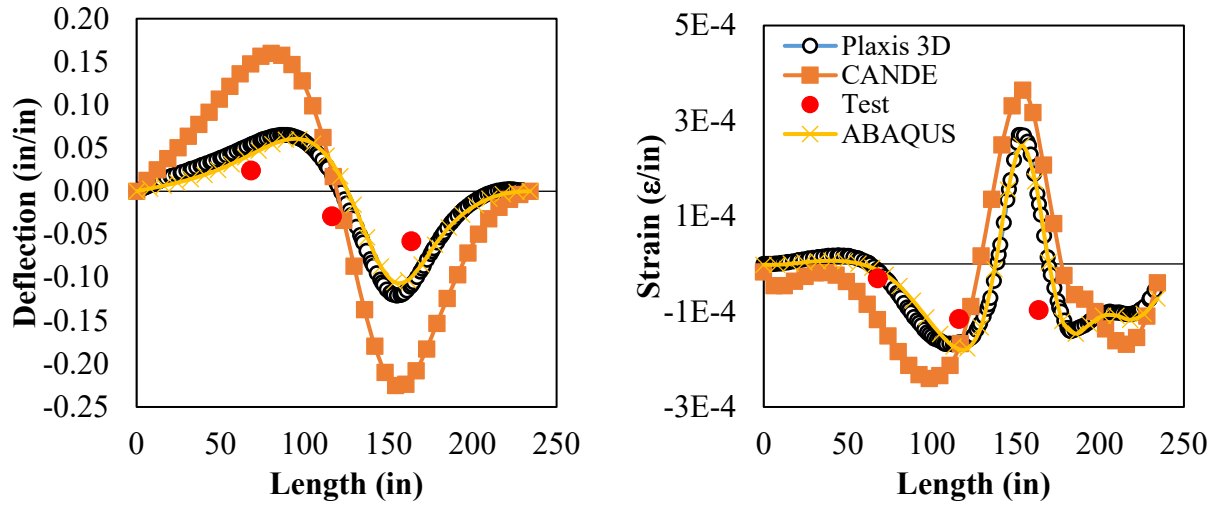


Figure 6.25. BIN 20441 measured and predicted responses: (left) deflection, (right) strain with load truck at “3/4” load position (load line 2).



**Figure 6.26. BIN 20441 measured and predicted responses: (left) deflection, (right) strain with load truck at “end” load position (load line 2).**



## CHAPTER 7: SIMPLIFIED RATING FACTOR METHODOLOGY FOR SHALLOW FILL SCENARIOS

### 7.1 Background

Existing simplified tools used to load rate metal culverts include spreadsheet-based approaches developed by the Ohio Department of Transportation (Sezen et al. 2009) and the Michigan Department of Transportation (MDOT 2016). The earliest version of simplified approach is the original ODOT spreadsheet that is based upon procedures outlined in the *National Corrugated Steel Pipe Association Design Data Sheet 19* (NCSPA 1995) and the AASHTO *Standard Specifications for Highway Bridges* (1992). However, regardless of the robustness of the structure and its performance, that method rates culverts as unsafe if the cover depth is less than the minimum cover required by AASHTO design specifications, which is the case for all of the culverts involved in the present study. The ODOT subsequently recognized and discussed the conservatism of their spreadsheet in “Verification of ODOT’s Load Rating Analysis Programs for Metal Pipe and Arch Culverts” (Sezen et al. 2009). Therefore, the rating methodology was revised in 2012 by ODOT using the arch buckling formulations presented in the *Guide to Stability Design Criteria for Metal Structures* (Galambos 1998), which was then evaluated by Ohio University for corrugated metal culverts under shallow soil covers (Sargand et al. 2015). The Michigan DOT subsequently developed their own load rating procedure that included replacing the rating factor equation that was based on the minimum cover requirement in the ODOT spreadsheet with an equation that is based upon the moments equations presented in “Design Procedures for Flexible Metal Culvert Structures” (Duncan et al. 1983; MDOT 2016).

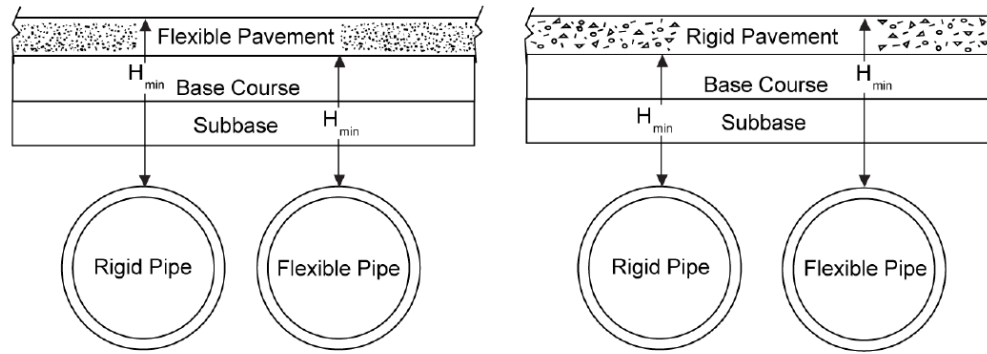
After carefully reviewing and examining the source and definition of each parameter used in these approaches and how the parameters affect the rating factors, it was found that some of these parameters were incorrectly assigned. Furthermore, for shallow cover culverts, pavement can play a significant role in reducing the moment due to live load (Burmister 1958, Poulos and Davis 1974, Abdel-Karim et al. 1990, Han et al. 2013, and Mlynarski et al. 2019), yet is merely counted as an additional layer of backfill in current rating methodologies. These weaknesses and the exclusion of pavement effect artificially amplify the structural response represented by the load rating procedures, and for culverts under shallow fill, ultimately result in rating factors that are significantly lower than their true values. The work presented in this chapter, therefore, aims to address these concerns and define an improved rating factor technique for culverts under shallow fill. The responses and rating factors calculated from these improved procedures are then compared with their corresponding results in CANDE to verify the improvement of these modifications and an example and comparisons are provided.

## **7.2 Definition and Origin of Minimum Cover Requirements**

The word “cover” is widely and broadly used in section 12 of AASHTO LRFD design specifications yet is not explicitly defined in “12.2—DEFINITIONS”. Related terminology used in section 12 and other relevant sources includes “soil cover” “height of cover” “cover height” “fill height” “fill depth” “depth of cover” “cover depth” “crown cover depth” “crown soil cover” “design height of cover” “earth cover” “minimum allowable cover dimension” “depth of crown of culvert below ground surfaces” “actual height of cover above top of culvert or above crown of arches or pipes” “vertical distance from the top of cover for design height to point of horizontal load application” “height of ground surface above top of pipe” “minimum cover height” “minimum cover height above the crown” “minimum depth of fill” “minimum depth of cover”

“height of cover limits” “minimum cover limits” and “minimum cover”. Section C12.6.6.3 (commentary for “12.6.6.3—Minimum Cover”) states that “Depending on the pipe material and the pavement type above it, the minimum cover may include the pavement thickness and base course, along with the sub-base.” Figure 7.1 from Section C12.6.6.3 indicates that flexible pavement thickness is not included in the minimum cover definition for flexible pavement over flexible pipes but is included for rigid pavement over flexible pipes. The opposite definition apparently applies to buried rigid pipes. Section C12.6.6.3 also includes the caveat that “thermal expansion in thermoplastic pipe can affect pavement performance under shallow fills.” Furthermore, observe the note at the bottom of Figure 7.1: “The minimum cover dimension is not to be confused with the fill height used for calculations purposes, which shall be from the top of the pipe to the top of the surface, regardless of the pipe type or pavement type”. The Corrugated Steel Pipe Design Manual (NCSPA 2018) states “the minimum cover is measured from the top (inside rise) of the pipe to the bottom of the asphalt pavement course and to the top of rigid pavements”. The MBE (AASHTO 2018) does not contain any definitions or resistance equations associated with cover or fill height over metal culverts. Therefore it is important to recognize that there is no single meaning of “cover” or “minimum cover”, but rather its definition depends on how the dimension is applied to the engineering or construction use.

The minimum cover requirements for the design of culverts under normal traffic load are defined in Section 12.6.6.3 “Minimum Cover” of both AASHTO LRFD and AASHTO Standard Specifications. Table 7.1 summarizes these requirements as Table 12.6.6.3-1 of the AASHTO *LRFD Bridge Design Specifications* (2020). Pertinent to this research project, it is important to note that arch structures are not specifically designated in Table 12.6.6.3-1, and the word “pipe”



$H_{min}$  = minimum allowable cover dimension

Note: The minimum cover dimension is not to be confused with the fill height used for calculation purposes, which shall be from the top of the pipe to the top of the surface, regardless of the pipe type or pavement type.

**Figure 7.1. “Figure 12.6.6.3-1—Minimum Cover Orientation” of AASHTO LRFD Section C12.6.6.3**

is included in each relevant designation. Section 12.7 addresses the design of “arch structures” but does not further stipulate minimum cover. Section 12.8 is applicable to “the structural design of buried long-span structural plate corrugated metal structures”, which includes arch structures, but “having a radius of curvature greater than 13.0 ft in the crown or side plates.” Table 12.8.3.1.1-1 presents minimum cover requirements for long-span structures as a function of top radius and steel thickness. Minimum cover requirements for construction scenarios are specified in the AASHTO *LRFD Bridge Construction Specifications* (AASHTO 2017), but the temporary cover construction scenario is not pertinent to rating factor analyses since ratings are done after, and often long after, the structure has been in service. NCSPA (2018) defines pipe as “a culvert having a non-rectangular cross-section, often assumed to be circular unless specified otherwise”. Therefore, even though arch structures such as the Anniston arch culverts involved in this project do not have the fully enclosed cross section that are typically associated with the word “pipe”, they nonetheless

fall under the terminology of “pipe” for many culvert design and analysis applications. From the standpoint of section 12 of the AASHTO design specifications, corrugated steel culvert structures are either “pipes” or “boxes”. NCSPA (2018) also states that “minimum covers for H20 and H25 highway loads are taken as the greater of span/8 or 12 inches for all corrugated steel pipe except spiral rib pipe”.

**Table 7.1. Minimum cover definition Table 12.6.6.3-1 of the AASHTO LRFD Bridge Design Specifications (2020).**

Type	Condition	Minimum Cover*
Corrugated Metal Pipe	—	$S/8 \geq 12.0$ in.
Spiral Rib Metal Pipe	Steel Conduit	$S/4 \geq 12.0$ in.
	Aluminum Conduit where $S \leq 48.0$ in.	$S/2 \geq 12.0$ in.
	Aluminum Conduit where $S > 48.0$ in.	$S/2.75 \geq 24.0$ in.
Structural Plate Pipe Structures	—	$S/8 \geq 12.0$ in.
Long-Span Structural Plate Pipe Structures	—	Refer to Table 12.8.3.1.1-1
Structural Plate Box Structures	—	1.4 ft. as specified in Article 12.9.1
Deep Corrugated Structural Plate Structures	—	See Article 12.8.9.4
Fiberglass Pipe	—	12.0 in.
Thermoplastic Pipe	Under unpaved areas	$ID/8 \geq 12.0$ in.
	Under paved roads	$ID/2 \geq 24.0$ in.
Steel-Reinforced Thermoplastic Culverts	—	$S/5 \geq 12.0$ in.
Reinforced Concrete Pipe	Under unpaved areas or top of flexible pavement	$B_c/8$ or $B'_c/8$ , whichever is greater, $\geq 12.0$ in.
Reinforced Concrete Pipe	Under bottom of rigid pavement	9.0 in.
* Minimum cover taken from top of rigid pavement or bottom of flexible pavement		

According to *The Corrugated Metal Conduit as a Compression Ring* (White et al. 1960), once a pipe has been installed in compacted backfill with sufficient fill height, its strength can be evaluated as a thin ring in compression. Under such condition the flexural resistance of the pipe wall is not considered to support a significant portion of the vertical loads; the loads are resisted through axial compression. To accommodate this resistance mechanism in practical applications, White (1960) stipulated that the minimum cover depth should be at least 1/8 the diameter of the

culvert, which was based upon field test experience and has been summarized in minimum heights-of-cover tables.

In research by Duncan (1979), experimental evidence and the results of finite element analyses indicated that metal culvert structures are effectively restrained from excessive deformation if they are surrounded by good quality backfill and under a depth of cover greater than one-fourth of the span. The stresses induced by vehicle loads diminish in magnitude and become more uniform with increasing depth. Under these circumstances, even without consideration of the flexural stiffness or moment capacity, the culverts are able to resist all imposed loads entirely through ring compression action. Furthermore, Duncan's later study (Duncan and Drawsky 1983) restated that field experience has demonstrated that flexural failure under normal live loads is unlikely if the cover depth is greater than 20% of the span or one foot (whichever is greater) and the backfill is adequately compacted.

Therefore, minimum cover specification has been established with several factors in mind, including construction loading, potential thermal effects, dynamic effects that could damage the pipe, etc., but the primary impetus behind the minimum cover in current specifications was to provide sufficient soil depth so that the primary resistance mechanism would be thrust in the structure wall rather than flexure. In addition to minimizing the demand on surrounding soil, the minimum cover stipulation also facilitates simple analysis and design approaches that do not depend on defining the position and magnitude of maximum moment and interaction between moment and thrust. However, from the load-rating standpoint, an existing culvert that does not meet the design minimum cover can still have sufficient resistance to have a rating factor greater than 1.



The other critical factor is whether pavement, specifically flexible pavement, should be considered in the definition of cover used in rating factor analyses. NCSPA (2018) acknowledges that “asphalt does at least as good a job of distributing wheel loads as soil”; however it then points out that it is not included in the minimum cover definition due to construction scenario concerns. Furthermore, as noted in the background section, those involved in developing and assessing the ODOT and MDOT spreadsheet methodologies concluded that the minimum cover defined for design was overly conservative when applied to rating factor analyses. It is therefore clear that pavement, rigid or flexible, should be involved in rating factor analyses, especially for shallow buried culverts.

### **7.3 Rating Factor Analysis Methodology**

As presented in Chapter 3, the culvert rating approach must consider strength and stability limit states. Furthermore, as alluded to above, the challenge with shallow fill culverts that do not meet minimum cover requirements is that the pure thrust resistance mechanism that is the basis of resistance equations in current design specifications cannot be assumed. In other words, rating of shallow fill culverts must involve assessment of available live load capacity under combined moment and thrust. Given that the position of the vehicle(s) that cause the maximum demand, as well as the critical position on the culvert, must be determined, significant added complexity therefore arises. This section outlines the deficiencies of currently used rating methods when applied to shallow fill culverts and derives potential alternatives.

#### **7.3.1 Modified ODOT Minimum Cover Definition**

Because of the recognized over-conservatism of reducing the load rating factor by the ratio of measured minimum cover to required minimum cover defined in AASHTO, the Ohio Department of Transportation modified this requirement by incorporating the critical-load

parameter defined in the *Guide to Stability Design Criteria for Metal Structures* (Galambos 1998). However, the critical intensity of distributed loads  $q$  for the three buckling modes from Galambos (Table 7.2) used to modify the original minimum cover requirement are essentially another form of thrust capacity critical buckling stress  $f_{cr}$  presented in AASHTO LRFD 12.7.2.4 that was also incorporated into the ODOT spreadsheet. The critical buckling stress in the cross-section area  $f_{cr}$  (AASHTO LRFD 12.7.2.4) can be converted to the corresponding critical uniformly distributed buckling pressure applied over the span of structure  $q_{cr}$  by the following derivation:

$$f_{cr} = \frac{12E_m}{\left(\frac{kS}{r}\right)^2} = \frac{12E_m}{\left(kS/\sqrt{\frac{I}{A}}\right)^2} = \frac{12E_m}{(kS)^2} \times \frac{I}{A} = \frac{12}{k} \times \frac{E_m I}{S^2 A} \quad (7.1)$$

$$\frac{q_{cr} S}{2A} = f_{cr} \quad (7.2)$$

$$q_{cr} = f_{cr} \frac{2A}{S} = \frac{12}{k} \times \frac{E_m I}{S^2 A} \times \frac{2A}{S} = \frac{24E_m I}{kS^3} = \frac{24}{k} \times \frac{E_m I}{S^3} \quad (7.3)$$

The corresponding critical buckling pressure  $q_{cr}$  in Eq. 7.3 comes from the classic buckling equation for a circular ring under hydrostatic pressure (the additional  $k$  was introduced to account for soil-structure interaction), while the critical intensity of distributed load  $q = \gamma \times \frac{EI}{L^3}$  in Galambos (1998) (Table 7.2) is also a buckling pressure for arches subjected to vertical uniform load. Both of these buckling criteria were derived in the *Theory of Elastic Stability* (Timoshenko and Gere 1961) for different structural shapes. In other words, the modified ODOT spreadsheet revised by critical-load parameters in Galambos theory redundantly used two similar buckling criteria.

**Table 7.2. Critical-load parameter for uniform elastic arches in pure compression (Galambos 1998).**

$\frac{h}{\bar{L}}$	Three-Hinged Arch		Two-Hinged Arch		Fixed Arch	
	$qL^3/EI$	$HL^2/EI$	$qL^3/EI$	$HL^2/EI$	$qL^3/EI$	$HL^2/EI$
<i>Parabolic arches subjected to vertical load uniformly distributed on a horizontal projection</i>						
0.10	22.5	28.1	29.1	36.3	60.9	76.2
0.15			39.5	32.9	85.1	70.9
0.20	39.6	24.8	46.1	28.8	103.1	64.5
0.25			49.2	24.6	114.6	57.3
0.30	49.5	20.6	49.5	20.6	120.1	50.0
0.35			47.8	17.1	120.6	43.1
0.40	45.0	14.1	45.0	14.1	117.5	36.7
0.50	38.2	9.6	38.2	9.6	105.3	26.3

### 7.3.2 Definition of “Span” for Long-Span Structures

According to White and Layer (1960) and Sezen et al. (2009), the circumferential thrust develops in proportion to the radius of curvature in the wall of a non-circular pipe arch culvert (Figure 7.2):

$$P = \frac{T}{R'} \quad (7.4)$$

$$\text{Thus, } T = P \times R' \quad (7.5)$$

where  $P$  is the soil pressure,  $R'$  is the radius of curvature at the point under consideration, and  $T$  is the circumferential thrust. Moreover, in an arch culvert (Figure 7.3), the vertical reaction  $V$  at the springline is defined as:

$$V = P \times \frac{S}{2} \quad (7.6)$$

Thus, the tangential thrust  $C$  is:

$$C = \frac{V}{\cos \phi} = P \times \frac{S}{2} / \cos \phi = P \times R \quad (7.7)$$

where  $\phi$  is the angle between the arch axis and the vertical line at footing,  $S$  is the arch span, and  $R$  is the radius of arch curvature. Therefore, for both shapes (pipe arch culvert in Figure 7.2 and arch culvert in Figure 7.3), the thrust is directly proportional to the top radius rather than the culvert span.

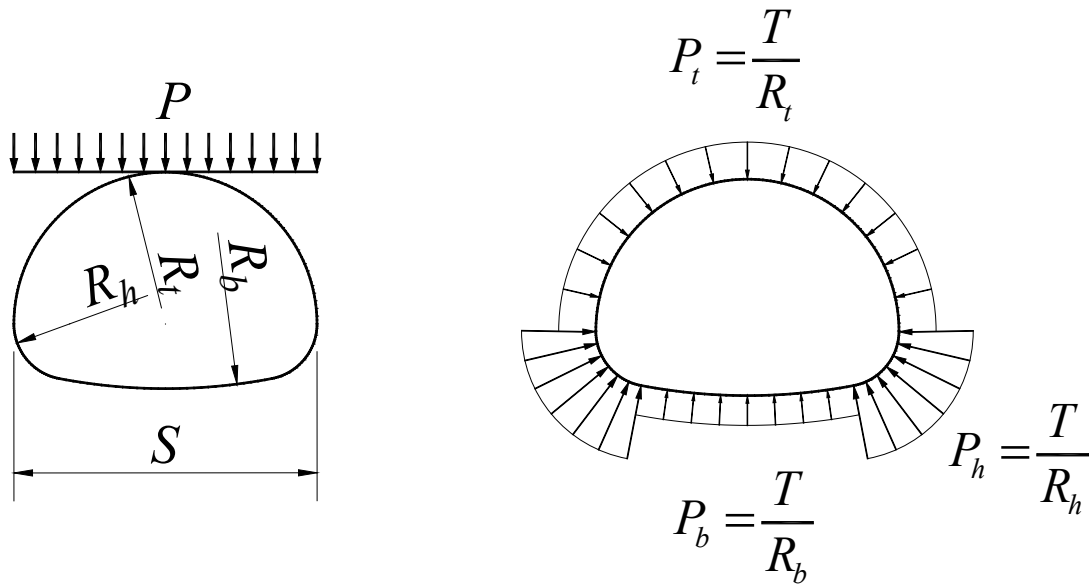


Figure 7.2. Circumferential thrust in non-circular culvert (Sezen et al. 2009).

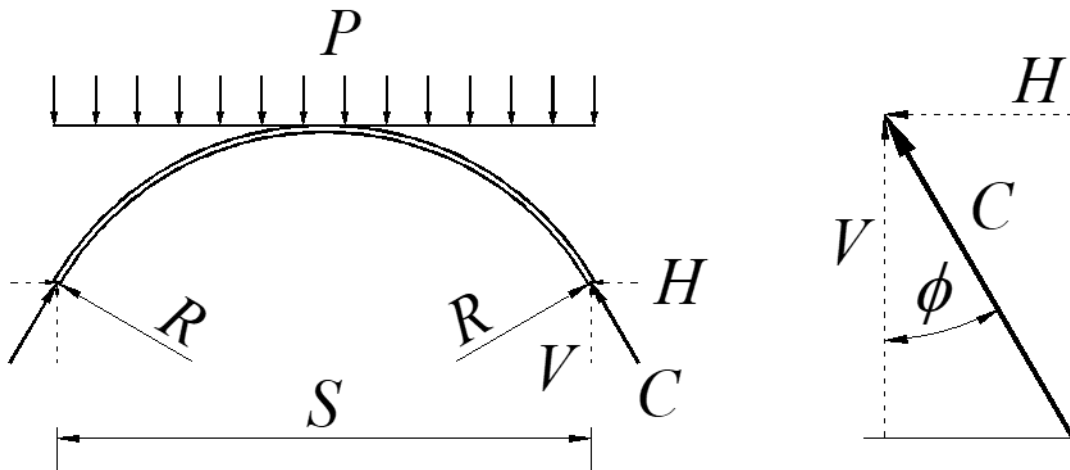


Figure 7.3. Tangential thrust in arch culvert (White and Layer 1960).

Accordingly, per 12.7.2.1 of the AASHTO Standard Specification (2002), AASHTO LRFD 12.8.3.2 (2020) and *NCSPA Design Data Sheet No. 19* section II-A-3, for all long span structures (horizontal ellipse, low and high profile arches, inverted pear shapes and pear arches) as well as other horizontal ellipses with a relatively large radius of curvature greater than 13.0 ft in the crown or side plates, twice the value of the top radius in lieu of span must be used to define the thrust. However, in the formulae for other calculations in long-span culverts, such as the reduction factor  $F_1$  in AASHTO LRFD 12.7.2.2-5 (2020), the critical load defined by Galambos (1998), the parameter  $C$  in the RF equation based on minimum cover requirements,  $\frac{H^2}{Ch^2}$ , and the moment calculations in MDOT spreadsheet, etc., the actual field measured span must be used. Using twice the top arc radius in these equations for long-span structures would artificially amplify the responses and thereby result in rating factors that are lower than actual representation of capacity.

### **7.3.3 Tire Contact Area**

The tire pressure is idealized as uniformly distributed over a rectangular contact area. The contact area of a wheel for vehicles other than the design truck and tandem, whose width is 20 inches and whose length is 10 inches, should be determined by AASHTO LRFD C3.6.1.2.5. The tire width =  $P/0.8$ , where  $P$  is design wheel load (kip) and is based on heaviest wheel load without dynamic load allowance. However, the tire length =  $6.4\gamma(1+IM/100)$  where  $\gamma$ =load factor;  $IM$ =dynamic load allowance percent and should be calculated based on the dynamic load allowance equal of 33%, the value at the top road surface with zero cover depth (*Appendix C: Proposed Revisions to AASHTO Specifications C3.6.1.2.6*); because the contact area only depends on the weight and impact of the truck on the road surface, it is unreasonable to apply the impact factor under a certain fill depth to the top surface calculation. The dynamic load allowance

$IM = 33(1.0 - 0.125D_E) \geq 0\%$  (AASHTO LRFD 3.6.2.2-1) computed with soil depth greater than zero should be only added to the calculation of pressure on the projected area below the surface, such as the live load vertical crown pressure per AASHTO LRFD C3.6.1.2.6b-7.

### 7.3.4 Thrust due to Live Load

As demonstrated by Sargand et al. (2018), the thrusts due to live load calculated using ring compression theory are significantly greater than those measured during field tests. This is because the live loads, regardless of the cover depth, are converted to an equivalent pressure that is applied across the entire culvert span. This inherent inaccuracy can be minimized by using the thrust formulae in 12.7.2.2 in AASHTO LRFD, where the width of the culvert on which the live load is applied parallel to span, " $C_L$ ", is restricted to the live load patch length " $l_w$ " at depth  $H$ . As illustrated in Figure 7.4, the  $l_w$  for shallow cover is much less than the culvert span and thus the value of wall thrust calculated due to live load is much less.

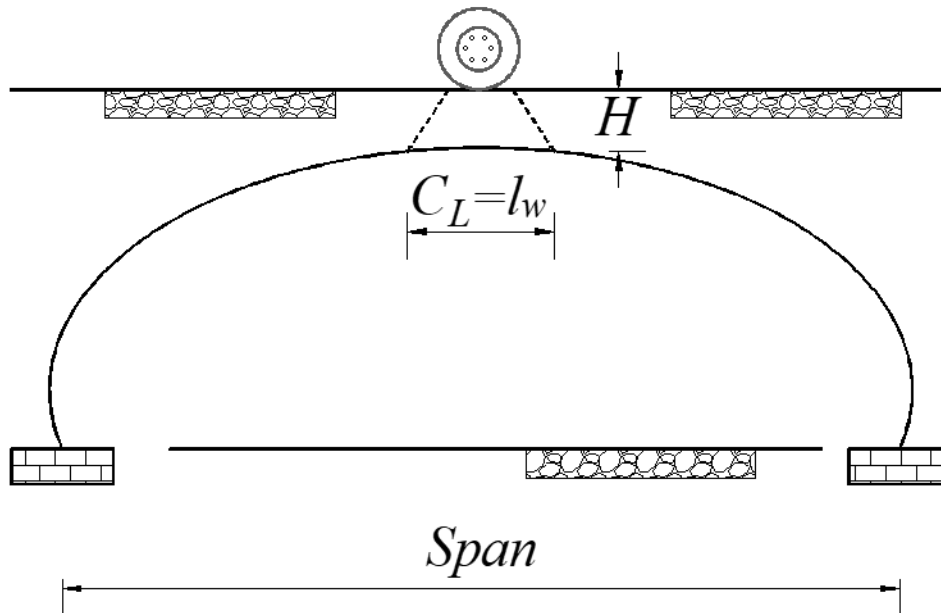


**Figure 7.4. Width of culvert on which the live load is applied parallel to span.**



### 7.3.5 Maximum Moment by the Duncan Method

The MDOT spreadsheet uses the moments due to dead load and live load defined by Duncan and Drawsky (1983), who concluded that the maximum moment occurs at the quarter point of the culvert when the live load is also over the quarter point:

$$M_1 = K_{M1} R_B \gamma S^3 \quad (7.8)$$

in which  $M_1$  = maximum moment with zero cover depth (k ft/ft) (due to part 1 in Figure 7.5);  $K_{M1}$  = moment coefficient that varies with flexibility number;  $R_B$  = moment reduction factor for backfill moments that varies with rise/span ratio;  $\gamma$  = unit weight of backfill (k/ft<sup>3</sup>);  $S$  = span (ft). The maximum moment  $M_1$  for the zero cover ( $H = 0$ ) condition at both the crown (with tension in the outer fiber) and the quarter point (with tension in the inner fiber) is calculated with the moment coefficient  $K_{M1}$  determined at zero depth of cover over the quarter point. Thus, the cover depth over the quarter point for  $K_{M1}$  is equal to  $0+R/2$ , where  $R$  is the rise.

The maximum moment  $M_2$  due to earth fill  $H$  over the top of culvert (part 2 in Figure 7.5) with tension in the inner fiber at the crown and tension in the outer fiber at the quarter point is:

$$M_2 = K_{M2} R_B \gamma S^2 H \quad (7.9)$$

which is in the opposite direction as  $M_1$ . The coefficient  $K_{M2}$  is calculated by the cover depth over the quarter point at final cover, which is equal to the actual cover depth under live load  $H$  plus  $R/2$ , while the  $H$  in  $K_{M2} R_B \gamma S^2 H$  is the minimum cover depth over the crown  $H$ .

The additional moment at the quarter point due to live load over the quarter point (Figure 7.5):

$$\Delta M_L = R_L K_{M3} S(LL) \quad (7.10)$$

which is in the same direction as  $M_1$ .  $R_L$  = reduction factor for live load moment, which varies with cover depth and flexibility number;  $K_{M3}$  = live load moment coefficient, which varies with flexibility number; and  $LL$  = equivalent line load (k/ft).  $R_L$ ,  $K_{M3}$  and  $LL$  are calculated based on the cover depth over the quarter point under the live load  $H + R/2$  (per Duncan 1979). Any of these parameters mistakenly calculated by  $H$  would result in an overestimation of the moment due to live load.

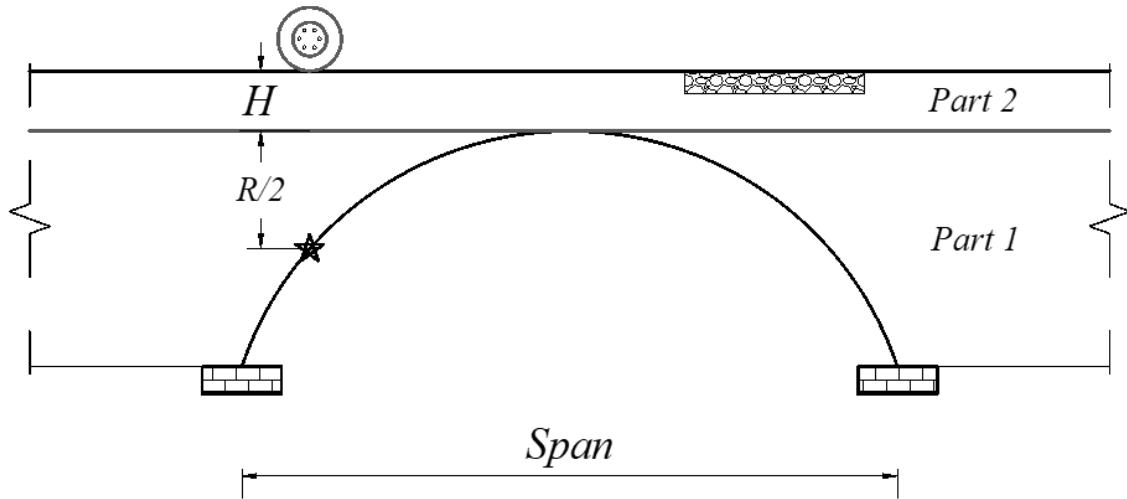


**Figure 7.5. Moment due to earth fill and live load at the quarter point.**

### 7.3.6 Maximum Moment by Castigliano's method

The maximum moment due to live load can be predicted in a simpler way than that calculated in Duncan method. According to *Structural Mechanics of Buried Pipes* (Watkins and Anderson 1999) and *Buried Flexible Steel Pipe Design and Structural Analysis* (Whidden 2009), the critical location of live load is determined when the surface wheel load approaches the culvert from left side and “punches through” a truncated pyramid of soil; the edge of the projected pressure area is at the crown as shown in Figure 7.6. The resultant downward deformation on the left shoulder results in opposite direction on the right side of the pipe. From Castigliano's equation, the maximum moment is:

$$M = 0.022Pr^2 \quad (7.11)$$

where  $M$  = maximum moment due to live load (k-ft/ft);  $P$  = the distributed vertical pressure over the crown due to live load (k/ft<sup>2</sup>); and  $r$  = the mean radius of the pipe. The maximum moment occurs at the point of minimum radius of curvature, which is approximately 12 degrees from the centerline. In this theory, the dead load (soil weight) is negligible because it is assumed to be small compared to the surface load.

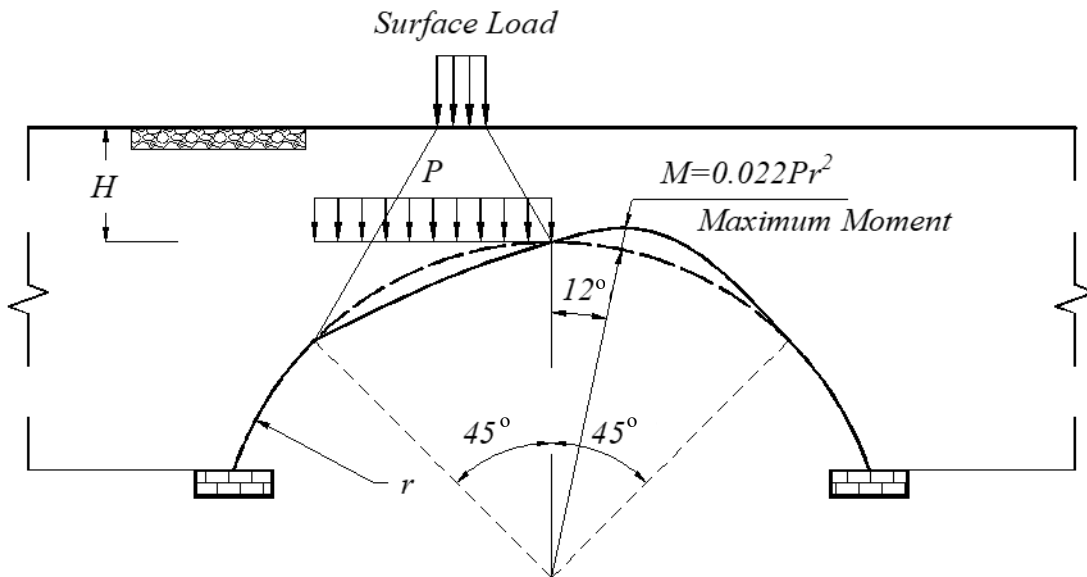


**Figure 7.6. Mechanics of flexible pipe under a surface load (Watkins and Anderson 1999).**

#### 7.4 Pavement Effect

Both experimental results and finite element analysis have demonstrated that pavement can significantly reduce the maximum internal forces in the culvert wall due to live load compared to the same fill depth without pavement (Abdel-Karim et al. 1990, Mlynarski et al. 2019). This is because, due to the higher shear moduli, the load-spreading effect through the pavement's thickness is much greater than the load spreading that would occur in the same thickness

of soil. However, this stress-reduction from pavement was not accounted for in any current simplified and spreadsheet-based load rating methodology; the pavement was only considered as an additional thickness layer of soil over the structure.

To account for the benefit of pavement in the load rating, the technique developed by Han et al. (2013) is adopted in the following. Han's equation demonstrated the relationship between the load spreading effect in the pavement and the stiffness ratio of two adjacent layers:

$$\tan \alpha_1 = \tan \alpha_0 \left[ 1 + 0.204 \left( \frac{E_{bc}}{E_{sg}} - 1 \right) \right] \quad (7.12)$$

where  $\alpha_1$  = pressure distribution angle in the base course under consideration;  $\alpha_0$  = reference pressure distribution angle for a uniform medium defined by  $E_{bc} = E_{sg}$ ;  $E_{bc}$  = elastic modulus of the base course under consideration; and  $E_{sg}$  = elastic modulus of the underlying subgrade.

#### 7.4.1 Culvert under Rigid Pavement

The rigid pavement considered in Han's study consisted of plain cement concrete (PCC), under which there were cement-treated base course, lime-treated subgrade, and a natural subgrade above the culvert. The elastic modulus of concrete pavement can be determined using the correlation given by ACI 318-11:

$$E_c = 57000 \sqrt{f'_c} \quad (7.13)$$

where  $E_c$  = elastic modulus of the concrete (psi) and  $f'_c$  = compressive strength of the concrete (psi). The typical concrete pavement design strength is 4000 psi, so the calculated elastic modulus of the concrete is 3.6e6 psi. The average elastic moduli of 750000 psi and 45000 psi are adopted for cement-treated base course and lime-treated subgrade respectively based on the AASHTO *Guide for Design of Pavement Structures* (1993). The average elastic modulus of the natural

subgrade is obtained from the elastic soil property in top layer of various backfills by Selig (1990) (Table 7.3).

**Table 7.3. Elastic soil properties for backfill (Selig 1990).**

Gravelly Sand (SW)						
Maximum Principal Stress Level (psi)	95% Standard Compaction			85% Standard Compaction		
	E (psi)	B (psi)	v	E (psi)	B (psi)	v
0 to 1	1,600	2,800	0.40	1,300	900	0.26
1 to 5	4,100	3,300	0.29	2,100	1,200	0.21
5 to 10	6,000	3,900	0.24	2,600	1,400	0.19
10 to 20	8,600	5,300	0.23	3,300	1,800	0.19
20 to 40	13,000	8,700	0.25	4,100	2,500	0.23
40 to 60	16,000	13,000	0.29	4,700	3,500	0.28
Sandy Silt (ML)						
Maximum Principal Stress Level (psi)	95% Standard Compaction			85% Standard Compaction		
	E (psi)	B (psi)	v	E (psi)	B (psi)	v
0 to 1	1,800	1,900	0.34	600	400	0.25
1 to 5	2,500	2,000	0.29	700	450	0.24
5 to 10	2,900	2,100	0.27	800	500	0.23
10 to 20	3,200	2,500	0.29	850	700	0.30
20 to 40	3,700	3,400	0.32	900	1,200	0.38
40 to 60	4,100	4,500	0.35	1,000	1,800	0.41
Silty Clay (CL)						
Maximum Principal Stress Level (psi)	95% Standard Compaction			85% Standard Compaction		
	E (psi)	B (psi)	v	E (psi)	B (psi)	v
0 to 1	400	800	0.42	100	100	0.33
1 to 5	800	900	0.35	250	200	0.29
5 to 10	1,100	1,000	0.32	400	300	0.28
10 to 20	1,300	1,100	0.30	600	400	0.25
20 to 40	1,400	1,600	0.35	700	800	0.35
60	1,500	2,100	0.38	800	1,300	0.40

The vertical pressure distribution angles from the concrete pavement to the cement-treated base course, from the cement-treated base course to the lime-treated subgrade, and the lime-treated subgrade to the natural subgrade are determined by Eq. 7.12.  $2 \times \tan \alpha_0$  is taken as 1.15 per AASHTO LRFD Table 3.6.1.2.6a-1 or 1.75 per AASHTO Standard 6.4.1. Thus, the  $\alpha_0$  is taken as  $30^\circ$  per AASHTO LRFD or  $41.2^\circ$  per the AASHTO Standard Specification, respectively. The distribution angle calculated for each rigid pavement layer is provided in Table 7.4.

**Table 7.4. Distribution Angle between Pavement Layers**

<b>Pavement layer</b>	$E_{bc}$ (psi)	$E_{sg}$ (psi)	<b>Distribution angle <math>\tan \alpha_1</math></b>
Concrete pavement	3600000	750000	1.02
Cement-treated base	750000	45000	2.41
Lime-treated subgrade	45000	1800	3.39
Natural subgrade	1800	—	0.58

Note:  $\alpha_0$  is taken as  $30^\circ$ , the elastic modulus of the natural subgrade is selected as 1800 psi from ML95 in Table 7.3.

Hence, the length of the rectangular distribution area on the metal culvert along the culvert axis due to a single wheel load “ $\alpha$ ” can be determined as follows:

$$\alpha = t_l + 2(h_1 \tan \alpha_1 + h_2 \tan \alpha_2 + h_3 \tan \alpha_3 + h_4 \tan \alpha_4) \quad (7.14)$$

where  $\alpha$  = length of the distributed area along the axis of culvert by one single wheel load;  $t_l$  = length of the tire footprint along the axis of culvert;  $h_1$ ,  $h_2$ ,  $h_3$ , and  $h_4$  = thicknesses of concrete pavement, cement-treated base, lime-treated subgrade, and natural subgrade, respectively; and  $\alpha_1$ ,  $\alpha_2$ ,  $\alpha_3$ , and  $\alpha_4$  = distribution angles between concrete pavement, cement-treated base, lime-treated subgrade, and natural subgrade, respectively.

The thicknesses of the cement-treated base layer  $h_2$  and the lime-treated subgrade layer  $h_3$  are fixed at 4 inches and 6 inches, respectively, which refers to the typical cross sections of the culvert models under rigid pavements field-tested by the Kansas Department of Transportation (Han et al. 2013). The thicknesses of the concrete layer  $h_1$ , and the natural subgrade layer  $h_4$  are variable.



A schematic of the vertical pressure distribution on the culvert under typical concrete pavement is shown in Figure 7.7. The length of the combined distribution area by the two wheel loads along the axis of culvert can be determined as follows:

$$b = a + s \tag{7.15}$$

where  $b$  = length of the combined distribution area along the axis of culvert, and  $s$  = spacing of the two wheel loads, center to center. The width of the distributed area in the direction perpendicular to the culvert axis is  $a - (t_l - t_w)$ , where  $t_w$  is the width of the tire footprint.

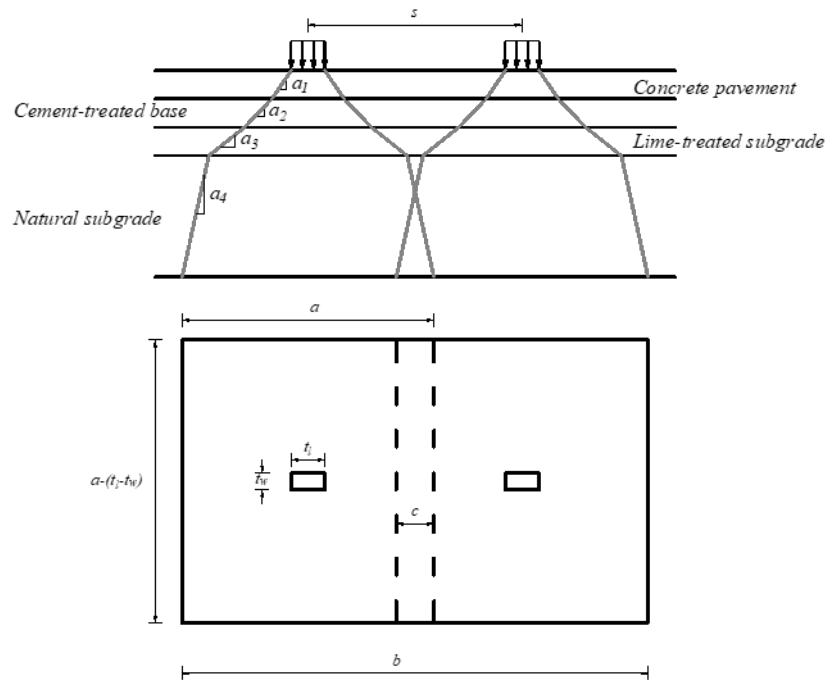


**Figure 7.7. Vertical pressure distribution under rigid pavement (Han et al. 2013).**

For rigid pavement, the applied loads are assumed to be distributed uniformly over the entire combined distribution area onto the culvert as shown in Figure 7.8. The magnitude of the uniform vertical pressure can be determined by dividing the total loads from both wheels by the total distribution area:

$$P_c = \frac{2P}{b(a - t_l + t_w)} \quad (7.16)$$

where  $P_c$  = the distributed vertical pressure over the culvert.

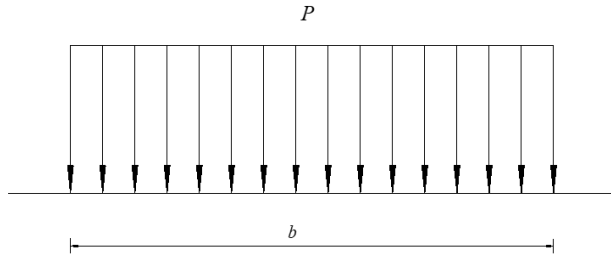


**Figure 7.8. Distributed Pressure over the Culvert under a Rigid Pavement**

#### 7.4.2 Culvert under Flexible Pavement

Flexible pavement consists of a hot mixed asphalt (HMA) layer, under which there is typically lime-treated subgrade and a natural subgrade above the culvert. The elastic modulus of the asphalt layer is approximated as 200000 psi. The average elastic modulus of 45000 psi is adopted for lime-treated subgrade as recommended by the *Guide for Design of Pavement Structures* (AASHTO 1993). The average elastic modulus of the natural subgrade is obtained from the elastic soil property in top layer of various backfills by Selig (1990) (Table 7.3).

The vertical pressure distribution angles from the asphalt concrete to the lime-treated subgrade, and the lime-treated subgrade to the natural subgrade are determined by Equation 7.12, where  $2 \times \tan \alpha_0$  is taken as 1.15 per AASHTO LRFD Table 3.6.1.2.6a-1 or 1.75 per AASHTO Standard 6.4.1. Thus, the  $\alpha_0$  is taken as  $30^\circ$  per AASHTO LRFD or  $41.2^\circ$  per the AASHTO Standard Specification, respectively. The distribution angle calculated for each flexible pavement layer is shown in Table 7.5:

**Table 7.5. Distribution Angle between Pavement Layers**

<b>Pavement layer</b>	$E_{bc}$ (psi)	$E_{sg}$ (psi)	<b>Distribution angle <math>\tan \alpha_1</math></b>
Asphalt concrete	200000	45000	0.98
Lime-treated subgrade	45000	1800	3.39
Natural subgrade	1800	—	0.58

Note:  $\alpha_0$  is taken as  $30^\circ$ , the elastic modulus of the natural subgrade is selected as 1800 psi from ML95 in Table 7.3.

Hence, “ $\alpha$ ” the length of the rectangular distribution area on the metal culvert along the culvert axis due to a single wheel load can be determined as follows:

$$\alpha = t_l + 2(h_1 \tan \alpha_1 + h_2 \tan \alpha_2 + h_3 \tan \alpha_3) \quad (7.16)$$

where  $\alpha$  = length of the distributed area along the axis of culvert by one single wheel load;  $t_l$  = length of the tire footprint along the axis of culvert;  $h_1$ ,  $h_2$ , and  $h_3$  = thicknesses of asphalt pavement, lime-treated subgrade, and natural subgrade, respectively; and  $\alpha_1$ ,  $\alpha_2$ , and  $\alpha_3$  = distribution angles between asphalt pavement, lime-treated subgrade, and natural subgrade, respectively. The thicknesses of the lime-treated subgrade layer  $h_2$  is fixed at 6 inches, which refers to the typical cross sections of the culvert models under flexible pavements field-tested by Kansas Department of Transportation (Han et al. 2013). The thicknesses of the asphalt layer  $h_1$ , and the natural subgrade layer  $h_3$  are variable. A schematic of the vertical pressure distribution on the culvert under pavement is shown in Figure 7.9.

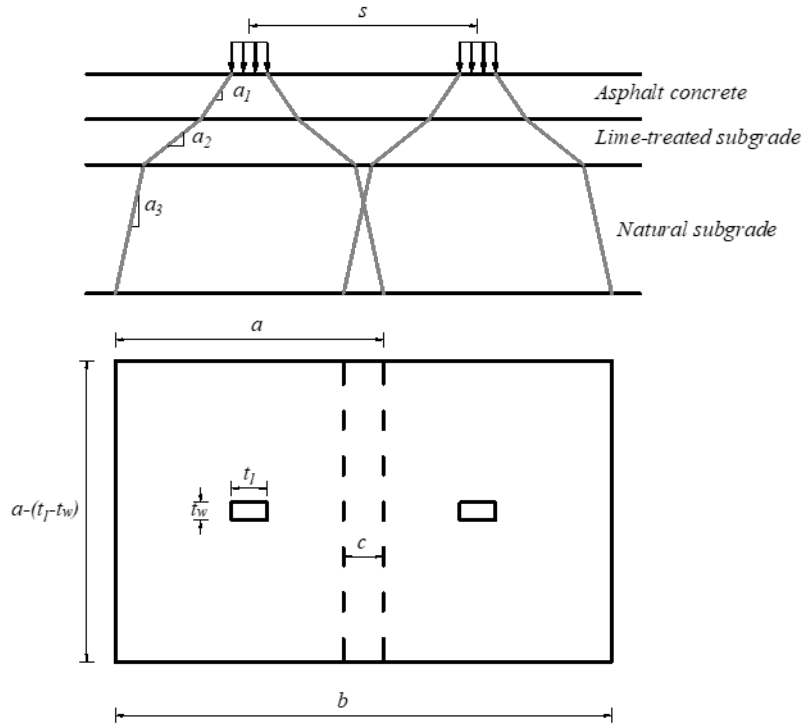


**Figure 7.9. Vertical Pressure Distribution through Flexible Pavement Layers**

For flexible pavement, the applied loads are assumed to be distributed independently over the distribution area from an individual wheel load onto the culvert. The uniform vertical pressure from a single wheel load is:

$$P_{c1} = \frac{P}{a(a - t_l + t_w)} \quad (7.18)$$

where  $P_{c1}$  = the distributed vertical pressure from an individual wheel load over the culvert. Within the overlapped area (Figure 7.10), the vertical pressure over the culvert can be determined by superposing the pressures due to two individual wheels:

$$P_{c2} = 2P_{c1} \quad (7.19)$$

where  $P_{c2}$  = distributed vertical pressure within the overlapped area over the culvert.

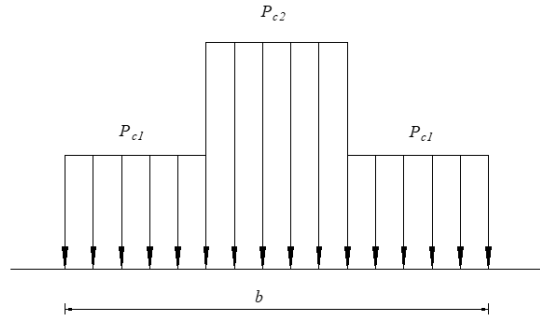


**Figure 7.10. Distributed Pressure over the Culvert under a Flexible Pavement**

The pavement benefit is only accounted for in the calculation of moment due to live load in the load rating, because the spreading effect of pavement affects the moment much more than the thrust due to live load in the metal structure.

#### 7.4.3 Pavement Effect in Duncan Method

In order to account for this pavement load-spreading effect in the calculation of moment due to live load by the Duncan method, the “*LL*” equivalent line load in the equation for  $\Delta M_L$  can be determined by AASHTO with consideration of above pavement benefit. The equivalent line load is uniform loading distributed along the line parallel to the axle of vehicle. In the Duncan method, the concept relating the intensity of *LL* to the magnitude of vehicle load was that both cause the same maximum vertical pressure (computed using Bousinesq elastic theory) at the same level over the culvert,

$$LL = \frac{AL}{K_4} \quad (7.20)$$

where  $K_4$  = a factor dependent on the wheel numbers on axle and the depth over culvert (ft),  $AL$  = axle load (k). However, the *LL* neither accounts for any pavement load-spreading effect, nor does it reflect any load distribution rules defined by AASHTO. Therefore, to address these two deficiencies the calculation of *LL* is replaced by:

$$LL = \frac{AL}{2a} \quad (7.21)$$

where  $a$  = length of the distributed area along the axis of culvert by one single wheel load (ft) calculated by Eq. 7.14 for rigid pavement or Eq. 7.17 for flexible pavement. If the distributed areas from two wheel loads overlap along the axis of culvert,

$$LL = \frac{AL}{a+s} \quad (7.22)$$

where  $a$  = length of the distributed area along the axis of culvert by one single wheel load (ft) calculated by Eq. 7.14 for rigid pavement or Eq. 7.17 for flexible pavement and  $s$  = spacing of the wheel loads (ft), center to center in a single axle.

#### 7.4.4 Pavement Effect in Castigliano's Method

In order to account for the pavement effect in the calculation of moment due to live load by the Castigliano method, the vertical pressure over the crown " $P$ " in the Eq. 7.11 should be determined by  $P_c$  in Eq. 7.16 for rigid pavement or  $P_{c1}$  in Eq. 7.18 or  $P_{c2}$  in Eq. 7.19 for flexible pavement.

#### 7.5 Worst-Case Position for Load Rating

Duncan (1979) concluded that the effects of backfill and live load with load positioned over the quarter point produce the greatest moment at the quarter point compared to the moment at any other location in the culvert. However, the position of live load over the quarter point will not necessarily result in the lowest rating factor. The position of live load over the crown or live load over the point between the crown and the quarter point where the moment due to backfill is approximately zero could also be the possible worst-case location (produces the lowest rating factor). Thus, theoretically, the rating factors should be calculated at all three positions of live



load (over the crown, over the quarter point and over the middle point between the crown and the quarter point) to obtain the critical value. This is because, for shallow buried culverts, the backfill will result in moment with tension in the inner fiber (culvert interior) at the quarter point and tension in the outer fiber at the crown of structure, as illustrated in Figure 7.11, and the live load applied at different positions over the culvert will result in different techniques for computing the rating factors.

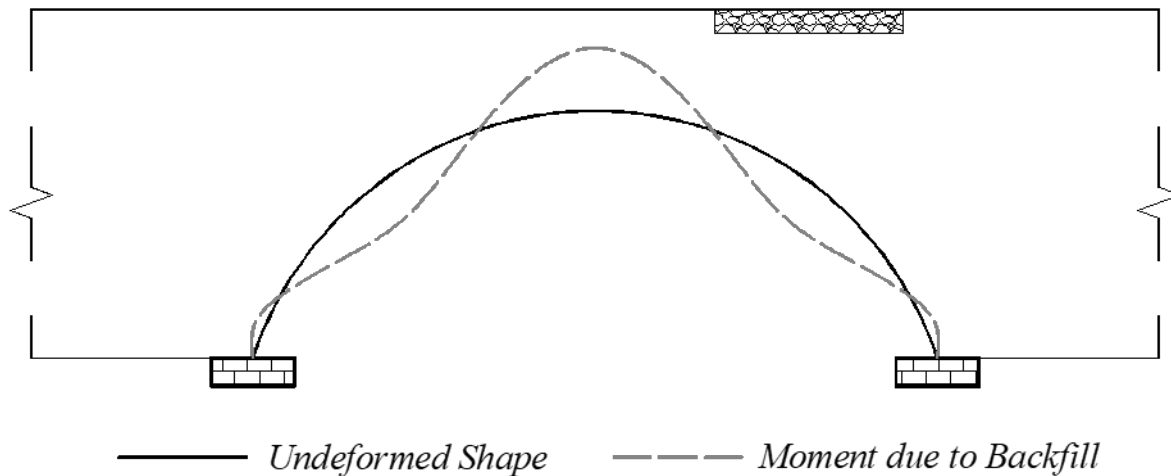


**Figure 7.11. Moment distribution due to backfill at final cover without live load (outside values denote outer fiber in tension, inside values denote inner fiber in tension).**

The rating factors based on the three possible worst-case positions of live load should therefore be calculated as follows:

**(1) When live load is over the crown** as in Figure 7.12, the moment due to live load causes tension in the inner fiber at the crown that is opposite to the fiber strain due to backfill. In this way, the live load must compensate for the moment due to backfill before the crown moves inward as is caused by the moment due to live load. In other words, the moment due to backfill at the crown tends to increase the resistance of the structure when the live load is over the crown. Hence, the rating factor based on moment should be calculated by:

$$RF_M = \frac{A_1 M_C + A_2 M_D}{A_3 M_L} \quad (7.23)$$

where  $M_C$  = plastic moment capacity of the culvert section;  $M_D$  = maximum moment at the crown due to dead load;  $M_L$  = additional moment at the crown due to live load; and  $A_1$ ,  $A_2$ ,  $A_3$  = factors for moment capacity, dead load and live load, respectively.

Per AASHTO LRFD section 3.4 and CANDE-2007 *Solution Methods and Formulations* section 6.4, the load factor  $\gamma$  and load modifier  $\eta_{EB}$  for earth fill loading should be selected to produce the worst-case structural response scenario. Thus,

$$A_2 M_D = \frac{\gamma_{\min}}{\eta_{EB}} M_1 - \gamma_{\max} \eta_{EB} M_2 = \frac{0.9}{1.05} M_1 - 1.95 \times 1.05 M_2 \quad (7.24)$$

where the definitions of  $M_1$  and  $M_2$  refer to Eq. 7.8 and Eq. 7.9. The parameters in the computation for  $M_L$  and its corresponding impact factor should be calculated based on the minimum cover depth  $H$  over the crown, where  $H$  denotes minimum cover over the crown.

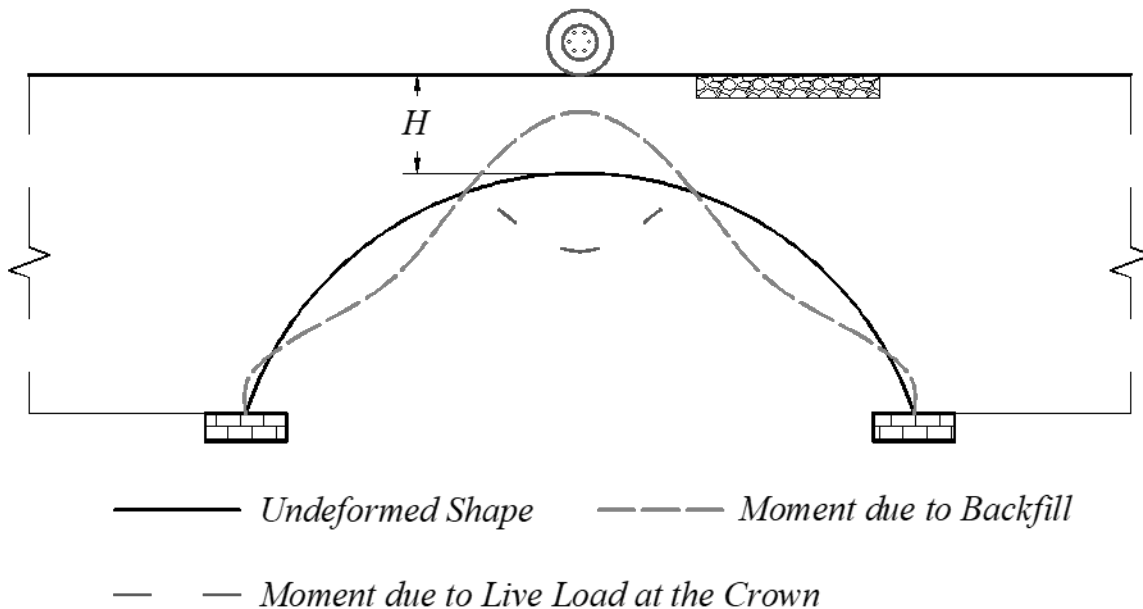


**Figure 7.12. Live load is over the crown (outside values denote outer fiber in tension, inside values denote inner fiber in tension).**

**(2) When live load is over the quarter point** as illustrated in Figure 7.13, the moment due to live load causes tension in the inner fiber at the quarter point that is the same as the fiber strain due to backfill (Duncan and Drawsky 1983). In this way, the moment due to backfill at the quarter point tends to decrease the resistance of the structure when the live load is over the quarter point. Hence, the rating factor based on moment should be calculated by:

$$RF_M = \frac{A_1 M_C - A_2 M_D}{A_3 M_L} \quad (7.25)$$

where  $M_C$  = plastic moment capacity of the culvert section;  $M_D$  = maximum moment at the quarter point due to dead load;  $M_L$  = additional moment at the quarter point due to live load; and  $A_1, A_2, A_3$  = factors for moment capacity, dead load and live load, respectively.

Likewise, per AASHTO LRFD section 3.4 and CANDE-2007 *Solution Methods and Formulations* section 6.4, the load factor  $\gamma$  and load modifier  $\eta_{EB}$  for earth fill loading should be selected to produce the worst-case moment at the quarter point. Thus,

$$A_2 M_D = \gamma_{\max} \eta_{EB} M_1 - \frac{\gamma_{\min}}{\eta_{EB}} M_2 = 1.95 \times 1.05 M_1 - \frac{0.9}{1.05} M_2 \quad (7.26)$$

Where the definitions of  $M_1$  and  $M_2$  refer to Eq. 7.8 and Eq. 7.9. The parameters in the computation for  $M_L$  and its corresponding impact factor should be calculated based on the actual cover depth  $H+R/2$  over the quarter point, where  $H$  denotes minimum cover over the crown, and  $R$  is the rise of culvert.

**(3) When the live load is over the middle point** between the crown and the quarter point where the moment due to backfill is zero as shown in Figure 14, the moment due to backfill at this point neither increases nor decreases the resistance of the structure. Hence, the rating factor based on

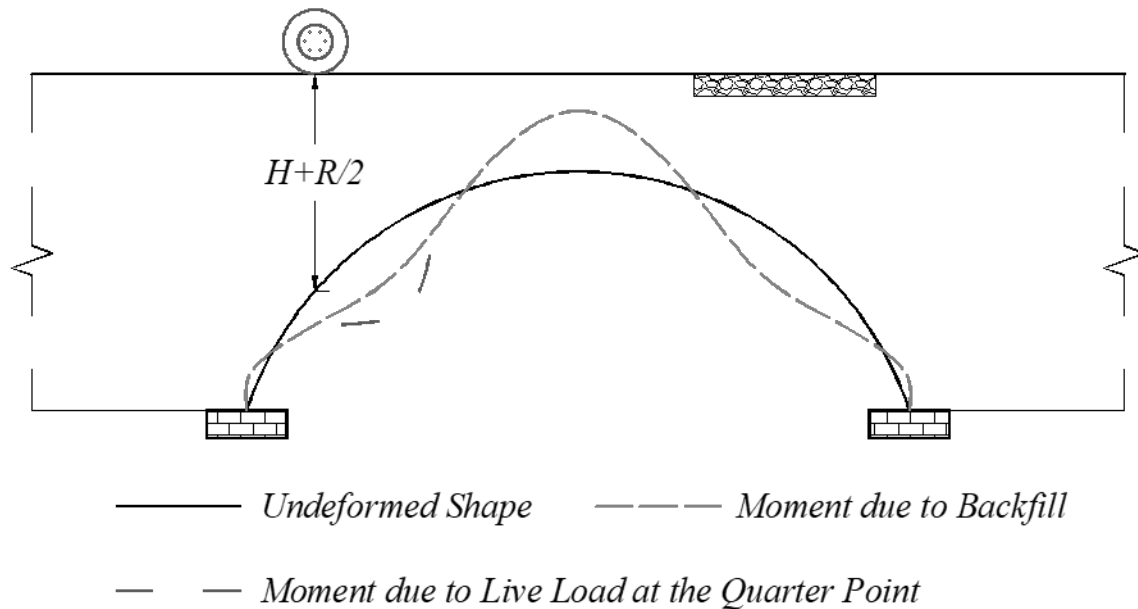


**Figure 7.13. Live load is over the quarter point (outside values denote outer fiber in tension, inside values denote inner fiber in tension).**

moment here should be calculated by:

$$RF_M = \frac{A_1 M_C}{A_3 M_L} \quad (7.27)$$

Where:

$M_C$  = plastic moment capacity of the culvert section;

$M_L$  = additional moment due to live load at the point between the crown and the quarter point where the moment due to backfill is zero;

$A_1, A_3$  = factors for moment capacity and live load, respectively.

The parameters in the computation for  $M_L$  and its corresponding impact factor should be calculated based on the actual cover depth  $H+R/4$  below the live load, where  $H$  denotes minimum cover over the crown,  $R$  is the rise of culvert.

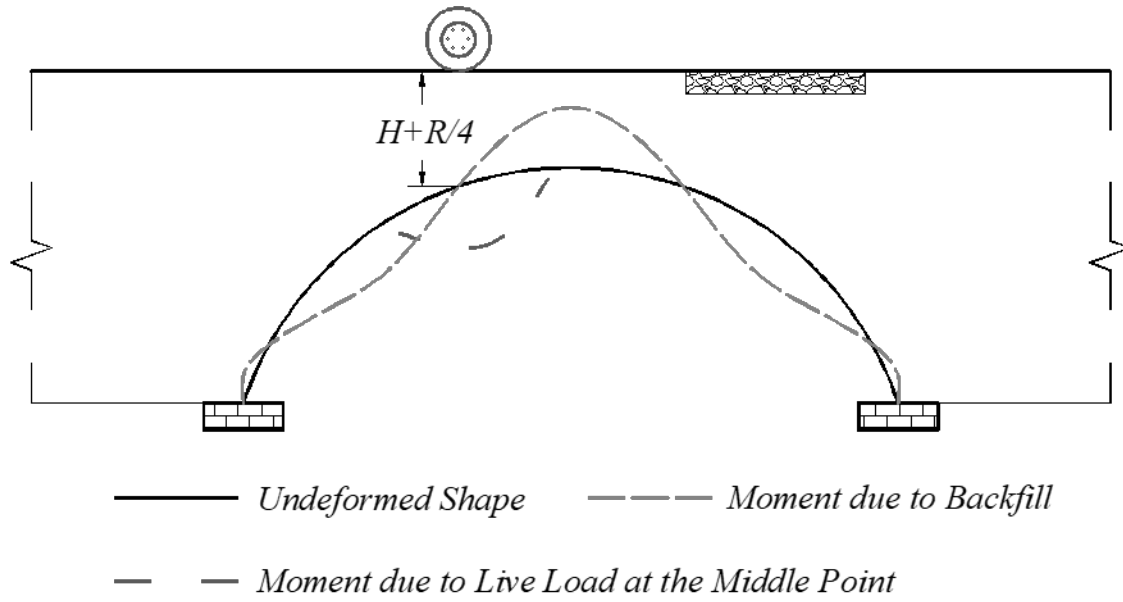


**Figure 14. Live load is over the middle point between the crown and the quarter point (outside values denote outer fiber in tension, inside values denote inner fiber in tension).**

When live load is over the crown, the numerator  $A_1M_C + A_2M_D$  in the rating factor equation is greater, but the moment due to live load in the denominator  $A_3M_L$  is also greater. However, when the live load is over the quarter point, the numerator  $A_1M_C - A_2M_D$  is less, but the denominator  $A_3M_L$  is also less. Similarly, when the live load is over the middle point between the crown and the quarter point, the numerator  $A_1M_C$  and denominator  $A_3M_L$  are both within the middle value compared with their values when live load is over the crown and over the quarter point. Therefore, numerically, it is difficult to determine which rating factor corresponding to these three different live load positions is the lowest. As a result, theoretically, it is necessary to compare the rating factors for these three cases and find out the lowest value in the simplified approach.

### 7.6 Rating Factor Equations for Culverts with Shallow Cover

The rating factor based on minimum cover requirement used by ODOT and the rating factor based on moment in MDOT are both problematic. The derivation of the rating factor based on minimum cover requirement in the ODOT approach is presented in Appendix E of the NCSPA *Design Data Sheet No. 19*. The following demonstrates the derivation and discusses its flaws.

For metal culverts buried under the minimum cover required by AASHTO,  $h$ , to withstand the load imposed by  $AL$  (axle load for design vehicle) the structure requires a plastic moment capacity of:

$$M_p = \frac{ALdF_p}{c} \left( \frac{S}{h} \right)^2 \quad (7.28)$$

Thus, for a given structure designed with the plastic moment capacity  $M_p$  defined in Eq. 7.28, as the thickness of the cover over the crown  $H$  becomes greater, heavier load  $RF(AL)$  can be applied to the culvert to maintain the same required plastic moment capacity:

$$\frac{ALdF_p}{c} \left( \frac{S}{h} \right)^2 = \frac{RF(AL)dF_p}{c} \left( \frac{S}{H} \right)^2 \quad (7.29)$$

After parameters cancel out,

$$RF = \frac{H^2}{h^2} \quad (7.30)$$

However, the axle load  $AL$  applied to minimum cover  $h$  for design on the left side of the equation is not necessarily the same as the  $AL$  on  $H$  for load rating on the right side. Plus, the factor of safety  $F_p$ , which depends on the cover-to-span ratio  $H/S$ , for minimum cover  $h$  on the left side of the equation is not equal to  $F_p$  for greater cover  $H$  on the right side. Thus, these two parameters,  $AL$  and  $F_p$ , will not cancel out. Moreover, the culvert is not necessarily designed to have the moment capacity determined by equation 7.28, which depends on the section properties of the metal culvert.

In this sense, the rating factor equation 7.30 that is based on cover heights in NCSPA Design Data Sheet No. 19 came from an overly simplified derivation.

For the rating factor based on moment in the MDOT method, the RF only defines how the maximum moment approaches its plastic moment capacity but ignores the limit state for combined effect of axial force and moment:

$$RF_M = \frac{A_1 M_C - A_2 M_D}{A_3 M_L} \quad (7.31)$$

In other words, Eq. 7.31 does not reflect any influence from thrust that might decrease the rating factor.

Two new rating factor definitions are therefore proposed to compensate for the inadequacies in the rating factors in ODOT and MDOT. The first comes from the factor of safety based on the development of a plastic hinge (Duncan and Drawsky 1983):

$$RF_{Duncan} = F_P = 0.5 \frac{P_P}{P} \left[ \sqrt{\left(\frac{M}{M_P}\right)^2 \left(\frac{P_P}{P}\right)^2 + 4} - \left(\frac{M}{M_P}\right) \left(\frac{P_P}{P}\right) \right] \quad (7.32)$$

where  $P$  = factored thrust due to both dead load and live load;  $P_P$  = factored wall yield strength;  $M$  = factored moment due to both dead load and live load; and  $M_P$  = factored plastic moment capacity.

The second is converted from AASHTO LRFD section 12.8.9.5:

$$\left(\frac{T_f}{R_t}\right)^2 + \left|\frac{M_u}{M_n}\right| \leq 1.00 \quad (7.33)$$

1.00 is reflects the minimum capacity of the structure against combined effect of thrust and moment and  $\left(\frac{T_f}{R_t}\right)^2 + \left|\frac{M_u}{M_n}\right|$  is the load effect. By taking the moment direction into consideration,

an improved rating factor is derived as:



$$RF_{AASHTO} = \frac{1 - \left[ \left( \frac{T_{fd}}{P_t} \right)^2 \pm \left| \frac{M_{ud}}{M_n} \right| \right]}{\left( \frac{T_{fl}}{P_t} \right)^2 + \left| \frac{M_{ul}}{M_n} \right|} \quad (7.34)$$

where  $T_{fd}$  = factored thrust due to dead load;  $T_{fl}$  = factored thrust due to live load;  $P_t$  = factored thrust resistance;  $M_{ud}$  = factored moment due to dead load;  $M_{ul}$  = factored moment due to live load; and  $M_n$  = factored moment resistance. The sign “ $\pm$ ” in the numerator is positive when the strain at the point on structure below the live load caused by moment due to dead load is in the same direction as that caused by moment due to live load, and vice versa. As discussed before, the factored thrusts and moments should be calculated based on different possible worst-case loading positions.

In the above new rating factor equations (Eq. 7.33 and Eq. 7.34), the Duncan method is incorporated to calculate the moment. However, because the formula for live load moment calculation proposed by Duncan was merely developed for the magnitude of change in quarter point moment due to live load over the quarter point, it cannot be used to predict the moment at other locations with live load over other positions. Thus, with the Duncan method incorporated for load rating, only the rating factors with live load over the quarter point were calculated while the rating factors for the other two possible worst-case positions of live load such as over the crown and over the middle point between crown and quarter point were not demonstrated. Hence, all the live load effects such as thrust should be also calculated based upon the live load over the quarter point.

## **7.7 Rating Factors based on Moment by Castigliano Method**

The moment equation Eq. 7.11 derived from Castigliano's method only dependent on the pressure at the crown “ $P$ ” and the radius of pipe “ $r$ ” is much simpler than that of the Duncan method that relies on calculation of many factors. Also, because the dead load effect is neglected, the rating factors can be calculated merely based on live load effect. Therefore, the introduction of the new maximum moment equation Eq. 7.11 and ignoring the dead load (Watkins and Anderson 1999, Whidden 2009) could greatly simplify the process of calculating the moment due to live load and the resultant rating factors.

According to Figure 7.6, to incorporate the moment equation by Castigliano for load rating, all the live load effects (such as thrust) should be calculated based upon the depth of minimum cover over the crown. Also, all dead load effects are neglected.

## **7.8 Proposed ALDOT Simplified Method**

The results of the in-depth examination of the ODOT and MDOT methods along with FEM based analysis were used to develop a next generation spreadsheet tool (ALDOT method). This spreadsheet computes the rating factor by ODOT and MDOT methods and compares that to the proposed ALDOT method. The spreadsheet will be provided to ALDOT for consideration.

## **7.9 Example and Comparison**

The following example is based on the second axle of the concrete truck (Figure 7.15) over the quarter point of culvert structure. All parameters in the simplified approaches and CANDE analyses are from the field test data of BIN 20441. Only the operating rating factors for LRFR load rating are presented.

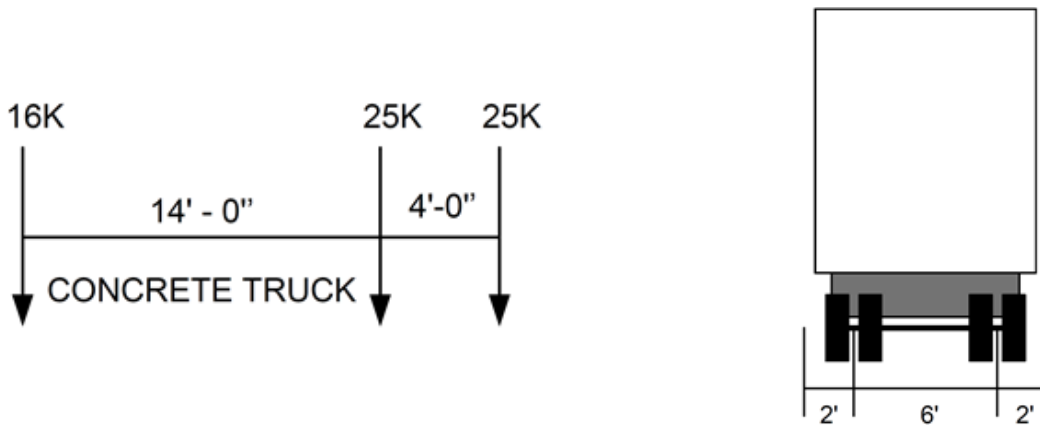


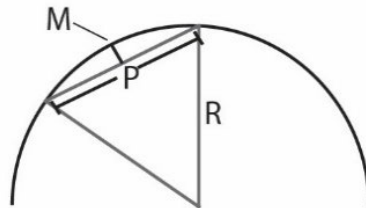
**Figure 15. Concrete Truck Configuration.**

### 7.9.1. Refined ODOT Approach

#### Structure Information

- Depth of fill:  $H = 13 \text{ in} / 12 = 1.083 \text{ ft}$
- Span length:  $S = 16.67 \text{ ft}$
- Rise:  $R = 4.33 \text{ ft}$

#### Determining Actual Top Radius ( $R_t$ )



$$R = \frac{M}{2} + \frac{P^2}{8M}$$

M = Mid-ordinate (distance from middle of curve to middle of chord)

P = Chord distance (length of straight edge)

R = Radius

Note: Maximum actual top radius ( $R_t$ ) is needed. Therefore measurements should be made at several locations to determine this value.

**Figure 7.16. Top radius definition (NCSPA 1995).**

- Straight edge length:  $P = 48in / 12 = 4 ft$
- Mid ordinate:  $M = 2.5in / 12 = 0.208 ft$
- Top radius:  $R_t = M / 2 + P^2 / (8M) = 9.704 ft$
- $R_t < 13 ft$ ; therefore, the culvert should be defined as typical corrugated metal pipe rather than long-span structural plate pipe structure (AASHTO LRFD 12.8.1).
- Asphalt thickness:  $H_{pav} = 2.5 in / 12 = 0.208 ft$
- Minimum allowable cover dimension (AASHTO LRFD C 12.6.6.3):  
 $H_{min} = H - H_{pav} = 0.875 ft < S/8 = 2.08 ft > 12 in$  (minimum cover requirement for corrugated metal pipe in AASHTO LRFD table 12.6.6.3-1)
- The minimum cover is less than the minimum allowable cover required per AASHTO.

#### Pipe Cross-Section Properties

- Pipe wall area:  $A_s = 3.321 in^2 / ft$
- Radius of gyration of corrugation:  $r = 0.5016 in$
- Moment of inertia:  $I \times 10^{-3} = 68.100 in^4 / in$

#### Pipe Seam Strength (AASHTO LRFD Section 12, APPENDIX A12)

- Pipe seam strength:  $132 k / ft$  (for 6"x1.5"x0.249"corrugation)

#### Backfill

- Soil density:  $\delta = 0.112 k / ft^3$
- Factor for distribution of live load with depth of fill based on backfill type (AASHTO LRFD 3.6.1.2.6):  $\phi_E = 1.15$

#### Load Factors

- Net load modifier for earth fill loading (AASHTO LRFD 12.5.4. and 1.3.4):  $\eta_R = 1.05$
- Maximum load factor for vertical earth pressure (AASHTO LRFD 3.4.1):  $\gamma_{EV \max} = 1.95$
- Minimum load factor for vertical earth pressure (AASHTO LRFD 3.4.1):  $\gamma_{EV \min} = 0.9$
- Live load factor for operating load rating (AASHTO MBE Table 6A.4.4.2.3a-1 and Table 6A.4.4.2.3b-1):  $\gamma_{LL} = 1.3$
- Condition factor (AASHTO MBE 2<sup>nd</sup> Edition Table 6A.4.2.3-1 & C6A.4.2.3-1):  $\phi_c = 1.0$

→ System factor (AASHTO MBE 2<sup>nd</sup> Edition Table 6A.4.2.4-1):  $\phi_s = 1.0$

### Critical Load Parameter for Arch

→ Rise and span ratio:  $R / S = 0.26$

→ Critical load parameter (Galambos 1998):  $\gamma_4 = \frac{q_{cr} S^3}{EI} = 115.7$

### Mechanical Properties

→ Minimum yield point of the metal:  $F_y = 33 \text{ ksi}$

→ Minimum tensile strength of the metal:  $F_u = 45 \text{ ksi}$

→ Modulus of elasticity of metal:  $E_m = 29000 \text{ ksi}$

### Resistance Factors

→ Percent of thickness remaining based on condition state (Sezen et al. 2009 Table 8.7):

$$\phi_{area} = 100\%$$

→ Buckling factor based on condition state (Sezen et al. 2009 Eq. 8.8):  $\phi_{buckling} = 1.00$

→ Seam strength reduction based on condition state (Sezen et al. 2009 Table 8.6):

$$\phi_{seam} = 100\%$$

→ Resistance factor for wall area and buckling (AASHTO LRFD Table 12.5.5-1):  $\phi_1 = 1.00$

→ Resistance factor for seam strength (AASHTO LRFD Table 12.5.5-1):  $\phi_2 = 0.67$

→ Soil stiffness factor (AASHTO LRFD 12.7.2.4):  $k = 0.22$

→ Pipe crown deflection: 0%

→ Buckling strength reduction factor (NCSPA *Design Data Sheet No. 19* Appendix B.1):

$$f = 1.00$$

### Calculate the Critical Buckling Stress (AASHTO LRFD 12.7.2.4)

→ If  $S < \frac{r}{k} \sqrt{\frac{24E_m}{F_u}}$ , then  $f_{cr} = F_u - \frac{F_u^2}{48E_m} \left( \frac{kS}{r} \right)^2$

→ If  $S > \frac{r}{k} \sqrt{\frac{24E_m}{F_u}}$ , then  $f_{cr} = \frac{12E_m}{(kS/r)^2}$

→ Compare:  $S(in) = 200.04 < \frac{r}{k} \sqrt{\frac{24E_m}{F_u}} = 283.55$

→ Therefore,  $f_{cr} = 33.80 \text{ ksi}$

### Thrust Capacity of the Wall

- Wall yield strength:  $\phi_1\phi_{loss}F_yA = 109.6 \text{ k/ft}$
- Wall buckling strength:  $f\phi_2\phi_{loss}f_{cr}A = 112.3 \text{ k/ft}$
- Seam strength:  $\phi_2\phi_{seam} = 88.4 \text{ k/ft}$
- Therefore, the thrust capacity of the wall:  $T_{cap} = \text{Min} [\phi_1\phi_{loss}F_yA, f\phi_2\phi_{loss}f_{cr}A, \phi_3(\text{Seam Strength})] = 88.4 \text{ k/ft}$

### Pipe Wall Thrust due to Earth Cover

- Pipe wall thrust due to earth cover:  $T_E = \sigma HR_t = 1.01 \text{ k/ft}$
- Compare the factored  $T_E = \eta_R\gamma_{EV \max}T_E$  in simplified approach with CANDE result:

Simplified	CANDE
2.071 k/ft	2.751 k/ft

- The CANDE value is obtained at the footing of culvert.

### Calculate the Pipe Wall Thrust due to Live Load plus Dynamic Load Allowance

- To incorporate the moment equation in the Duncan method for load rating, the live load effects should be calculated based upon the live load over the quarter point. Thus, the actual cover for calculation is:  $H + R/2 = 13 \text{ in} / 12 + 4.33 \text{ ft} / 2 = 3.25 \text{ ft}$
- Multiple presence factor (AASHTO LRFD 3.6.1.1.2-1):  $m = 1.2$
- Adjust  $m$  based on ADTT (AASHTO LRFD C3.6.1.1.2): 0.9
- After ADTT adjustment:  $m_{adj} = 1.08$
- Live load dynamic load allowance at surface for calculation of surface tire contact area (AASHTO LRFD 3.6.2.2 and *Appendix C: Proposed Revisions to AASHTO Specifications C3.6.1.2.6*):  $IM_{suf} = 33(1.0 - 0.125D_E)$
- $D_E = 0 \text{ ft}$
- $IM_{suf} = 33\%$
- $(1 + IM_{suf}) = 1.33$
- The "second axle" wheel load for the concrete truck with  $m_{adj}$ :  $P_{m_{adj}} = 15.9 \times 1.08 = 17.17 \text{ kips}$
- The surface tire contact area for the concrete truck (AASHTO LRFD C3.6.1.2.5),

- Tire width:  $W_T = P_{m_{adj}} / 0.8 = 21.47 \text{ in}$
- Tire length:  $L_T = 6.4\gamma_{LL}(1 + IM_{surf}) = 11.07 \text{ in}$
- Distribution of wheel load through earth fill (AASHTO LRFD 3.6.1.2.6), live load patch width at depth at the quarter point  $H + R / 2$  when the second axle is over the quarter point:  $W_L = W_T + \varphi_E(H + R / 2) + 0.06S = 6.52 \text{ ft}$
- Live load patch length at depth of quarter point  $H + R / 2$  when the second axle is over the quarter point:  $L_L = L_T + \varphi_E(H + R / 2) = 4.66 \text{ ft}$
- The wheel spacing on axle:  $6 \text{ ft}$
- The axle spacing:  $4 \text{ ft}$
- Live load patch area at depth of quarter point  $H + R / 2$  when the second axle is over the quarter point:
- If  $W_L > 6 \text{ ft}$  (overlapping in a single axle), the patch width under a wheel =  $(W_L + 6 \text{ ft}) / 2$
- If  $W_L \leq 6 \text{ ft}$  (no overlapping in a single axle), the patch width under a wheel =  $W_L$
- If  $L_L > 4 \text{ ft}$  (overlapping between adjacent axles), the patch length under a wheel =  $(L_L + 4 \text{ ft}) / 2$
- If  $L_L \leq 4 \text{ ft}$  (no overlapping between adjacent axles), the patch length under a wheel =  $L_L$
- Then, the patch area under a wheel:  $A_{LL} = (W_L + 6 \text{ ft}) / 2 \times (L_L + 4 \text{ ft}) / 2 = 26.28 \text{ ft}^2$   
(overlapping in a single axle and between adjacent axles)
- Live load dynamic load allowance at depth of quarter point  $H + R / 2$  when the second axle is over the quarter point for calculation of responses:  $IM = 33(1.0 - 0.125D_E)$
- $D_E = H + R / 2 = 3.25 \text{ ft}$
- $IM = 19.6\%$
- $(1 + IM) = 1.196$
- Pressure at the quarter point due to second axle over the quarter point plus dynamic load allowance and adjusted multiple presence factor:  
 $\rho_{(L+IM)\&m_{adj}} = 2 \times P_{(L+IM)\&m_{adj}} / A_{LL} = 2 \times 17.17 \times 1.196 / 58.34 = 0.704 \text{ ksf}$
- Pipe wall thrust due to live load plus dynamic load allowance and adjusted multiple presence factor (AASHTO LRFD 12.7.2.2):  $T_{(L+IM)\&m_{adj}} = \frac{\rho_{(L+M)\&m_{adj}}(C_L)F_1}{2}$



where  $C_L = L_L = 4.66 \text{ ft} < S = 16.67 \text{ ft}$

$$\rightarrow F_1 = \text{Max} \left( \frac{0.75(S)}{L_L}, \frac{15}{12(S)}, 1 \right) = \left( \frac{0.75(S)}{L_L} \right) = 2.68$$

$$\rightarrow T_{(L+IM)\&m_{adj}} = \frac{0.704 \text{ksf} \times 4.66 \text{ft} \times 2.68}{2} = 4.402 \text{ k/ft}$$

→ Compare the factored  $T_{(L+IM)\&m_{adj}} = \gamma_{LL} T_{(L+IM)\&m_{adj}}$  in simplified approach with CANDE result:

Simplified	CANDE
4.993 k/ft	5.287 k/ft

→ The CANDE value is obtained at the footing of culvert with second axle stopped over the quarter point.

#### Calculate the Critical Intensity of Distributed Load

→ Critical intensity of distributed load (Galambos 1998):  $q_{cr} = \gamma_4 \frac{EI}{S^3}$

→  $E = E_m = 29000 \text{ ksi}$

→  $q_{cr} = 0.0285 \text{ ksi}$

#### Calculate the Maximum Distributed Load over the Crown

→ Distribution of wheel load through earth fill (AASHTO LRFD 3.6.1.2.6),

→ Live load patch width at cover depth  $H$  over the crown:  $W_L = W_T + \varphi_E(H) + 0.06S = 4.03 \text{ ft} < 6 \text{ ft}$  (no overlapping in a single axle)

→ Live load patch length at cover depth  $H$  over the crown:  $L_L = L_T + \varphi_E(H) = 2.17 \text{ ft} < 4 \text{ ft}$  (no overlapping between adjacent axles)

→ Live load patch area at cover depth  $H$  over the crown:  $A_{LL} = W_L \times L_L = 8.75 \text{ ft}^2$

→ Live load dynamic load allowance at cover depth  $H$  over the crown for calculation of maximum distributed load:  $IM = 33(1.0 - 0.125D_E)$

→  $D_E = H = 1.08 \text{ ft}$

→  $IM = 28.5\%$

→  $(1 + IM) = 1.285$

→ Maximum distributed load at the crown due to live load plus dynamic load allowance and adjusted multiple presence factor:

$$\rho_{(L+IM)\&m_{adj}} = P_{(L+IM)\&m_{adj}} / A_{LL} = 15.9 \times 1.285 \times 1.08 / 8.75 = 2.52 \text{ ksf}$$

→ Factored maximum distributed load at the crown due to both live load and earth cover:

$$q_{\max} = \gamma_{EV \max} \eta_R \sigma H + \gamma_{LL} \rho_{(L+IM)\&m_{adj}} = 1.95 \times 1.05 \times 0.112 \times 1.08 + 1.3 \times 2.52 = 3.53 \text{ ksf} = 0.0245 \text{ ksi}$$

### Compare the Critical Intensity of Distributed Load and the Maximum Distributed Load over the Crown

→  $q_{cr} > q_{\max}$  (safe)

→ Modified minimum cover:  $h_{\text{mod}} = H = 1.08 \text{ ft}$

### Calculate the Operating Load Rating Factor for Ring Compression Structure

→ Rating factor based on wall strength:  $RF_{O-W} = \frac{\varphi_c \varphi_s T_{cap} - \gamma_{EV \max} \eta_R T_E}{\gamma_{LL} T_{(L+IM)\&m_{adj}}}$

→ Condition factor (AASHTO MBE Table 6A.4.2.3-1 and C6A.4.2.3-1):  $\varphi_c = 1.00$

→ System factor (AASHTO MBE Table 6A.4.2.4-1):  $\varphi_s = 1.00$

$$\rightarrow RF_{O-W} = \frac{1.00 \times 1.00 \times 88.4 - 1.95 \times 1.05 \times 1.01}{1.3 \times 4.402} = 15.09$$

→ Rating factor based on minimum cover requirement:  $RF_{O-C} = \frac{H^2}{C(h_{\text{mod}})^2}$

$$\rightarrow C = 2.36 \frac{H}{S} + 0.528 = 0.68 \leq 1.0$$

$$\rightarrow RF_{O-C} = 1.47$$

→ Operating rating factor:  $RF_o = \text{Min}(RF_{O-W}, RF_{O-C}) = 1.47$

## **7.9.2 Refined MDOT Simplified Approach (Duncan and Drawsky 1983)**

### Determine the Plastic Moment Capacity

→ Plastic moment capacity:  $M_p = 4.34 \text{ k} * \text{ft} / \text{ft}$

### Calculate the Flexibility Number for the Condition of Zero Cover Depth

→ Depth of fill:  $H = 0 \text{ ft}$

→ Depth of cover over the quarter point for  $H = 0 \text{ ft}$ :  $H + R / 2 = 4.33 / 2 = 2.165 \text{ ft}$

→ Secant modulus of backfill for  $H = 0 \text{ ft}$  (based on ML95 from Duncan and Drawsky,

1983):  $E_s = 45.578 \text{ k/ft}^2$

→ Flexibility number for  $H = 0 \text{ ft}$ :  $N_f = \frac{E_s S^3}{EI}$

→  $E = E_m = 29000 \text{ ksi} \times 12^2 = 4176000 \text{ k/ft}^2$

→  $N_f = 1283$

Determine the Moment Coefficients for the Condition of Zero Cover Depth

→ For  $N_f \leq 5000$ ,  $K_{M1} = 0.0046 - 0.0010 \times \log_{10} N_f$ ,

→ For  $N_f \geq 5000$ ,  $K_{M1} = 0.0009$

→ Then,  $K_{M1} = 0.0014918$

→ For  $0.2 \leq R/S \leq 0.35$ ,  $R_b = 0.67 + 0.87(R/S - 0.2)$ ,

→ For  $0.35 \leq R/S \leq 0.50$ ,  $R_b = 0.80 + 1.33(R/S - 0.35)$ ,

→ For  $0.5 \leq R/S \leq 0.60$ ,  $R_b = 2R/S$

→ Then,  $R_b = 0.7220$

Calculate the Maximum Moment at Both the Quarter Point and the Crown for the Condition of Zero Cover Depth and No Live Load

→ Maximum moment with zero cover depth:  $M_1 = K_{M1} R_b \gamma S^3$

→  $\gamma = \sigma = 0.112 \text{ k/ft}^3$

→  $M_1 = 0.559 \text{ k} * \text{ft/ft}$

Calculate the Flexibility Number for Cover Depth over the Quarter Point

→ Cover depth over the crown:  $H = 1.08 \text{ ft}$

→ Depth of cover over the quarter point:  $H + R/2 = 1.08 \text{ ft} + 4.33 \text{ ft} / 2 = 3.25 \text{ ft}$

→ Secant modulus for backfill at the depth of cover over quarter point based on ML95 from Table 7 in Duncan and Drawsky, 1983):  $E_s = 49.369 \text{ k/ft}^2$

→ Flexibility number for the depth of cover over the quarter point:  $N_f = \frac{E_s S^3}{EI} = 1390$

Determine the Moment Coefficients for Cover Depth over the Quarter Point

→ For  $N_f \leq 5000$ ,  $K_{M2} = 0.018 - 0.004 \times \log_{10} N_f$ ,

→ For  $N_f \geq 5000$ ,  $K_{M2} = 0.0032$

- Then,  $K_{M2} = 0.005428$
- For  $N_f \leq 100000$ ,  $K_{M3} = 0.120 - 0.018 \times \log_{10} N_f$ ,
- For  $N_f \geq 100000$ ,  $K_{M3} = 0.030$
- Then,  $K_{M3} = 0.0634$
- $R_L = \frac{0.265 - 0.053 \log_{10} N_f}{[(H + R/2) / S]^{0.75}} = 0.3356$
- $M_2 = K_{M2} R_B \gamma S^2 H = 0.132 \text{ k} * \text{ft} / \text{ft}$

Calculate the Maximum Moment at Quarter Point due to Earth Fill

- The maximum moment at quarter point due to earth fill:  $M_B = M_1 - K_{M2} R_B \gamma S^2 H$
- $\gamma = \sigma = 0.112 \text{ k} / \text{ft}^3$
- $H = 1.08 \text{ ft}$
- $M_B = 0.427 \text{ k} * \text{ft} / \text{ft}$
- Compare the factored  $M_B = \gamma_{EV \max} \eta_R M_1 - \frac{\gamma_{EV \min}}{\eta_R} K_{M2} R_B \gamma S^2 H$  in simplified approach with CANDE result:

Simplified	CANDE
1.031 k * ft / ft	0.396 k * ft / ft

- The CANDE value is obtained at the quarter point of culvert.

Calculate the Equivalent Line Load with Consideration of Pavement for the Calculation of Moment due to Live Load

- Elastic modulus of the asphalt pavement (Han et al. 2013):  $E_1 = 200000 \text{ psi}$
- Elastic modulus of the lime-treated subgrade (Han et al. 2013):  $E_2 = 45000 \text{ psi}$
- Elastic modulus of the natural subgrade (the elastic modulus in top layer of ML95 in Table 7.3):  $E_3 = 1800 \text{ psi}$
- Thicknesses of asphalt pavement:  $h_1 = H_{pave} = 2.5 \text{ in}$
- Thicknesses of lime-treated subgrade (Han et al. 2013):  $h_2 = 6 \text{ in}$

→ Thicknesses of natural subgrade:  $h_3 = H + R/2 - h_1 - h_2 = 30.48$  in Reference vertical pressure distribution angle in the backfill (AASHTO LRFD Table 3.6.1.2.6a-1):

$$\tan \alpha_0 = \tan 30^\circ = LLDF/2 = 1.15/2 = 0.575$$

→ Vertical pressure distribution angle in the asphalt pavement (Han et al., 2013):

$$\tan \alpha_1 = \tan \alpha_0 \left[ 1 + 0.204 \left( \frac{E_1}{E_2} - 1 \right) \right] = 0.98$$

→ Vertical pressure distribution angle in the lime-treated subgrade:

$$\tan \alpha_2 = \tan \alpha_0 \left[ 1 + 0.204 \left( \frac{E_2}{E_3} - 1 \right) \right] = 3.39$$

→ Vertical pressure distribution angle in the natural subgrade:

$$\tan \alpha_3 = \tan \alpha_0 = 0.58$$

→ Length of the distributed area at the quarter point by one single wheel load:

$$a = W_T + 2(h_1 \tan \alpha_1 + h_2 \tan \alpha_2 + h_3 \tan \alpha_3) = 8.13 \text{ ft}$$

→ Wheel spacing on axle: 6 ft

→ Equivalent line load with consideration of pavement:

$$\text{If } a > 6 \text{ ft (overlapping in a single axle), } K_4 = a + 6 \text{ ft}$$

$$\text{If } a \leq 6 \text{ ft (no overlapping in a single axle), } K_4 = 2a$$

$$\text{Then, } K_4 = a + 6 \text{ ft} = 14.13 \text{ ft (overlapping in a single axle)}$$

→ The load supported on a single axle or on tandem axles if the spacing between the axles is less than one third the span of the culvert:  $AL = 50 \text{ kips}$  (because the spacing between the axles 4 ft is less than one third the span of the culvert  $16.67/3=5.56$  ft)

$$\rightarrow \text{The equivalent line load: } LL = \frac{AL}{K_4} = 3.54 \text{ k/ft}$$

#### Calculate the Additional Moment at Quarter Point due to Live Load

→ The pavement effect is only accounted for in the calculation of moment due to live load because it affects moment much more than thrust.

$$\rightarrow \text{Additional moment at quarter point due to live load: } \Delta M_L = K_{M3} R_L S(LL) = 1.26 \text{ k} * \text{ft/ft}$$

#### Calculate the Reduction Ratio due to Pavement for the Calculation of Moment due to Live Load

- Elastic modulus of the flexible pavement (CANDE Tool Box 2019):  $E_1 = 200000 \text{ psi}$
- Elastic modulus of the underlying backfill (the elastic modulus in top layer of ML95 in Table 3):  $E_2 = 1800 \text{ psi}$

- Reference vertical pressure distribution angle in the backfill (AASHTO LRFD Table 3.6.1.2.6a-1):  $\tan \alpha_0 = \tan 30^\circ = LLDF/2 = 1.15/2 = 0.575$

- Vertical pressure distribution angle in the pavement (Han et al., 2013):

$$\tan \alpha_1 = \tan \alpha_0 \left[ 1 + 0.204 \left( \frac{E_1}{E_2} - 1 \right) \right] = 13.49$$

- Length of the distributed area at the quarter point by one single wheel load:

$$a = W_T + 2 \left[ H_{pav} \tan \alpha_1 + (H_{\min} + R/2) \tan \alpha_0 \right] = 10.91 \text{ ft}$$

- Width of the distributed area at the quarter point by one single wheel load:

$$a - (W_T - L_T) = 10.04 \text{ ft}$$

- Distributed area at the quarter point by one single wheel load:

$$a \left[ a - (W_T - L_T) \right] = 109.49 \text{ ft}^2$$

- Wheel spacing on axle:  $6 \text{ ft}$

- Pressure at the quarter point due to heaviest axle over the quarter point plus dynamic load allowance and adjusted multiple presence factor with consideration of pavement:

- If  $a > 6 \text{ ft}$  (overlapping within the distributed area),

$$\rho_{(L+IM)\&m_{adj}\&pave} = 2 \times \frac{P_{(L+IM)\&m_{adj}}}{a \left[ a - (W_T - L_T) \right]}$$

- If  $a \leq 6 \text{ ft}$  (no overlapping within the distributed area),

$$\rho_{(L+IM)\&m_{adj}\&pave} = \frac{P_{(L+IM)\&m_{adj}}}{a \left[ a - (W_T - L_T) \right]}$$

- Then,  $\rho_{(L+IM)\&m_{adj}\&pave} = 0.38 \text{ ksf}$  (overlapping)

- Reduction ratio of axle load due to pavement in the calculation of moment due to live

$$\text{load: } R_{pave} = \frac{\rho_{(L+IM)\&m_{adj}\&pave}}{\rho_{(L+IM)\&m_{adj}}} = \frac{0.38}{0.70} = 0.53$$

- The pavement effect is only accounted for in the calculation of moment due to live load because it affects moment much more than thrust.

Calculate the Additional Moment at Quarter Point due to Live Load

- The pavement effect is only accounted for in the calculation of moment due to live load because it affects moment much more than thrust.
- Additional moment at quarter point due to live load:  $\Delta M_L = K_{M3} R_L S(LL)$
- Equivalent line load:  $LL = \frac{R_{pave} \times AL}{K_4}$
- Axle load for concrete truck (the load on a single axle, or on tandem axles spaced at less than one third the span of the culvert):  $R_{pave} \times AL = 0.53(31.8 + 31.4) = 33.67 \text{ kips}$
- Factor for calculating equivalent line load at depth of cover over the quarter point:  
 $H + R / 2 = 3.25 \text{ ft}$  (based on 4 wheels per axle from Duncan and Drawsky, 1983):  
 $K_4 = 9.17 \text{ ft}$
- $\Delta M_L = 1.30 \text{ k} * \text{ft} / \text{ft}$

Calculate the Operating Load Rating Factor Based on Plastic Moment Capacity

- Rating factor based on plastic moment capacity:  $RF_{O-M} = \frac{\phi_c \phi_s \phi_f M_p - \gamma_{EV \max} \eta_R M_B}{\gamma_{LL} M_{(L+IM) \& m_{adj}}}$
- Resistance factor for flexure (AASHTO LRFR 6.5.4.2):  $\phi_f = 1.0$
- Live load dynamic load allowance at quarter point:  $IM = 33(1.0 - 0.125 D_E)$
- $D_E = H + R / 2 = 3.25 \text{ ft}$
- $IM = 19.6\%$
- $(1 + IM) = 1.196$
- Additional moment at quarter point due to live load plus dynamic load allowance and adjusted multiple presence factor:  $M_{(L+IM) \& m_{adj}} = (1 + IM) m_{adj} \Delta M_L = 1.68 \text{ k} * \text{ft} / \text{ft}$
- Compare the factored  $M_{(L+IM) \& m_{adj}} = \gamma_{LL} M_{(L+IM) \& m_{adj}}$  in simplified approach with its CANDE result:

Simplified	CANDE
2.109 k * ft / ft	1.430 k * ft / ft

- The CANDE value is obtained at the quarter point of culvert with heaviest axle stopped over the quarter point.
- $RF_{O-M} = 1.51$



### 7.9.3 Rating Factor Based on AASHTO

#### Calculate the Operating Load Rating Factor Based on AASHTO LRFR 12.8.9.5

→ Operating load rating factor based on AASHTO LRFR 12.8.9.5:

$$RF_{O-AASHTO} = \frac{1 - \left[ \left( \frac{T_{fd}}{P_t} \right)^2 + \left| \frac{M_{ud}}{M_n} \right| \right]}{\left( \frac{T_{fl}}{P_t} \right)^2 + \left| \frac{M_{ul}}{M_n} \right|}$$

→ Factored thrust due to dead load:  $T_{fd} = \gamma_{EV \max} \eta_R T_E = 2.07 \text{ k/ft}$

→ Factored thrust due to live load:  $T_{fl} = \gamma_{LL} T_{(L+IM)\&m_{adj}} = 5.72 \text{ k/ft}$

→ Factored thrust resistance:  $P_t = \phi_h F_y A$

→ Resistance factor for plastic hinge (AASHTO LRFR Table 12.5.5-1):  $\phi_h = 0.9$

→ Area of pipe wall:  $A = A_s = 3.321 \text{ in}^2/\text{ft}$

→  $P_t = 98.63 \text{ k/ft}$

→ Factored moment due to dead load:  $M_{ud} = \gamma_{EV \max} \eta_R M_1 - \frac{\gamma_{EV \min}}{\eta_R} K_{M2} R_B \gamma S^2 H = 1.03$

$k * \text{ft}/\text{ft}$

→ Factored moment due to live load:  $M_{ul} = \gamma_{LL} M_{(L+IM)\&m_{adj}} = 2.19 \text{ k} * \text{ft}/\text{ft}$

→ Factored moment resistance:  $M_n = \phi_h M_p = 0.9 \times 4.34 = 3.91 \text{ k} * \text{ft}/\text{ft}$

→  $RF_{O-AASHTO} = 1.31$

### 7.9.4 Rating Factor Based on Duncan (1983)

#### Calculate the Operating Load Rating Factor Based on the Factor of Safety against Development of Plastic Hinge

→ Operating load rating factor based on the factor of safety against development of plastic hinge (Duncan and Drawsky, 1983):

$$RF_{O-Duncan} = F_P = 0.5 \frac{P_P}{P} \left[ \sqrt{\left( \frac{M}{M_P} \right)^2 \left( \frac{P_P}{P} \right)^2 + 4} - \left( \frac{M}{M_P} \right) \left( \frac{P_P}{P} \right) \right]$$

→ Factored thrust due to both dead load and live load:

$$P = T_{fd} + T_{fl} = \gamma_{EV \max} \eta_R T_E + \gamma_{LL} T_{(L+IM)\&m_{adj}} = 7.79 \text{ k/ft}$$

→ Factored wall yield strength:  $P_p = P_t = \phi_h F_y A = 98.63 \text{ k/ft}$

→ Factored moment due to both dead load and live load:

$$M = M_{ud} + M_{ul} = \gamma_{EV \max} \eta_R M_1 - \frac{\gamma_{EV \min}}{\eta_R} K_{M2} R_B \gamma S^2 H + \gamma_{LL} M_{(L+IM)\&m_{adj}} = 3.22 \text{ k * ft/ft}$$

→ Factored plastic moment capacity:  $M_p = M_n = \phi_h M_p = 0.9 \times 4.34 = 3.91 \text{ k * ft/ft}$

→  $RF_{O-Duncan} = 1.20$

### 7.9.5 Comparison between Simplified Approaches and CANDE

#### The Operating Load Rating Factor from ODOT Method

→  $RF_O = \text{Min}(RF_{O-W}, RF_{O-C}) = RF_{O-C} = 1.47$

#### The Operating Load Rating Factor from MDOT Method

→  $RF_O = \text{Min}(RF_{O-W}, RF_{O-M}) = RF_{O-M} = 1.51$

#### The Operating Load Rating Factor from AASHTO Method

→  $RF_O = \text{Min}(RF_{O-W}, RF_{O-AASHTO}) = RF_{O-AASHTO} = 1.31$

#### The Operating Load Rating Factor from Duncan Method

→  $RF_O = \text{Min}(RF_{O-W}, RF_{O-Duncan}) = RF_{O-Duncan} = 1.20$

#### The Comparison of Responses and Rating Factors between Simplified Methods and CANDE

Structural Responses	Simplified	CANDE
Max Factored Thrust due to Dead Load (k/ft)	2.07	2.75
Max Factored Thrust due to Live Load (k/ft)	4.99	5.29
Factored Moment at The Quarter Point due to Dead Load (k*ft/ft)	1.03	0.396

Factored Moment at The Quarter Point due to Live Load (k*ft/ft)	2.11	1.43
<b>Rating Factors</b>	<b>Simplified</b>	<b>CANDE</b>
ODOT RF	1.47	2.3
MDOT RF	1.57	
AASHTO RF	1.36	
Duncan RF	1.23	

### 7.9.6 Rating Factors Based on Castigliano's Equation

According to Figure 7.6, to incorporate the simpler moment equation by Castigliano for load rating, the live load effects should be calculated based upon the cover depth over the crown:

$$H = 13 \text{ in.}$$

#### Calculate the Pipe Wall Thrust due to Live Load plus Dynamic Load Allowance

→ Maximum distributed load at the crown due to live load plus dynamic load allowance and adjusted multiple presence factor:

$$\rho_{(L+IM)\&m_{adj}} = P_{(L+IM)\&m_{adj}} / A_{LL} = 15.9k \times 1.285 \times 1.08 / 8.75 \text{ ft}^2 = 2.52 \text{ ksf}$$

→ Pipe wall thrust due to live load plus dynamic load allowance and adjusted multiple

presence factor (AASHTO LRFD 12.7.2.2):  $T_{(L+IM)\&m_{adj}} = \frac{\rho_{(L+M)\&m_{adj}} (C_L) F_1}{2}$

→  $C_L = L_L = 2.17 \text{ ft} < S = 16.67 \text{ ft}$

→  $F_1 = \text{Max} \left( \frac{0.75(S)}{L_L}, \frac{15}{12(S)}, 1 \right) = \left( \frac{0.75(S)}{L_L} \right) = 5.77$

→  $T_{(L+IM)\&m_{adj}} = \frac{2.52 \text{ ksf} \times 2.17 \text{ ft} \times 5.77}{2} = 15.77 \text{ k/ft}$

→ Compare the factored  $T_{(L+IM)\&m_{adj}} = \gamma_{LL} T_{(L+IM)\&m_{adj}}$  in simplified approach with CANDE result:

Simplified	CANDE
17.809 k/ft	11.674 k/ft

→ The CANDE value is obtained at the footing with second axle stopped over the crown.

### Calculate the Maximum Moment due to Live Load

→ The pavement effect is only accounted for in the calculation of moment due to live load because it affects moment much more than thrust.

→ Thicknesses of natural subgrade:  $h_3 = H - h_1 - h_2 = 4.50 \text{ in}$

→ Length of the distributed area at the crown by one single wheel load:

$$a = W_T + 2 \left[ H_{pav} \tan \alpha_1 + (H_{\min}) \tan \alpha_0 \right] = 8.42 \text{ ft}$$

→ Width of the distributed area at the crown by one single wheel load:

$$a - (W_T - L_T) = 7.55 \text{ ft}$$

→ Distributed area at the crown by one single wheel load:

$$a \left[ a - (W_T - L_T) \right] = 63.54 \text{ ft}^2$$

→ Wheel spacing on axle: 6 ft

→ Pressure at the crown due to second axle approaching the pipe from the left side of the centerline plus dynamic load allowance and adjusted multiple presence factor with consideration of pavement:

If  $a > 6 \text{ ft}$  (overlapping within the distributed area),

$$\rho_{(L+IM)\&m_{adj}\&pave} = 2 \times \frac{P_{(L+IM)\&m_{adj}}}{a \left[ a - (W_T - L_T) \right]}$$

If  $a \leq 6 \text{ ft}$  (no overlapping within the distributed area),

$$\rho_{(L+IM)\&m_{adj}\&pave} = \frac{P_{(L+IM)\&m_{adj}}}{a \left[ a - (W_T - L_T) \right]}$$

→ Live load dynamic load allowance at crown:

$$IM = 33(1.0 - 0.125D_E)$$

$$D_E = H = 1.08 \text{ ft}$$

$$IM = 28.5\%$$

$$(1 + IM) = 1.285$$

$$\rightarrow \text{Then, } \rho_{(L+IM)\&m_{adj}\&pave} = \frac{P_{(L+IM)\&m_{adj}}}{a[a - (W_T - L_T)]} = \frac{12.5 \times 1.285 \times 1.08}{29.03} = 0.60 \text{ ksf (No}$$

overlapping)

→ Maximum moment on the right side of the centerline due to live load plus dynamic load allowance and adjusted multiple presence factor:

$$M_{(L+IM)\&m_{adj}} = 0.022 Pr^2 = 0.022 \times \rho_{(L+IM)\&m_{adj}\&pave} \times R_T = 1.44 \text{ k * ft/ft}$$

→ Compare the factored  $M_{(L+IM)\&m_{adj}} = \gamma_{LL} M_{(L+IM)\&m_{adj}}$  in simplified approach with CANDE result:

Simplified	CANDE
1.610 k * ft/ft	1.973 k * ft/ft

→ The CANDE value is obtained at the quarter point of culvert with the second axle stopped over the quarter point.

### Calculate the Operating Load Rating Factor Based on Plastic Moment Capacity with Castigliano's Equation

→ Rating factor based on plastic moment capacity (dead load is neglected):

$$RF_{O-M}^s = \frac{\phi_c \phi_s \phi_f M_p}{\gamma_{LL} M_{(L+IM)\&m_{adj}}}$$

→ Resistance factor for flexure (AASHTO LRFR 6.5.4.2):  $\phi_f = 1.0$

$$\rightarrow RF_{O-M}^{Castigliano} = \frac{1 \times 1 \times 1 \times 4.34}{1.3 \times 1.24} = 2.70$$

### Calculate the Operating Load Rating Factor Based on AASHTO LRFR 12.8.9.5 with Castigliano's Equation

→ Operating load rating factor based on AASHTO LRFR 12.8.9.5 (dead load is neglected):

$$RF_{O-AASHTO}^s = \frac{1}{\left(\frac{T_{fl}}{P_t}\right)^2 + \left|\frac{M_{ul}}{M_n}\right|}$$

- Factored thrust due to live load:  $T_{fl} = \gamma_{LL} T_{(L+IM)\&m_{adj}} = 17.81 \text{ k/ft}$
- Factored thrust resistance:  $P_t = \phi_h F_y A = 98.63 \text{ k/ft}$
- Factored moment due to live load:  $M_{ul} = \gamma_{LL} M_{(L+IM)\&m_{adj}} = 1.61 \text{ k * ft/ft}$
- Factored moment resistance:  $M_n = \phi_h M_p = 0.9 \times 4.34 = 3.91 \text{ k * ft/ft}$
- $RF_{O-AASHTO}^{Castigliano} = 2.25$

**Calculate the Operating Load Rating Factor Based on The Factor of Safety against Development of Plastic Hinge with Castigliano's Equation**

- Operating load rating factor (dead load is neglected) based on the factor of safety against development of plastic hinge (Duncan and Drawsky, 1983):

$$\rightarrow RF_{O-Duncan}^{Castigliano} = F_p = 0.5 \frac{P_p}{P} \left[ \sqrt{\left(\frac{M}{M_p}\right)^2 \left(\frac{P_p}{P}\right)^2 + 4} - \left(\frac{M}{M_p}\right) \left(\frac{P_p}{P}\right) \right]$$

- Factored thrust due to live load:  $P = \gamma_{LL} T_{(L+IM)\&m_{adj}} = 17.81 \text{ k/ft}$
- Factored wall yield strength:  $P_p = P_t = \phi_h F_y A = 98.63 \text{ k/ft}$
- Factored moment due to live load:  $M = \gamma_{LL} M_{(L+IM)\&m_{adj}} = 1.61 \text{ k * ft/ft}$
- Factored plastic moment capacity:  $M_p = M_n = \phi_h M_p = 0.9 \times 4.34 = 3.91 \text{ k * ft/ft}$
- $RF_{O-Duncan}^{Castigliano} = 2.08$

**7.9.7 Comparison between Simplified Approaches and CANDE**

**Calculate the Operating Load Rating Factor for Ring Compression Structure with Castigliano's Equation**

- Rating factor based on wall strength calculated with cover depth over the crown (dead load is neglected):  $RF_{O-W}^{Castigliano} = \frac{\phi_c \phi_s T_{cap}}{\gamma_{LL} T_{(L+IM)\&m_{adj}}}$
- Condition factor (AASHTO MBE Table 6A.4.2.3-1 & C6A.4.2.3-1):  $\phi_c = 1.00$
- System factor (AASHTO MBE Table 6A.4.2.4-1):  $\phi_s = 1.00$
- $RF_{O-W}^{Castigliano} = \frac{1.00 \times 1.00 \times 88.4}{1.3 \times 13.70} = 4.97$
- The Operating Load Rating Factor from MDOT Method with Castigliano's Equation

$$RF_O^{Castigliano} = \text{Min}(RF_{O-W}^{Castigliano}, RF_{O-M}^{Castigliano}) = RF_{O-M}^{Castigliano} = 2.70$$

→ The Operating Load Rating Factor from AASHTO Method with Castigliano's Equation

$$RF_O^{Castigliano} = \text{Min}(RF_{O-W}^{Castigliano}, RF_{O-AASHTO}^{Castigliano}) = RF_{O-AASHTO}^{Castigliano} = 2.25$$

→ The Operating Load Rating Factor from Duncan Method with Castigliano's Equation

$$RF_O^{Castigliano} = \text{Min}(RF_{O-W}^{Castigliano}, RF_{O-Duncan}^{Castigliano}) = RF_{O-Duncan}^{Castigliano} = 2.08$$

Comparison of Responses and Rating Factors between Simplified Methods and CANDE

<b>Structural Responses</b>	<b>Simplified</b>	<b>CANDE</b>
Factored Thrust due to Live Load (k /ft)	17.8	11.7
Factored Moment due to Live Load (k*ft/ft)	1.61	1.97
<b>Rating Factors</b>	<b>Simplified</b>	<b>CANDE</b>
Castigliano MDOT RF	2.70	2.3
Castigliano AASHTO RF	2.25	
Castigliano Duncan RF	2.08	

**7.10 Simplified Methodology Summary**

The currently used simplified approaches for load rating developed by ODOT and MDOT are considered to be too conservative for shallow buried metal culverts with cover depth less than minimum requirement defined by AASHTO. The conservatism is mainly attributed to the inappropriate selection of some parameters in the equations for calculation of structural responses and the ignorance of load-spreading effect of pavement in these simplified procedures. After reclarifying and reselecting these mis-chosen parameters and utilizing appropriate techniques to



account for pavement effect, the responses and rating factors calculated from the refined simplified approaches are found to be reasonably closer to their corresponding numerical results in CANDE.

Two new equations are developed based on AASHTO LRFD 12.8.9.5 and Duncan (1983) respectively to account for the combined effect of thrust and moment for load rating. Rating factors calculated from these two new equations, originally created to evaluate the development of plastic hinge, also agree well with the result predicted by CANDE.

A simpler equation from Watkins and Anderson (1999) and Whidden (2009) to calculate the maximum moment due to live load by Castigliano's method is introduced. This simpler equation can also generate accurate maximum live load effect and close rating factors relative to the CANDE results and thus is seen as another correct way for the calculation of live load moment incorporated into the simplified approach in this study.

However, the remodified simplified approaches based on ODOT and MDOT are only a measure of expediency. As the depth of cover gets thinner and thinner, neither the assumption that the culvert structure is under ring compression would be established any longer, nor the way to convert the earth weight and live load as uniformly pressure over the entire span of culvert is applicable anymore. The future work may involve developing new equations for non-ring compression culvert structures to calculate the responses and rating factors under extreme shallow cover or even no cover over the crown and creating new formulas to calculate the moment at different positions than at the quarter point, such as at the crown or at the point between the crown and the quarter point, so as to find out the worst-case loading position for load rating.

## CHAPTER 8: RATING OF THE ANNISTON CULVERTS

### 8.1 Rating Factor Methodology Summary

One of the key objectives of the project was to use the developed methodologies and data to form a best estimate of rating factors for the nine Anniston culverts against the Alabama posting vehicles. However, the various available methods result in significantly different rating outcomes and each offers disparate advantages and disadvantages. This chapter therefore assesses, compares and summarizes the rating outcomes calculated using the methods defined in the prior chapters, and ultimately culminates in final rating factor recommendations for the nine Anniston culverts. Critical observations about each analysis option are summarized first.

#### 8.1.1 Original ODOT Spreadsheet

The original ODOT spreadsheet is based on the NCSPA *Design Data Sheet #19* and provides the easiest calculation approach. However, by definition, it will result in rating factors that are less than 1 when the cover over the crown is less than the minimum cover defined by AASHTO design specifications, regardless of the robustness of the actual constructed culvert. The Anniston culverts therefore result in a rating factor of less than 1 using this methodology. Also, the original ODOT spreadsheet is only LFR.

#### 8.1.2 Modified ODOT Spreadsheet

The modified ODOT spreadsheet is also easy to use, but also tends to result in a rating factor that is much lower than the actual available resistance for low cover situations. Recognizing the inherent weakness of basing the RF on cover depth, the modified ODOT spreadsheet approach added buckling theory to the limit state. However, it appears that the buckling modification is

incorporated in a way that is likely inaccurate. LRFR was added to the modified ODOT spreadsheet approach.

### **8.1.3 MDOT Spreadsheet**

The MDOT spreadsheet approach improved the rating factor definitions that account for loading and structural resistance and eliminated the rating factor equations that are based solely on cover depths. LFR and LRFR versions are available. Detractions include that the calculations of the dead load (DL) and live load (LL) are complicated and confusing, and the load spreading effect of pavement, which can have a significant impact in low cover situations, is not considered.

### **8.1.4 AU Modified MDOT (ALDOT Spreadsheet)**

As presented in Chapter 7, the MDOT methodology and spreadsheet tool was augmented through this project. Primary improvements included (1) the ability to address the load spreading effect of pavement and based, (2) reassignment of critical parameters that were confusing, and (3) introduction of new moment and new rating factor equations.

It should be recognized at this point that any and all simplified approaches involve inherent and potentially severe flaws when applied to shallow cover situations. The most prominent include: (1) given the nonlinearities and geometric complexities, there are no simple structural analysis methods that can accurately resolve the relatively localized tire pressure loading at the roadway surface into internal forces in the culvert walls at the ultimate strength condition; and (2) the simplified methods do not explicitly account for the culvert shape; for example with the Anniston culverts, the rating factor calculation for the arch culvert with a particular fill and geometry profile is exactly the same as that of the comparable pipe arch culvert. The “simplified” approaches presented in the literature and incorporated into the spreadsheet tools mentioned above rely on a limited set of empirical data and therefore are very approximate at best when applied to

shallow cover situations. Although the intent was to develop conservative simple methodologies (the calculated rating factor would be lower than reflected by the actual capacity), this is not guaranteed.

#### **8.1.4 2D / Plane Strain (CANDE)**

As discussed in detail in Chapter 6, CANDE is a plane strain finite element code that was developed specifically for culvert analyses. It simulates compaction associated with construction phases and incorporates critical sources of nonlinearities such as soil plasticity models and soil-structure interaction. It therefore tends to be much more versatile and accurate than the “simplified approach” spreadsheet tools. It can account for load and resistance factors and can directly calculate the rating factors associated with the various limit states. The critical load position can be automatically analyzed.

Detractions include the inevitable inaccuracies associated with converting a three dimensional scenario into plane strain analysis. The impact of this approximation is much more pronounced for shallow cover live load controlled scenarios than for deep buried culverts. Also, given the inherent nonlinearities, to achieve an accurate rating factor from CANDE, the magnitudes of the loads, in their critical positions, must be increased until failure is simulated (a rating factor of 1 is reached), and then the ratio of that failure load magnitude over the factored load represents the actual rating factor. Numerical convergence issues are inevitable. The pavement effect cannot be properly simulated with the elastic beam elements that are available within CANDE because the tension and shear that could occur at the ultimate load would likely exceed the linear elastic stress limits of pavement. This is a cumbersome process that is not easily understood by typical practicing transportation engineers. Even though CANDE was developed specifically for culvert design and analysis, its use for rating factor analysis is complex and requires

high level of FEM expertise and experience. CANDE will output rating factors based on extrapolating the results from applying the factored load, but those results will likely be significantly inaccurate and over-predictive (unconservative) for shallow cover scenarios. To illustrate the need for carefully increasing the load magnitude until failure is simulated, in the following sections, CANDE analyses in which the prescribed factored loading is applied and the rating factor results from extrapolation is referred to as “Level 1” analyses; analyses in which the load magnitude is increased until failure is simulated is referred to as “Level 2”.

### **8.1.5 3D Nonlinear FEM**

Three-dimensional finite element modeling using general purpose FEM software, such as with ABAQUS and PLAXIS 3D used for this project and highlighted in Chapter 6, has the greatest potential of any analytical method for being accurate. It is also the most versatile, but since was not developed for load rating, it is unable to directly output rating factors and therefore significant effort and expertise is required to transform the finite element results into rating calculations. Furthermore advanced software and the required computation resources tend to be costly. Using general purpose FEM software for rating purposes is generally not an option for the typical transportation engineering office.

### **8.1.6 Load Testing**

Load testing is not a stand-alone rating technique, but it can improve the accuracy of the other analytical methods. Its value is apparent in scenarios such as the Anniston culverts where the backfill depths do not meet current design and construction requirements, the backfill materials and quality are unknown, and existing analytical tools conclude that posting is necessary whereas performance does not indicated any significant capacity concerns. Detractions include that load testing is costly, accessibility-dependent, requires high level of expertise and experience since

there are no existing standards, and a significant pretest analysis investment must be made to ensure that the structure will not fail under test loading. The following sections demonstrate the use of the field test data presented in Chapter 5 for improving the accuracy of analytical rating factor calculations.

## 8.2 Rating Factor Calculation using Field Test Data

To improve rating accuracy using the load test data, the load effects measured at the critical point (the point with maximum response to the applied load) must be compared with the values predicted by a theoretical or analytical approach at the same point due to the test vehicle at its corresponding position. The procedures initially defined in NCHRP Research Result Digest Issue No. 234 “Manual for Bridge Rating through Load Testing” (TRB 1998) and currently in the MBE (AASHTO 2018) associate the computations used to define theoretical load rating factor with the load testing data using a factor “ $K$ ” as defined in equations 8.1 through 8.4.  $K$  is equal to 1 if no load test data is available or if the load test results agree with the theoretical or analytical results. If  $K$  is greater than 1 then the response of the structure is more favorable as observed from the load test than predicted theoretically; hence, the rating factor may be increased. If  $K$  is less than 1 then the theoretical rating factor is reduced because the load test responses are more severe than theoretically predicted (TRB 1998).

$$RF_T = RF_C K \quad (8.1)$$

where  $RF_T$  is the rating factor corrected using load test data,  $RF_C$  is the theoretical load rating factor and  $K$  is the adjustment factor defined in equation 2:

$$K = 1 + K_a K_b \quad (8.2)$$

where  $K_a$  accounts for both the benefit from the load test and the section factor resisting the applied load (equation 8.3) while  $K_b$  accounts for the load test results compared with theoretical calculations, follow-up inspections, and the presence or absence of special features (equation 8.4).

$$K_a = \frac{\varepsilon_C}{\varepsilon_T} - 1 \quad (8.3)$$

where  $\varepsilon_T$  is the maximum measured member strain during load test and  $\varepsilon_C$  is the corresponding theoretical strain for the test vehicle at the same position in the load test.

$$K_b = K_{b1} K_{b2} K_{b3} \quad (8.4)$$

where  $K_{b1}$  accounts for the extent to which the contribution of test measurement can be relied on at the rating load level and ranges from 0 to 1;  $K_{b2}$  accounts for inspection and ranges from 0.8 to 1; and  $K_{b3}$  accounts for different failure modes and presence of failure indicators, and ranges from 0.7 to 1.

To illustrate the use of the test data presented in Chapter 5 for improving the accuracy of a rating factor,  $RF_C$  is required, which can be derived from simplified approaches or advanced analytical approaches such as the use of finite element software. The following is based upon methodology adopted by the Michigan Department of Transportation (Ahlborn et al. 2013, MDOT 2016). The Alabama Department of Transportation defines seven posting vehicles ranging from 11.3 MT (12.5T) school bus to 38.1 MT (42T) “6 AXLE (3S3)” truck (ALDOT 2021). For illustration purposes, the 29.9 MT (33T) concrete truck defined in Figure 8.1 was used since it results in the lowest analytical rating factor for the tested culverts. Additionally, the MDOT approach uses moments calculated at quarter points as the basis for the demand calculations.



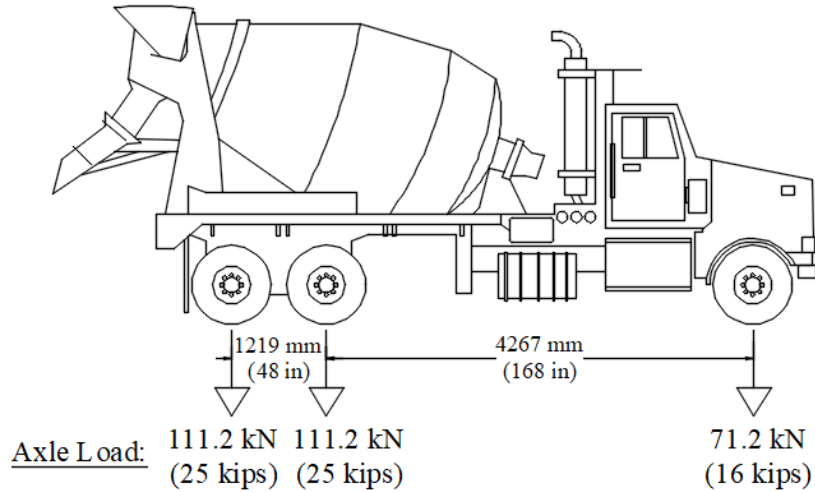


**Figure 8.1. Concrete truck used for RF comparisons**

For the culvert scenario, the LRFR theoretical rating factor is defined by:

$$RF_C = \frac{\phi_c \phi_s \phi_f \phi M_P - \gamma_{EV} \eta_R M_B}{\gamma_{LL} (M_{L+IM})} \quad (8.5)$$

where  $M_P$  = plastic moment capacity (per length);  $M_B$  = maximum moment (per length) at quarter point due to backfill loads at final cover;  $M_{L+IM}$  = additional moment (per length) at quarter point due to live load plus impact over quarter point;  $\phi_c$ ,  $\phi_s$ ,  $\phi_f$  = condition factor, system factor and flexural resistance factor, respectively; and  $\gamma_{EV}$ ,  $\gamma_{LL}$ ,  $\eta_R$  = load factor for vertical earth pressure and live load respectively and load modifier relating to redundancy. The maximum moment at quarter points is defined by:

$$M_B = K_{M1} R_B \gamma S^3 - K_{M2} R_B \gamma S^2 H \quad (8.6)$$

and the additional moment at quarter point due to live load over quarter point can be calculated by:

$$M_L = K_{M3} R_L S(LL) \quad (8.7)$$

in which  $K_{M1}$ ,  $K_{M2}$ ,  $K_{M3}$  are coefficients for moment due to backfill at zero cover, at final cover and live load respectively (dimensionless);  $R_B$ ,  $R_L$  are reduction factors for moment due to backfill and live load respectively (dimensionless);  $S$ ,  $H$  are span and cover depth;  $\gamma$  is unit weight of backfill; and  $LL$  is the equivalent line load.

According to the MBE,  $K_a$  should be determined by comparing the maximum member strain measured during load tests,  $\epsilon_T$ , with  $\epsilon_c$ , which is defined as “the corresponding calculated strain due to the test vehicle, at its position on the bridge which produced  $\epsilon_T$  (AASHTO 2018). The maximum inner fiber strains measured during the load tests occurred at the crown when test truck was positioned over the crown, whereas the MDOT method provides an empirical equation to calculate the live load moment only at the quarter point with live load over the quarter point. In order apply the MDOT approach,  $K_a$  as calculated by two alternative comparisons of strains: (1)  $K_a$  was calculated by comparing the measured strain at quarter point,  $\epsilon_{Tq}$ , with the test truck positioned over the quarter point during load test with the corresponding theoretical strain at quarter point due to test truck over the quarter point,  $\epsilon_C$ ; and (2)  $K_a$  was calculated by comparing the maximum measured strain at the crown,  $\epsilon_{Tc}$ , with the test truck positioned over the crown during load test with the theoretical strain at quarter point due to test truck over the quarter point,  $\epsilon_C$

$K_{bl}$  should be determined from the MBE using the ratio of test truck load effect,  $T$ , to the gross rating load effect,  $W$ , and whether the member behavior can be extrapolated to  $1.33W$ . In the present study,  $T$  refers to the calculated unfactored live load moment at the quarter point due to the test truck positioned over the quarter point, and  $W$  refers to the calculated unfactored live load moment at the quarter point due to concrete truck plus impact. To check the criterion for extrapolation to  $1.33W$ , the analytical culvert structure is loaded with 1.33 times concrete truck

weight plus impact over the quarter point to determine whether the maximum stress due to both 1.33 times concrete truck weight plus impact and earth fill weight is less than the minimum yield stress of steel (33 ksi).

The resulting theoretical rating factors  $RF_C$ , adjustment factor  $K$  and rating factor based on load testing  $RF_T$  are presented in Table 8.1. As can be noted, the adjustment factors  $K$  calculated using  $\epsilon_{Tc}$  and  $\epsilon_C$  (marked as gray) are more reasonable than  $K$  calculated using  $\epsilon_{Tq}$  and  $\epsilon_C$ . It seems unreasonable that a culvert with 13-inch cover would be able to support more than 9 times the concrete truck weight. This is because the measured strain at quarter point due to test truck over the quarter point ( $\epsilon_{Tq}$ ) is generally too small to represent the true load effect under loading compared with the maximum measured strain at the crown due to test truck over the crown,  $\epsilon_{Tc}$ . Even though  $K_a$  determined by comparing  $\epsilon_{Tq}$  and  $\epsilon_C$  does not precisely follow the MBE definition, based on which the corresponding theoretical strain at the crown due to test truck over the crown should be used, both  $\epsilon_{Tc}$  and  $\epsilon_C$  are representative of maximum strain under loading in each case. Therefore,  $K_a$  generated by comparing  $\epsilon_{Tc}$  and  $\epsilon_C$  better represents the benefit derived from the load test.

**Table 8.1. Quantities used in calculating rating factors for culverts 1 and 2 for the 33T concrete truck.**

Variable	Culvert 1	Culvert 2
<b>CALCULATION OF <math>RF_C</math></b>		
Cover/fill height (in.)	15	13
$M_p$ (k-ft/ft)	4.34	4.34
$S$ (ft)	16.67	16.50
$R$ (ft)	4.33	4.33

$\gamma$ (k/ft <sup>3</sup> )	0.112	
$E$ (k/ft <sup>2</sup> )	4176000	
$I$ (ft <sup>4</sup> /ft)	3.94E-5	
$A$ : section area (in <sup>2</sup> /ft)	3.321	
$SF$ : section modulus (in <sup>3</sup> /ft)	0.9408	
$E_S$ for zero cover depth (k/ft <sup>2</sup> )	45.58	45.58
$N_f$ for zero cover depth (dimensionless)	1282	1244
$K_{M1}$ (dimensionless)	0.0015	0.0015
$R_B$ (dimensionless)	0.72	0.72
$E_S$ for final cover depth (k/ft <sup>2</sup> )	49.96	49.38
$N_f$ for final cover depth (dimensionless)	1405	1348
$K_{M2}$ (dimensionless)	0.0054	0.0055
$K_{M3}$ (dimensionless)	0.063	0.064
$R_L$ (dimensionless)	0.32	0.34
$AL$ (k)	50	50
$K_4$ (ft)	9.49	9.18
$\phi_c$ (AASHTO MBE 3rd Edition Table 6A.4.2.3-1 & C6A.4.2.3-1)	1.00	
$\phi_s$ (AASHTO MBE 3rd Edition Table 6A.4.2.4-1)	1.00	

$\phi_f$ (AASHTO LRFR 6.5.4.2 & 7.5.4.2)	1.00	
$\gamma_{EV}$ (AASHTO LRFR Table 3.4.1-2)	1.95 (Max) or 0.9 (Min)	
$\gamma_{LL}$ (AASHTO MBE Table 6A.4.4.2.3a-1 & Table 6A.4.4.2.3b-1)	1.30	
$\eta_R$ (AASHTO LRFD 12.5.4. & 1.3.4)	1.05	
$M_B$ (k-ft/ft)	0.41	0.42
$M_{L+IM}$ (k-ft/ft)	2.30	2.48
$RF_C$	1.11	1.03
<b>CALCULATION OF <math>RF_T</math></b>		
$\varepsilon_C$ (in/in)	9.63E-04	10.32E-04
$\varepsilon_{Tq}$ (in/in)	1.46E-04	0.59E-04
$\varepsilon_{Tc}$ (in/in)	2.70E-04	2.43E-04
$K_a$ by comparing $\varepsilon_C$ and $\varepsilon_{Tq}$	5.59	16.49
$K_a$ by comparing $\varepsilon_C$ and $\varepsilon_{Tc}$	2.57	3.25
$T$ (k-ft/ft)	2.27	2.43
$W(1+I)$ (k-ft/ft)	2.30	2.48
Calculated max stress due to 1.33 times concrete truck and earth fill (ksi)	46.05 > 33	49.21 > 33
Whether member behavior can be extrapolated to 1.33 $W$	No	No

$K_{b1}$	0.5	0.5
$K_{b2}$	1.0	1.0
$K_{b3}$	1.0	1.0
$K_b$	0.5	0.5
$K$ by comparing $\varepsilon_{Tq}$ and $\varepsilon_C$	3.80	9.25
$K$ by comparing $\varepsilon_{Tc}$ and $\varepsilon_C$	2.28	2.62
$RF_T$ adjusted by $\varepsilon_{Tq}$ vs $\varepsilon_C$	4.22	9.55
$RF_T$ adjusted by $\varepsilon_{Tc}$ vs $\varepsilon_C$	2.54	2.71

Using the MDOT spreadsheet method and the field test data, the theoretical rating factor for the lowest cover case was increased from approximately 1.0 to 2.7, which represents an increase from barely sufficient to the ample sufficiency that was expected given the condition and performance of the structures. However, simplified stress prediction methods are available only for quarter-point locations for this category of structure, which may not represent the true maximum points of stress and strain. It should be recognized that the approach illustrated here and presented in the MBE was not developed specifically for very nonlinear systems such as shallow fill culverts. To be properly implemented for the culvert load rating scenario, field test data used to develop the adjustment factor,  $K$ , must be carefully associated with the controlling rating factor mechanism, which is not possible unless advanced analyses such as finite element methods are used.

### 8.3 Rating Factor Comparison

To illustrate the difference in rating factor outcome, the methods defined in prior chapters and summarized in section 8.1 were used to calculate the rating factor associated with the

concrete truck loads defined in Figure 8.1 for the Anniston arch culvert with 13-inch cover above the crown (BIN 20441). The first row of Table 8.2 (“Analytical RF”) demonstrates the extreme variation that can occur. Of these methods, the “3D FEM” should result in the most accurate representation of capacity. Note the difference between CANDE L1 and CANDE L2 (Level 1 and Level 2, respectively). Also, of the four simplified methods, the AU/MDOT provides the best correlation, yet is still “conservative”.

The “Test *K* factor” essentially reflects the relationship between field-measured strain and strain computed by each respective method. Higher values indicate that the measured strain was lower than the computed strain. For the test results to be applied to a given analytical method, that method must be capable of calculating the strain at the position of strain measurement, hence the “NA” for the ODOT methods. Note, for example, that the smallest *K* factor of 1.06 for the 3D FEM is an artifact of the accuracy and versatility of the 3D FEM; in other words, there is a close correlation between the test and analytical results.

**Table 8.2. Rating factor (RF) comparisons for BIN 20441 using 33T concrete truck**

	<b>ODOT1</b>	<b>ODOT2</b>	<b>MDOT</b>	<b>AU/MDOT</b>	<b>CANDE L1</b>	<b>CANDE L2</b>	<b>3D FEM</b>
<b>Analytical RF</b>	0.40	1.47	1.03	2.05	6.44	2.40	2.80
<b>Test <i>K</i> factor</b>	NA	NA	2.62	1.61	1.88	1.88	1.06
<b>Adjusted RF</b>	NA	NA	2.70	3.30	12.11	4.51	2.97

## **8.4 Anniston Culverts Rating Factors**

ALDOT requested that the research team provide ratings for the nine Anniston/McClellan culverts. As prior presented and discussed, there are several approaches and tools that could be used for the rating task, with each having advantages and disadvantages over others, and with each potentially resulting in significantly different rating values. To come up with reportable and defensible rating factors for the ALDOT inventory, CANDE 2019 was used following recommended procedures defined in the CANDE manuals. Rating factors resulting from the “Level 1” approach in which the load magnitudes of the standard vehicles are applied are first presented. The effect of the “Level 2” approach is then presented for two fill heights to emphasize the difference between the two approaches.

### **8.4.1 Input and Methodology**

The operating rating factors for nine Anniston/McClellan culverts were evaluated for the seven ALDOT posting vehicles and an ALDOT load truck case using the finite element software CANDE 2019. Bridge inspection data sheets were provided by ALDOT for each of the culverts and used as the basis for constructing the models. Eight of the nine culverts are low profile arch (LPA) structures and one is pipe arch (PA) with minimum fill ranging from 12 to 19 inches. All of the LPA spans are 16.7 ft., have flexible pavement and were observed to be in good condition. The PA has a span of 12.7 ft. and no pavement. Note that  $L/8$ , which corresponds to the minimum design cover, for the LPAs is 25 inches and  $L/8$  for the PA is 19 inches; therefore none of the Anniston culverts meet current cover depth requirements for new construction. The bridge data sheet for BIN 20432 indicates skew; however, visual inspection indicates that the side rails are skewed but the culvert alignment is perpendicular to the roadway and did not impact the rating.



Table 8.3 lists the parameters that were used for each culvert model, which are also defined in Chapter 4 along with a thorough description of each culvert.

**Table 8.3. Anniston culvert properties.**

<b>BIN</b>	<b>Shape</b>	<b>Fill (inch)</b>	<b>Span (ft)</b>	<b>Height (ft)</b>	<b>Condition</b>	<b>Skew (deg)</b>	<b>Pavement (inch)</b>
18609	PA	12	12.7		7	0	0
18615	LPA	14	16.7	4.3	6	0	2.5
19875	LPA	18	16.7	4.3		0	2.5
20431	LPA	16	16.7	4.3	6	0	2.5
20432	LPA	15	16.7	4.3	6	40*	2.5
20433	LPA	15	16.7	4.3	7	0	2.5
20441	LPA	13	16.7	4.3	6	0	2.5
20442	LPA	12	16.7	4.3	7	0	2.5
20444	LPA	19	16.3	4.3	6	0	2.5

\*data sheet notes "skewed," but pipes are not skewed relative to traffic direction

### 8.4.2 Modeling Approach and Assumptions

CANDE 2019 and CANDE Toolbox 2019 were used to calculate the rating factors. The modeling approach is described thoroughly in Chapter 6. The documentation recommendations and best practices for CANDE 2019 were followed. The image and notes in Figure 8.2 define the adopted modeling methodology. The ratings are based on the following choices, decisions, and interpretations about the use of CANDE 2019 and the current state of the culverts.

- LRFR factors were incorporated;
- Axle loading worst-case positions were determined for each load case;
- The Duncan-Selig soil plasticity model was used for the in-situ soil and all backfill soil elements indexed to field measured properties;

- Elastic properties of the rock and footing are based on best estimates;
- Compaction due to gravity was simulated but construction equipment compaction was not simulated due to the age of the structures;
- Beam elements representing 2.5-inch thick asphalt pavement were included for all of the LPA culverts; simulating pavement had a significant effect on the rating factors.

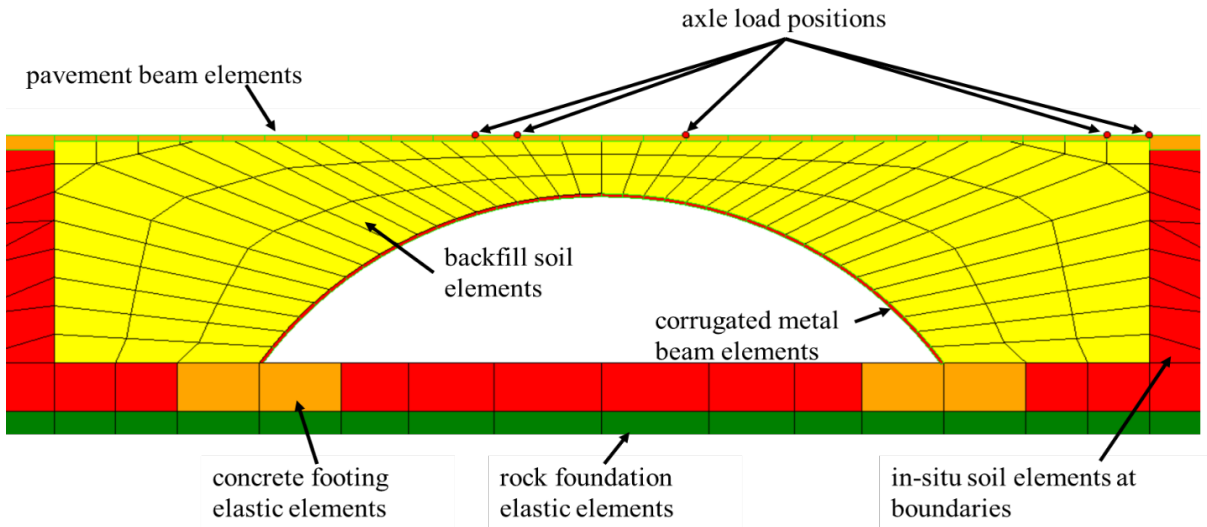


**Figure 8.2. Annotated CANDE 2019 Model for a low profile arch culvert typical of this project.**

### 8.4.3 Load Case Definitions

The load cases evaluated were 1) the ALDOT posting vehicles (Figure 8.3); 2) the HS-20 Standard Truck; and 3) ALDOT load truck configuration LC-5. All of the potential posting vehicle loads were used to rate each culvert. The HS-20 rating was provided for the FHWA National Bridge Inventory (Figure 8.4).

### 8.4.4 Rating Factor Results

The CANDE Level 1 rating factors for all culverts and load cases are summarized in Table 8.4. It can be noted that some of these rating factors are quite large. Parametrically, this is affected by the existence of the pavement wearing layer that was present at all of the LPA culverts. The

rating factors for the PA culvert were much less, primarily due to the lack of pavement. The controlling criterion for all of the LPA culverts was “seam thrust,” while the controlling criterion for the PA culvert (18609) was “plastic penetration.” It must be again emphasized that the analysis methodology and response results involve extreme nonlinearities and therefore the rating factors cannot be interpreted as capacity multipliers (i.e., a RF of 9.0 for the tri-axle truck does not mean that the structure can resist 9 times the tri-axle truck loading).

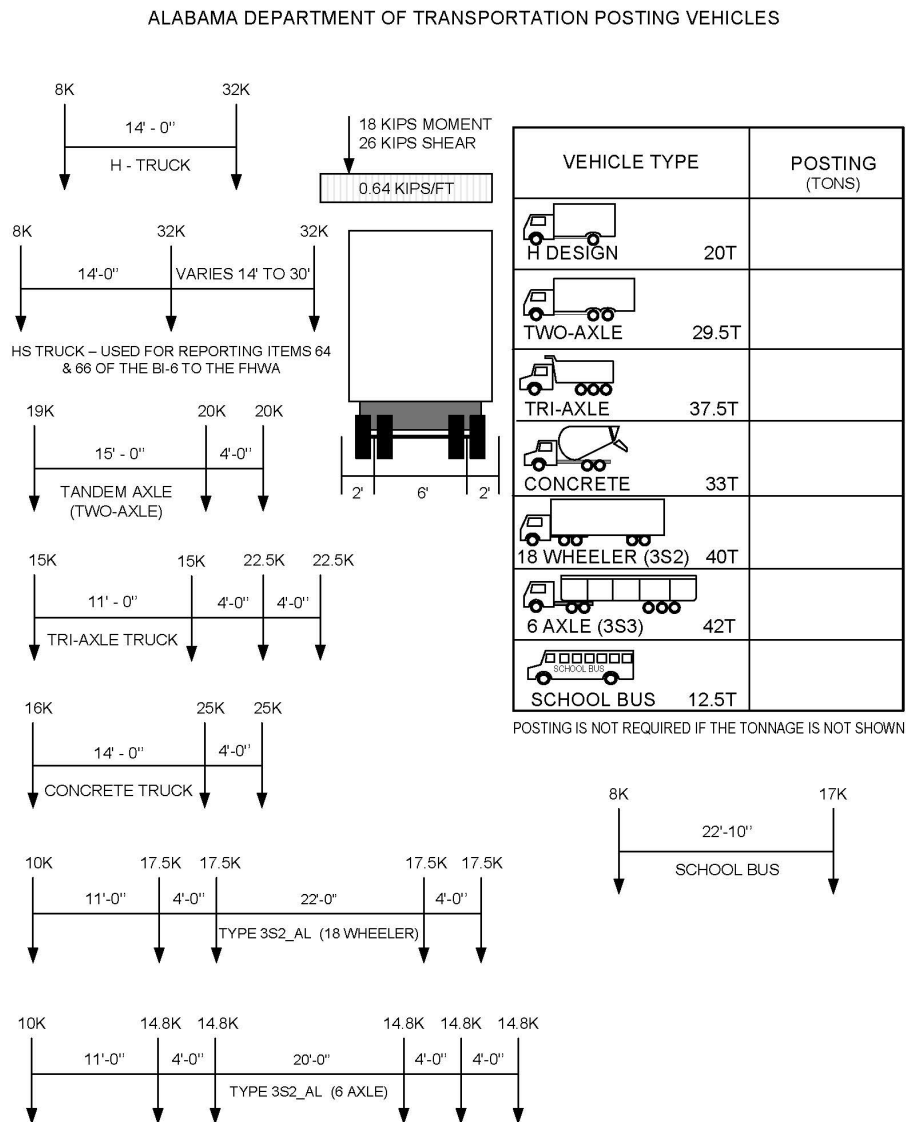


**Figure 8.3. Load case definitions.**

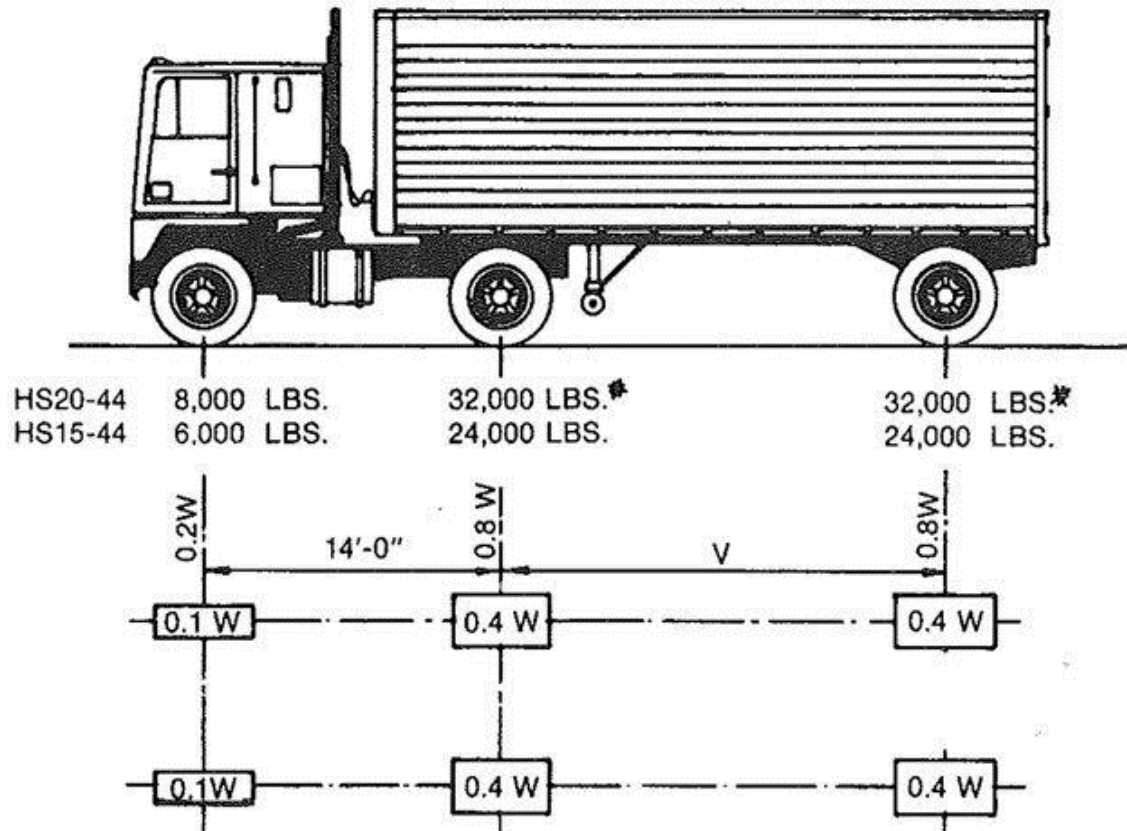


Figure 8.4. HS-20 load configuration.

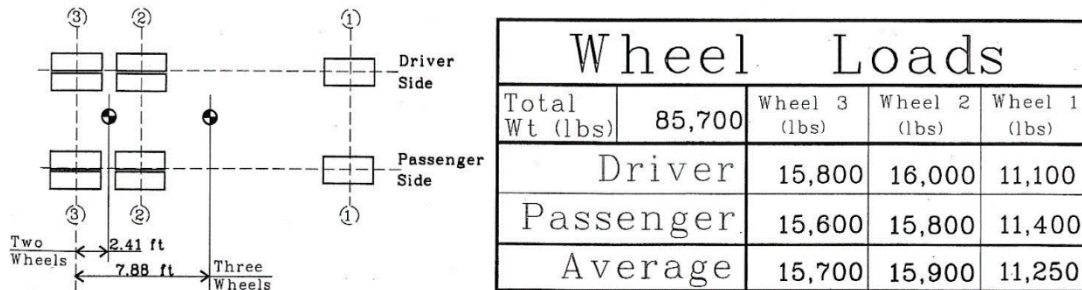


Figure 8.5. Test truck LC-5 configuration.

Table 8.4. Rating factors for Anniston Culverts based on CANDE Level 1 Analyses

<b>D-S summary</b>	<b>Operating Rating Factor (LRFR)</b>								
	<b>PA</b>	<b>LPA</b>	<b>LPA</b>	<b>LPA</b>	<b>LPA</b>	<b>LPA</b>	<b>LPA</b>	<b>LPA</b>	<b>LPA</b>
<b>Vehicle/BIN</b>	<b>18609</b>	<b>18615</b>	<b>19875</b>	<b>20431</b>	<b>20432</b>	<b>20433</b>	<b>20441</b>	<b>20442</b>	<b>20444</b>
<b>Test Truck LC-5</b>	1.3	7.8	8.0	7.9	7.9	7.9	7.8	7.8	8.0
<b>H DESIGN</b>	1.2	12.8	13.4	13.1	12.9	12.9	12.6	12.5	13.5
<b>TWO-AXLE</b>	2.5	11.7	11.8	11.8	11.7	11.7	11.7	11.7	11.8
<b>TRI-AXLE</b>	1.6	9.0	9.3	9.2	9.1	9.1	9.0	8.9	9.4
<b>CONCRETE</b>	1.7	9.5	9.6	9.5	9.5	9.5	9.5	9.4	9.6
<b>18 WHEELER</b>	3.8	13.4	13.5	13.5	13.5	13.5	13.4	13.4	13.5
<b>6 AXLE</b>	3.8	12.7	12.9	12.8	12.8	12.8	12.7	12.6	13.0
<b>SCHOOL BUS</b>	6.5	23.8	23.8	23.8	23.8	23.8	23.8	23.8	23.8
<b>HS-20</b>	1.2	12.1	12.4	12.2	12.2	12.2	12.0	12.0	12.5
	<b>Inventory Rating Factor (LRFR)</b>								
<b>HS-20</b>	1.0	9.4	9.8	9.6	9.5	9.5	9.2	9.1	9.9

To illustrate the effect of the “Level 2” approach of increasing the load magnitude until an RF of 1 was achieved, two more series of CANDE analyses were conducted: (1) 13 inch cover over the crown (BIN 20441) and (2) 18 inch cover over the crown (BIN 19875). For these analyses, the RFs presented in Table 8.5 were obtained by increasingly adding 0.5 time truck weight on culverts with the heaviest axle over the crown until RF=1. For example, RF=4 indicates the solution converges at 4 but not at 4.5 times truck weight. All other input and modelling approach is the same as the Level 1 analyses. This data demonstrates that, although CANDE guidance was carefully adhered, the rating factors that result from the Level 1 analyses are not accurate, and not

conservative from a safety standpoint. The reason that all of the culverts listed in Table 8.4 are not presented in Table 8.5, and that the Level 2 rating factors presented in Table 8.5 are to the nearest 0.5, is that the Level 2 analyses are trial-and-error and very time intensive.

**Table 8.5. Operating Rating Factors Comparisons between Level 1 and Level 2 CANDE Analyses**

	13 inch cover		18 inch cover	
	Level 1	Level 2	Level 1	Level 2
<b>Test Truck LC-5</b>	7.8	2	8.0	2.5
<b>H DESIGN</b>	12.6	2	13.4	2.5
<b>TWO-AXLE</b>	11.7	2.5	11.8	3.5
<b>TRI-AXLE</b>	9.0	2.5	9.4	4
<b>CONCRETE</b>	9.5	2	9.6	3
<b>18 WHEELER</b>	13.4	3	13.5	4
<b>6 AXLE</b>	12.7	4	13.0	5
<b>SCHOOL BUS</b>	23.8	3	23.8	4
<b>HS-20</b>	12.0	2	12.5	2

## CHAPTER 9: CONCLUSIONS AND RECOMMENDATIONS

Existing methodologies and tools for load rating of corrugated metal culverts were thoroughly investigated through numerical modeling and field testing. The basis and accuracy of three existing spreadsheet rating tools, two from the Ohio DOT and one from the Michigan DOT, were investigated for shallow-cover applications. Two existing culverts that are more than 80 years old and whose cover over the crown is significantly less than current design and construction requirements were instrumented and load tested. The plane strain finite element software, CANDE, that was developed specifically for culvert analysis and design and is widely used, plus two general-purpose finite element software, Abaqus and Plaxis, were extensively employed to understand the soil-structure interaction phenomena and assess culvert rating methodology. Recommendations for addressing the deficiencies of the existing “simplified” spreadsheet tools for low cover situations were developed and incorporated into a new spreadsheet-based tool. The following outlines the most prominent observations and conclusions:

- All three of the currently available spreadsheet tools are based upon assumptions and theory that will result in a conservative rating (a RF prediction that is lower than the actual representation of the available resistance). Therefore, if the use of those tools results in a “sufficient” rating then additional analyses and testing is not likely warranted. However, for low cover situations, these approaches may be ultra conservative and result in the indication that posting is required when in reality it is not.
- The resistance mechanisms for arch culverts (arch bases connected to rigid foundations) are significantly different from pipe arch culverts (fully enclosed pipe on compacted soil foundation), yet there is no difference in rating factor evaluation using the simplified approaches.

- The AASHTO *Manual for Bridge Evaluation* (MBE) is lacking with regard to methodology for rating corrugated metal culverts, especially for shallow cover situations in which localized effects from live loads are significant.
- Because of the extreme nonlinearities from soil-structure interaction, it is very difficult to develop an accurate and broadly applicable “simplified” method for rating metal culverts in which localized effects from live loads are significant. As with the Anniston culverts, advanced analytical and load testing will likely be required for situations in which the cover is less than that required for new construction.
- One of the challenges associated with rating existing culverts that have been in service for many years is defining the condition of the material (pavement, base, soil, etc.) that is below the roadway surface. Destructive testing and coring are typically not suitable options, and nondestructive characterization provides only limited insight. For example, the condition and thickness of the pavement and base materials, compaction of the soil, and the effects of roots from large trees were unknown variables with the Anniston culverts.
- Minimum cover requirements, for example  $L/8$  that is applicable to the Anniston culvert geometries, are based on a variety of practical factors that are not pertinent to the rating process and outcome; for example a minimum thickness of soil is required to minimize the likelihood of damage during roadway construction. In other words, the fact that a given existing culvert does not meet the minimum design and construction cover requirement does not mean that the structure is unsafe, but some of the rating procedures use the minimum design and construction cover requirement as the basis of a RF calculation.
- It is also important to recognize that the minimum cover requirements were established to ensure that live loads would be sufficiently attenuated through the soil so that predominate resistance mechanism in the culvert wall would be axial thrust, rather than flexure. In other words, the soil compression ring mechanism is enforced. The minimum cover results in a uniform distribution of live loading over the majority of the culvert, which greatly simplifies the calculation of live load effects.
- The shear resistance of typical flexible (asphalt) pavement and base is significantly greater than that of soil. However, this is not explicitly considered in the “simplified” rating approaches and tools, and becomes increasingly critical with shallower cover situations.



Merely considering the pavement effect can result in a change in rating outcome from posting-required to sufficient.

- Load testing can provide valuable data that can be used to improve confidence and accuracy of rating calculations. However, load testing is relatively costly, and must be combined with advanced numerical simulations (finite element modeling). Rating factors cannot be extracted from load testing alone because it is only practical to collect data from a few discrete locations. Load test data is valuable for validating the numerical models and adjusting the analytical rating factor calculations accordingly. A general procedure for using load test data for bridge rating is presented in the MBE, but was not developed for culvert rating and thus warrants improvement.
- The overall outcome of the Anniston culverts analyses and load tests was high confidence that the rating factors for the eight low profile arch structures is greater than 1.0. However, the pipe arch that is beneath a dirt road may require posting. It must be recognized though that the research team could not access all of the Anniston culverts and load testing was performed on only two culverts.
- Although CANDE has the ability to explicitly output rating factors, anyone using it for rating of shallow-cover flexible culverts must recognize that an accurate RF can only be achieved by increasing the live load magnitudes until an RF of 1 is achieved, which is a very cumbersome and time-intensive process. Furthermore, no sufficient method for modeling the pavement in this context is available. Pavement can be sufficiently simulated for design purposes using beam elements, but those elements remain elastic regardless of the load intensity, which violates the mechanics required for load rating. Alternatively, the properties of pavement can be assigned to plane strain elements, as with soil, but the meshing capability at the location of pavement is not sufficiently refined.

Recommendations resulting from the program include the following:

- Agencies should employ advanced analyses and load testing if rating calculations using simplified methods indicates that posting is required but the culvert is performing without indication of distress.

- A standard procedure for load testing of flexible shallow-cover culverts and guidance for the use of the data for load rating of culverts should be developed.
- Additional research is required to develop and validate reasonable “simplified” approaches that would distinguish between different culvert geometries, such as the PA and LPA culverts involved in this investigation.
- Additional research into the effects of flexible pavement and its incorporation into simplified rating procedures is needed.
- Additional research is needed to verify and improve the simplified rating procedures developed through this project.

## REFERENCES

- Abdel-Karim A. M., Tadros M. K. and Benak A. J. (1990). "Live Load Distribution on Concrete Box Culverts." *Transportation Research Record*, 1288, 136-151.
- Alabama Department of Transportation (ALDOT 2021). *Bridge Inspection Manual*. Alabama Department of Transportation Maintenance Bureau, 1409 Coliseum Blvd. <https://www.dot.state.al.us/publications/Maintenance/pdf/Bridge/BridgeInspectionManual.pdf>.
- Ahlborn T. M., Gilbertson C. G., Kiefer J. A. and Colling T. K. (2013). *Assessment of ODOT Culvert Load Rating Spreadsheets for use in Michigan*. Michigan Tech University CSD-2012-012, Michigan Department of Transportation Research Report RC-1590.
- American Association of State Highway and Transportation Officials (AASHTO 1992). *Standard Specifications for Highway Bridges*, 15<sup>th</sup> Edition, Washington, DC.
- American Association of State Highway and Transportation Officials (AASHTO 1993). *Guide for Design of Pavement Structures*. Washington DC.
- American Association of State Highway and Transportation Officials (AASHTO 2002). *Standard Specifications for Highway Bridges*, 17<sup>th</sup> Edition. Washington DC.
- American Association of State Highway and Transportation Officials (AASHTO 2017). *LRFD Bridge Construction Specifications*, Fourth Edition. Washington, D.C.
- American Association of State Highway and Transportation Officials (AASHTO 2018). *The Manual for Bridge Evaluation*, 3<sup>rd</sup> Edition, Washington DC.
- American Association of State Highway and Transportation Officials (AASHTO 2020). *LRFD Bridge Design Specifications*, 9<sup>th</sup> Edition, Washington DC.
- Bentley. (2021a). *Plaxis 3D: Material Models Manual*. Plaxis connect edition v21.01. Last updated: March 04, 2021. <https://communities.bentley.com>.
- Bentley. (2021b). *Plaxis 3D: Reference Manual*. Plaxis connect edition v21.01. Last updated: March 04, 2021. <https://communities.bentley.com>.
- Burmister D. M. (1958). "Evaluation of pavement systems of the WASHO road test by layered system method." Bulletin 177, Highway Research Board, 26-54.

- CANDE Tool Box (2019). "CANDE Tool Box Manual for Load Rating." August 20, 2019.
- CNA Consulting Engineers, Simpson, Gumpertz and Heger (NCHRP 2009). "Appendix C: Proposed Revisions to AASHTO Specifications." National Cooperative Highway Research Program Project 15-29.
- Duncan J. M. (1979). "Behavior and Design of Long-Span Metal Culvert." *Journal of Geotechnical Engineer Division*, ASCE, Vol. 105, No GT3, pp. 399-418.
- Duncan J. M. and Drawsky R. H. (1983). "Design procedures for flexible metal culvert structures." Report No. UCB/GT/83-04, University of California, Berkeley.
- Elshimi T. M. (2011). "Three-Dimensional Nonlinear Analysis of Deep-Corrugated Steel Culverts", Queen's Graduate Theses and Dissertations, Department of Civil Engineering Graduate Theses, Queen's University, Kingston, Ontario, Canada.
- Galambos T. V. (1998). *Guide to Stability Design Criteria for Metal Structures*, 5<sup>th</sup> Ed." Wiley, New York.
- Han J., Acharya R., Parsons R. L., Khatri D. (2013). "Improved Load Distribution for Load Rating of Low-Fill Box Structures." Report No. K-TRAN: KU-12-3, University of Kansas.
- Jaky J. (1944). "The Coefficient of Earth Pressure at Rest", *Journal of the Society of Hungarian Architects and Engineers*, Budapest, pp. 355–358 (in Hungarian).
- Kang J. S., Han T. H., Kang Y. J., Yoo C. H. (2009). "Short-term and long-term behaviors of buried corrugated high-density polyethylene (HDPE) pipes." *Composites: Part B*. 40.
- Katona M. G., Smith J. M., Odello R. S., and Allgood J. R. (1976). CANDE: A Modern Approach for the Structural Design and Analysis of Buried Culverts, Federal Highway Administration Report No. FHWA-RD-77-5.
- Katona M. G. (CANDE 2007). "Culvert Analysis and Design Solution Methods and Formulations." National Cooperative Highway Research Project NCHRP 15-28.
- Katona M. G. (CANDE 2019). "Culvert Analysis and Design Solution Methods and Formulations." AASHTO and TRB, Washington, D.C., 2019.
- McGrath T. J., Moore I. D., Selig E. T., Webb M. C. and Taleb B. (2002). *Recommended Specifications for Large-Span Culverts*. NCHRP Report 473, Transportation Research Board, Washington, DC.
- Michigan Department of Transportation (MDOT 2016). "MDOT CMP LRFR (ver 2\_0).xlsx Structural Analysis Documentation (SAD)." Structural Analysis Documentation, Design Division Bridge Management Section, Creightyn McMunn, Load Rating Program Manager.

- Mlynarski M., Katona M. G. and McGrath T. J. (2008). *Modernize and Upgrade CANDE for Analysis and LRFD Design of Buried Structures*. NCHRP Report 619. National Academies of Sciences, Engineering, and Medicine. Washington, DC: The National Academies Press.
- Mlynarski M., Clancy C., McGrath T. J. and Katona, M. G. (2019). *Proposed Modifications to AASHTO Culvert Load Rating Specifications*. Final report for NCHRP Project 15-54. National Academies of Sciences, Engineering, and Medicine. Washington, DC: The National Academies Press.
- National Corrugated Steel Pipe Association (NCSPA 1995). “Load Rating and Structural Evaluation of In-Service, Corrugated Steel Structures. Design sheet No. 19.” Washington, D.C., pp. 1-12.
- National Corrugated Steel Pipe Association (NCSPA 2008). *Corrugated Steel Pipe Design Manual*. Dallas TX.
- National Corrugated Steel Pipe Association (NCSPA 2013). *Installation Manual for Corrugated Steel Pipe and Structural Plate*. Dallas, TX.
- Petersen D. L., Nelson C. R., Li G., McGrath T. J. and Kitane Y. (2010). *Recommended Design Specifications for Live Load Distribution to Buried Structures*. National Academies of Sciences, Engineering, and Medicine. Washington, DC: The National Academies Press.
- Poulos H. G. and Davis E. H. (1974). “Elastic Solutions for Soil and Rock Mechanics.” Wiley.
- Sargand S. M., White K., Khoury I., Hussein H., Mutashar R., Jordan B., and Russ A. (2015). Task 4 – Validation of ODOT Shallow Cover Rating Factor Methodology for Metal Pipe & Arch Culverts, Rep. No. FHWA/OH-2015/15, Structures Research Service Report to Ohio Department of Transportation, February 2015, Civil Engineering Dept., Ohio University, Athens, OH. 150 pp.
- Sargand S., White K., Masada T., and Wang C. (2018). “Evaluation of load-rating procedure for metal culverts under shallow soil covers.” *J. Pipeline Syst. Eng. Pract.*, 9(1), ASCE, February.
- Selig E. T. (1988). “Soil Parameters for Design of Buried Pipelines.” *Pipeline Infrastructure*, B. A. Bennett, Ed., ASCE, New York, NY, pp. 99–116.
- Selig E. T. (1990). *Soil Properties for Plastic Pipe Installations*. Buried Plastic Pipe Technology, STP1093, G. S. Buczala and M. J. Cassady, Eds., ASTM, Philadelphia, PA, pp. 141–158.
- Sezen H., Fox P. P. and Yeau K. Y. (2009). “Verification of ODOT’s load rating analysis programs for metal pipe and arch culverts.” Rep. No. FHWA/OH-2009/6, Ohio Dept. of Transportation, Columbus, OH.

- Spangler M. G. (1941). *The structural design of flexible pipe culverts*. Bulletin 153, Iowa State College, Ames.
- Tehrani A. D., Kouchesfehiani Z. K. and Najafi M. (2020). Review and recommendations for structural testing of buried gravity storm drain pipes and culverts. *Canadian Journal of Civil Engineering*, September.
- Timoshenko S. P. and Gere J. M. (1961). *Theory of Elastic Stability*. Second Edition, McGraw-Hill Book Co. Inc., New York.
- Transportation Research Board (TRB 1998). *Manual for bridge rating through load testing*. NCHRP Research Result Digest, Issue No. 234, Transportation Research Board, Washington D.C., United States.
- United States Army Corps of Engineers (USACE 1991). *Design of Pile Foundations*. EM 1110-2-2906, Washington, DC.
- Wang C. (2016). “Load factor load rating of in-service, corrugated metal pipe structures.” Spreadsheet, Ohio Dept. of Transportation, Columbus, OH.
- Watkins R. K. and Spangler M. G. (1958). “Some characteristics of the modulus of passive resistance of soil—A study in similitude,” *Proc. of the Highway Research Board*, Highway Research Board, Washington, D.C.
- Watkins R. K. and Anderson L. R. (1999). *Structural Mechanics of Buried Pipes* (1st ed.). CRC Press.
- Webb M., Selig E., Sussmann J. and McGrath T. (1999). “Field Tests of a Large-Span Metal Culvert.” *Transportation Research Record*, 16522. 99-0425.
- Whidden W. R. (2009). *Buried Flexible Steel Pipe, Design and Structural Analysis*, ASCE Manuals and Reports on Engineering Practice No. 119, Prepared by the Task Committee on Buried Flexible (Steel) Pipe Load Stability Criteria & Design of the Pipeline Division of the American Society of Civil Engineers, 1801 Alexander Bell Drive, Reston Virginia, 20191.
- White H. L. and Layer J. P. (1960). “The Corrugated Metal Conduit as a Compression Ring.” *Proceedings of the Highway Research Board*, Highway Research Board, Vol. 39, pp. 389-397.